2013

Development Of Novel Redox Sensors And Processes Towards Biological Applications

Jigna Patel
University of Central Florida

DEVELOPMENT OF NOVEL REDOX SENSORS AND PROCESSES TOWARDS BIOLOGICAL APPLICATIONS

by

JIGNA PARBHU PATEL

B.S. University of Central Florida, 2007

A dissertation submitted in partial fulfillment of the requirements
for the degree of Doctor of Philosophy
in the Department of Chemistry
in the College of Sciences
at the University of Central Florida
Orlando, Florida

Summer Term
2013

Major Professor: Diego J. Díaz and Cherie L.Yestrebsky

ABSTRACT

Research on the cure and early detection of diseases such as diabetes, Alzheimer's, and Parkinson's is becoming of great interest due to the increasing number of people affected by them every year. An accurate and quick detection of various damaging species is highly critical in treatments of such diseases not only for exploring possible cures but also for early detection. If these diseases are detected during the initial stages than the possibility of curing them is much higher. Motivated by this, many researchers today have developed numerous types of sensing devices that can detect various physiological and biological compounds. However, most of these sensors are enzyme based. They have several setbacks such as the lack of sensitivity, restricted selectivity, short shelf life, and biological fouling. To overcome these obstacles, we examine the use of nanoceria modified Pt and Au electrodes for the detection of glucose and reactive oxygen species such as hydrogen peroxide. Amperometric detection of glucose and hydrogen peroxide is critical for biological applications for diabetes and possible Alzheimer's and Parkinson's patients. This dissertation focuses on the exploration of non-enzymatic detection of glucose and reactive oxygen species which has the prospective to be used for biological applications, in addition to an investigation of an odor control technology that uses these reactive oxygen species for the treatment of wastewater plants. The combination of bi-metallic composites with nanoceria showed increased oxidation ability towards glucose and hydrogen peroxide. The following dissertation expands on the relationship between bi-metallic nanoceria composite materials and its electro-oxidation of glucose and hydrogen peroxide towards biological sensing along with an investigation of an odor control technology that utilizes generates hydroxyl radical fine particle mist for the degradation of hydrogen sulfide odor in wastewater treatment plants.

This work is dedicated to God, my family, and my friends.

ACKNOWLEDGMENTS

First and foremost, I would also like to thank my research advisors Dr. Diego Díaz, Dr. Cherie Yestrebsky, and Dr. Clausen. Dr. Diaz, you have supported me throughout my studies and sacrificed a great deal of time and energy on my behalf and for this I am truly and forever grateful. Thank you for sharing your knowledge and for the extraordinary example you have been to me. Dr. Yestrebsky, I am eternally indebted to you for your willingness to take me on as your student during an uncertain period during my education. Thank you for the encouragement, support, guidance, and time you have given me. I greatly appreciate it. Dr. Clausen, thank you for your availability, knowledge, assistance, and time. To all my committee members: Dr. Michael Hampton and Dr. James Harper, thank you for your patience, availability, advice, and all your help during my dissertation. I am truly grateful for all that you have done for me. I would also like to sincerely thank Dr. Hyoung Jin Cho "Joe" and Dr. Sudipta Seal and their research group members for all of their help, guidance, and support throughout the years, without whom my research would have not been possible.

Now, I would like to a moment to thank my incredible family. Mom and Dad, thank you for the lifelong sacrifices you made for my life's betterment and for your unending loving encouragement and believing in me. I am truly blessed to have you as my parents, and I hope I continue to make you proud always. I would like to acknowledge my grandparents for all the blessings, encouragement, and sacrifices from the other side of the world. To my brother Bhavin and sister-in-law Hemali, your encouragement and support has meant a lot to me. For all my wonderful friends, without you I would not be where I am today; thank you for always being there for me. And finally, I would like to take a moment to thank a very special person to whom I

will be eternally grateful to, and that is my dear friend Sagar Shah. If it weren't for him, I would have never begun my graduate school journey and never would have known my true potential. My heartiest gratitude will always be with you Sagar, as you are, and always will be a truly meaningful and inspiring person in my life who has cared for me, guided me, believed in me, and forever changed my life.

I would also like to thank all of my colleagues in the electrochemistry and the industrial research lab. Without all of your encouragement and friendship, this dissertation would not have been possible. Jordan Anderson for helping me throughout my research and being a great example. Carlos Ledezma, thank you for your guidance, willingness to help me at all times, and for synthesizing compounds for my research. Josh Knorr and Victor Diaz for working alongside me day after day and for always taking my jokes/sarcasm in a cheerful manner. Carolina Franco for constantly putting up with me during the internship and being a great friend. Thank you for helping and supporting me at all times. Ted Gorman for all the laughs and just being yourself. Benny Pearman for being an active part of our lab even though you worked far away and for being such a caring friend. Simone Novaes-Card and Tamra Legron-Rodriguez for making it a pleasure to come to work and for always being there for me in my time of need. Thanks for all the laughs and affection. I have learned so much from you both. It has been a pleasure to do research alongside you all. Thank you Dr. Yestrebsky and Dr. Clausen's industrial research lab for taking me in and making me feel like a part of your family.

During my internship at Parkson/Vapex Environmental Technologies, several people deserve special recognition for their hospitality and assistance: Robert Jeyaseelan, Travis Douglas, Darrel Resch and his entire team were instrumental in shaping my experience there.

Thank you all. Finally, I would like to give a special thank you to the many people that have provided administrative support during my time in the chemistry department. In conclusion, the years I spent at UCF will be with me throughout my life and I will cherish them forever.

TABLE OF CONTENTS

LIST OF FIGURES

LISTS OF TABLES

LISTS OF ACRONYMS/ABBREVIATIONS

AA	Ascorbic Acid
AFM	Atomic Force Microscopy
BSA	Bovine Serum Albumin
Cu-UPD	Copper Underpotential Deposition
CV	Cyclic Voltammetry
DAFC	Direct Alcohol Fuel Cell
E	Potential
ECA	Electrochemical Active Area
EIS	Electrochemical Impedance Spectroscopy
GOx	Glucose Oxidase
HPLC	High Performance Liquid Chromatography
I, i	Current
IEP	Isoelectric Point
KL	Koutecky-Levich
NHE	Normal Hydrogen Electrode

PBS	Phosphate Buffer Solution
Q	Charge
RDE	Rotating Disk Electrochemistry
ROS	Reactive Oxygen Species
RPM	Revolutions Per Minute
s	Seconds
SEM	Scanning Electron Microscopy
SHE	Standard Hydrogen Electrode
t	Time
TEA	Triethanolamine
UV-Vis	Ultraviolet-Visible
UPD	Underpotential Deposition
V	Voltage

CHAPTER 1: INTRODUCTION

Sensors

A sensor is classified as a transducer that converts one form of measurable energy into another form which can be measured and processed through integrators and signal modifiers, in order to suit the information that is required. Sensors can be composed of a wide variety of substances and are capable of detecting a variety of types of energies. There are six main categories of energy that supply the input to the sensor which are summarized in Table 1. A majority of the sensors utilize the changes in concentration of an individual analyte which is then transformed into an electrical signal.

Table 1: Six major categories of energy sensors stating the parameters measured along with examples of each.

Category	Properties	Examples of Sensors
Chemical	Concentration, reaction rate, redox potential	pH sensors, oxygen sensors, CO detectors
Electrical	Current, voltage, resistance, capacitance, frequency	Voltmeter, ohmmeter
Magnetic	Field intensity, moment, permeability, flux density	Magnetic compass, metal detectors
Mechanical	Acceleration, force, stress, pressure	Flow meters, pressure gauge, motion sensors
Radiant	Intensity, energy, phase, wavelength, polarization	Light sensor, photo detectors
Thermal	Heat, temperature, flux	Thermometers, thermocouples, calorimeter

The basic constituents of a sensor are depicted in Figure 1. They include a sample insertion, followed by the sensing method which then yields a signal that is processed and readout of a measurement is obtained.

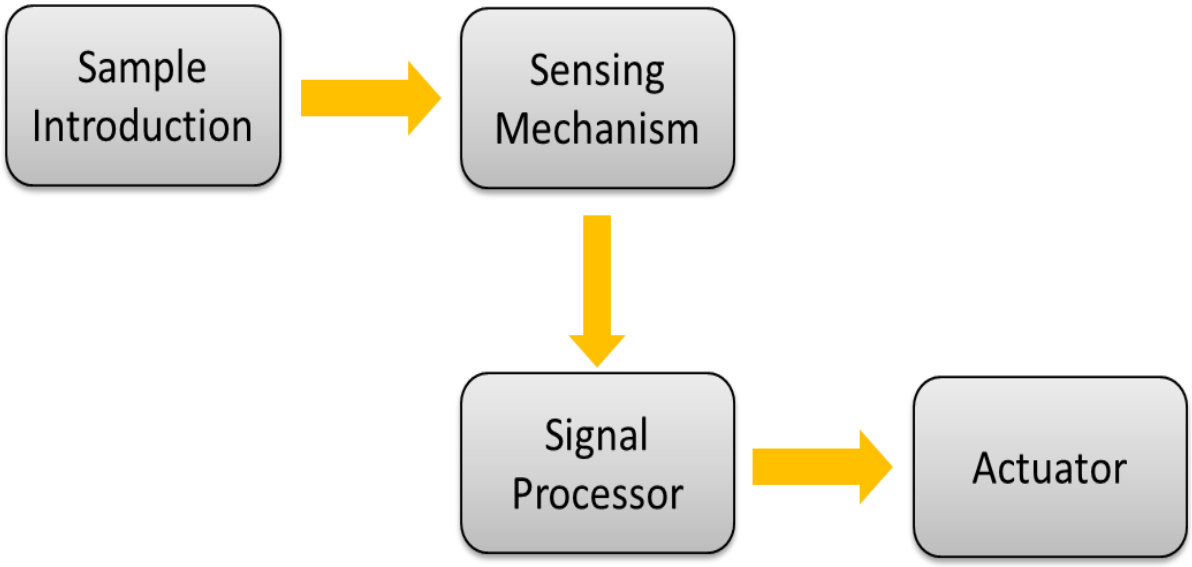

Figure 1: Schematic diagram showing the typical components of a sensor and the flow process that the sample of interest follows through the system yielding a data readout.

A biosensor is defined as a device that detects, records, and transmits information regarding a physiological change or process essentially to monitor the presence of various chemicals in a biological substance. Amongst the various types of biosensors, the electrochemical method of sensing offers the opportunity for a portable, economical, sensitive, and rapid methodology for the detection of glucose and reactive oxygen species such as hydrogen peroxide. Electrochemical detection methods using a variety of chemically modified electrodes have also been employed and will be the focus of this dissertation.

Use of Nano-scale Metal Oxides for Sensors

Over the years, many researchers have investigated various nano-scale metal oxide composite electrodes for biological sensing applications. These innovative metal oxide devices are cost-effective, highly sensitive due to the large surface-to-volume ratio of the nanostructure, and have exceptional selectivity under physiological conditions.[1] The catalytic ability of transition metal oxides such as CuO and NiO for the nonenzymatic direct electro-oxidation of glucose is another one of the appealing properties for glucose detection. These electrodes require minimum fabrication cost and have shown to be stable glucose sensors. Some metal oxides such as ZnO and CeO_2 demonstrate excellent biocompatibility, have a high isoelectric point (IEP), and have relatively easy synthetic procedures for generating a nanostructure that enables reliable immobilization of glucose oxidase (GOx).[2]

One metal oxide that has been generating a great deal of attention is cerium oxide (CeO_2). Ceria specifically is defined as the combination of the two cerium oxides with Ce^{+3} and Ce^{+4}. Recently, Anderson et al. have studied the utilization of Pt/nanoscale ceria composite electrodes for the electrochemical oxidation of alcohols in direct alcohol fuel cells (DAFCs).[3] This research has shown that nanocrystalline ceria can act as a beneficial catalyst for the electrochemical oxidation of methanol and ethanol. There is a great deal of interest in utilizing ceria as a catalyst material due to its ability to store and release oxygen (oxygen carrying capacity) without much distortion in the lattice. This is due to the ability of the cerium atom to undergo reversible oxidation / reduction processes from Ce^{+4} to Ce^{+3}.[4] Ceria has also been studied as an excellent material for electron exchange reactions.[5] Nanoceria presents unique catalytic behavior because of its increased surface area and oxygen vacancies.[4a] The oxygen vacancy sites are located at the surface of the nanoceria lattice. The

relatively high abundance of the vacancies is believed to be responsible for the unique electrochemical behavior.[6] Ceria and nanoceria have been employed in many catalytic systems such as catalytic converters, industrial gas exhausts, steam reforming, biological anti-oxidants, free radical scavengers, and fuel cells.[3a, 7] Ceria nanoparticles have also been used as chromogenic indicators in an enzyme assay for the detection of glucose.[8] Nanoceria is typically synthesized from the oxidation of cerium cations in aqueous solutions by adjusting the pH to a proper value for the specific ceria formation according to the Pourbaix diagram.

The nature of the interactions of ceria with glucose and other mono- and poly-saccharides has been thoroughly studied.[9] The Ce^{+4} state of cerium is observed to induce the oxidation of glucose by inducing C_1-C_2 or C_2-C_3 cleavages of the glucose into arabinose or erythrose and glyoxal.[10] More recently Asati, et. al. showed oxidase-like activity for cerium oxide nanoparticles with respect to the oxidation of dyes and *o*-phenylenediamine.[11] The oxidation mechanism is believed to include the formation of a chelate complex, followed by its disproportionation and hydrolysis on the reaction medium. The ability of ceria and Ce^{+4} to selectively hydrolyze glucose can be utilized in a metal/ceria composite electrode for the oxidation of glucose, and thus for the preparation of non-enzymatic glucose and hydrogen peroxide sensors. In the present work we study the behavior of such electrodes made with Pt and Au metals in order to address the catalytic enhancement and poison tolerance of the electrodes as well as their ability to discern between analyte and interferents such as ascorbic acid. The aim of this dissertation is to examine ceria modified electrode for possible sensing application along with a study of redox reactions in the treatment of odor causing compounds for the wastewater industry.

CHAPTER 2: ELECTROCHEMICAL OXIDATION OF NANOCERIA MODIFIED GOLD AND PLATINUM ELECTRODES TOWARDS AN ENZYMELESS GLUCOSE SENSOR

Background

Glucose Detection

Diabetes mellitus is a chronic but treatable group of metabolic diseases that affect about 200 million people worldwide.[12] This figure is projected to reach more than 300 million by 2030.[13] Hypoglycemia (low glucose levels) episodes can cause blackouts, lethargy, impaired mental functioning, irritability, and loss of consciousness while extremely low glucose levels can be life-threatening. Hyperglycemia (high glucose levels) can cause circulatory disease, stroke, amputations, blindness, kidney failure, and nerve degeneration.[14] The lack of a cure for the disease has made it imperative for the patients to frequently test their physiological glucose levels to determine if the current treatment is working effectively and also to avoid a diabetic emergency such as hypoglycemia (low blood sugar, less than 3 mM) or hyperglycemia (high blood sugar, greater than 7 mM).[15] As a result, there is a critical need for an accurate, highly sensitive, low-cost, and stable glucose sensor.

The first enzymatic glucose sensor was introduced by Updike and Hicks in 1967.[16] Since then, a great deal of research has been performed on glucose biosensors. The electrochemical glucose sensors are essentially categorized into three major groups depending on the measurement principles: potentiometric, amperometric, impedemetric or conductometric sensors.[2] Potentiometry is commonly used to measure glucose concentrations greater than 10^{-5} M, which is in the physiological range in most cases. The potential difference between the reference electrode and the working electrode is measured at zero

current flow. The ideally nonpolarizable reference electrode provides a constant potential and the working electrode presents the change in potential depending on the glucose concentration.[17] Amperometry is a reasonably sensitive electrochemical technique in which the measurement of interest is current. The current is linearly dependent on the analyte concentration by applying a constant bias potential. An amperometric biosensor consists of either two or three electrodes. The impedemetric or conductometric biosensor is the least common of the three types of glucose sensors. In this technique, an impedance spectrum is generated within a broad frequency range by the use of electrochemical impedance spectroscopy (EIS). For this study, an amperometric glucose sensor based on a nanoceria modified Au and Pt electrode will be explored.

The majority of these common glucose sensing techniques today rely on the amperometric response of an enzyme modified electrode in the presence of glucose. Most of the electrodes are modified with either glucose oxidase or glucose dehydrogenase enzyme.[18] The electrochemical reactions of glucose in the presence of these enzymes generate a current dependent on the concentration of glucose present in the sample being tested. Enzyme based glucose sensors offer high sensitivity and selectivity for the oxidation of glucose and are generally produced by immobilizing an enzyme onto a supporting electrode.[12, 15] Over the past four decades, glucose oxidase (GOx)-based glucose sensing has been of a significant interest in research and in the sensor market mostly due to the need to monitor glucose in biological and clinical areas. In general, the key reaction in the process of determining glucose concentrations and fabricating glucose biosensors is the oxidation of glucose into gluconolactone by the enzyme glucose oxidase. Glucose oxidase catalyzes the oxidation of glucose to produce gluconic acid according to the reaction shown below:

$$C_6H_{12}O_6 + O_2 + H_2O \xrightarrow{GOx} C_6H_{12}O_7 + H_2O_2 \quad \textbf{(1)}$$

Although very popular, such enzyme based glucose meters suffer from inaccuracies of up to 15% even when used optimally and much higher otherwise.[19] An inaccuracy of 15% can be extremely dangerous for patients in need of careful glucose monitoring and for hypoglycemic patients. Such inaccuracies can be due to temperature, sampling errors such as inadequate cleanliness or blood volume, concomitant interferences, high cost, and enzyme degradation. Among the main concerns with degradation are the loss of activity of the enzyme due to aging, as well as due to denaturation of the enzyme as it is affected by temperature, humidity, pH, potential/current cycles, and other possible chemical interferences.[12] The requirement of immobilizing the enzyme on the electrode's surface may also decrease the functionality of the enzyme as the modification of an electrode surface with the enzyme can induce changes on the enzyme's molecular structure affecting the enzyme's activity. Thus, the use of an enzyme on the glucose meter test strip can lead to inaccurate values due to the loss of enzyme activity.[20]

Enzymeless Glucose Detection

In order to overcome the enzyme's loss of activity and to improve the accuracy, there is a growing interest in developing glucose meters and sensors that do not require the use of enzymes. The use of different electrode materials for the electrochemical oxidation of glucose has been studied thoroughly, using pure metals such as Pt,[21] Au,[22] metal alloys,[23] and carbon structures such as diamond and nanotubes.[24] In general, it has been observed that such electrode materials can exhibit an amperometric response to glucose, but at the same time have several limitations. First, most enzymeless electrodes lack the degree of selectivity

required for their use on biological samples such as blood or plasma, where species such as ascorbic acid or uric acid may interfere. Also, the incomplete electrochemical oxidation of glucose generates several byproducts that can interact strongly or absorb into the electrode, resulting in the degradation or poisoning of the electrode material.[25]

The general principle for the use of an enzymeless electrode is that it should "mimic" the behavior of glucose oxidase, by a non-mediated, direct electrochemical oxidation of glucose. Glucose appears electrochemically active in neutral and alkaline environments, as it is oxidized when a positive potential is applied to the electrode.[26] However, these electrodes usually lack the exquisite selectivity of an enzyme and often use expensive precious metals.[25] The sensitivity of the electrode is decreased because the overall kinetics of glucose electro-oxidation are too slow. Previous mechanism studies show that the overall kinetics of glucose oxidation are too slow to produce significant faradaic current and that most of the pure metals including platinum present unsatisfactory sensitivity to glucose.[26] To overcome such kinetic limitations, the electrochemical oxidation of glucose often requires the application of high overpotential.[27] The need to apply relatively high potentials increases the probability of finding electrochemically active interfering species. For example, endogenous interfering species, such as L-ascorbic acid, uric acid, and 4-acetamidophenol can also be oxidized in the potential range of glucose oxidation, which then results in decreased selectivity.[28] Besides low sensitivity, platinum electrodes also exhibit other problems associated with poisoning by the adsorbed intermediates and poor selectivity.[29] For glucose monitoring in blood or plasma, selectivity may perhaps be the key issue for non-enzymatic and potentiometric sensors.

Over the years, only a few attempts have been reported with respect to fabricating amperometric and potentiometric glucose sensors without using enzymes.[30] Shoju and

Freund have employed polymeric membranes with boronic acid units, which have an affinity for the diol unit of saccharide. This sensor did respond to glucose but showed even higher sensitivity to fructose than glucose.[26] As for amperometric sensors, researchers have applied a myriad of different electrodes including nanoporous gold and platinum,[21b, 22, 27b] copper,[23b, 31] alloys like Pt/Pb[15, 23a] and Pt-Ir[12, 32] composites such as MnO_2/carbon nanotubes (CNTs)[24b, 25, 33] and Pt/WO_3,[26] CNTs, mesoporous or nanoporous carbon,[34] and boron doped diamond[35] among others.

However, most of these electrodes have shown limitations due to the degree of poisoning by chloride ion and adsorptive species; some are so serious that the amperometric signal is extremely small upon continued operation.[26] The electrodes show very limited selectivity with no recognition unit for glucose and therefore it is difficult to distinguish glucose from other electroactive interferences that can be present in a biological sample. Due to the relative large size of the glucose molecule in physiological conditions, interfering species cannot be excluded by the use of conventional size-selective membranes.[26] Recognizing that there is great room for improvement, novel non-enzymatic alternatives were being sought by our research group.

Experimental

Materials and Reagents

All aqueous solutions of D-glucose and Ascorbic Acid (AA) were prepared using triply distilled water with 18 MΩ·cm resistivity (Barnstead B-Pure). Dextrose (Baker Reagent, Anhydrous) and Ascorbic Acid (Mallinckrodt) were used to prepare various solutions of each in phosphate buffer solution (PBS). Aqueous D-glucose and ascorbic acid

solutions were prepared by serial dilution method (1.0 mM, 5.0 mM, 10.0 mM, and 20.0 mM) in PBS. A pH = 7.2 – 7.4 PBS buffer solution was prepared using 0.1 M monosodium phosphate monohydrate (Fisher) and 0.1 M sodium phosphate dibasic anhydrous (Fisher) and the pH was adjusted with sodium hydroxide (Acros) or with phosphoric acid (Fisher). The phosphate buffer solution was used as the supporting electrolyte.

High purity potassium hexachloroplatinate (K_2PtCl_6, Aldrich) and auric chloride ($AuCl_3$, Alfa Aesar) were used as the source of platinum and gold for electrodepostion procedures, respectively. In addition, cerium(IV) oxide nanopowder (nanoceria, Aldrich or as prepared by previously published results)[36] was also used for preparation of the composite electrode's deposition. Sulfuric acid (Fisher) was utilized as the supporting electrolyte for all deposition experiments. Copper sulfate, $CuSO_4$ (Acros), was used to make 0.10 M Cu^{2+} solutions for copper underpotential deposition procedures. All chemicals were ACS reagent grade or better and used as received unless specified otherwise.

Apparatus

A three electrode apparatus was used for all cyclic voltammetry and electrodeposition procedures without regard to liquid junction potentials. The working electrodes consisted of 2 mm diameter platinum and gold electrodes (CH Instruments, Inc) with an Ag/AgCl electrode (CH Instruments, Inc) used as the reference electrode, and a platinum wire electrode (CH Instruments, Inc) used as the counter electrode. Electrochemical experiments were performed on a CH Instruments model CHI400A (CH Instruments, Inc) potentiostat. Cyclic voltammetry experiments were run at scan rates ranging from 0.10 V/s to 0.25 V/s. The platinum and gold working electrodes were polished by circular rotation on a diamond

lapidary machine (Hi-Tech), using 1 micron diamond polishing fluid (Buehler) combined with fluid extender (Buehler). Once polished, the cleanliness of the surfaces of the platinum and gold working electrodes was assessed through analysis of the cyclic voltammogram of each electrode in 0.5 M H_2SO_4. A custom made 50.0-mL electrochemical cell was used for the electrodeposition experiments and a 20.0-mL electrochemical cell (CH Instruments) was used for all CV experiments. A schematic diagram of the experimental electrochemical cell setup utilized is shown in Figure 2. Scanning Electron Microscopy (SEM) was performed on Zeiss ULTRA-55 FEG SEM. Atomic force microscopy (AFM) was performed on Solver EC, NT-MDT with a 1-3 nm curvature radius DLC (diamond-like carbon) tip in the contact mode.

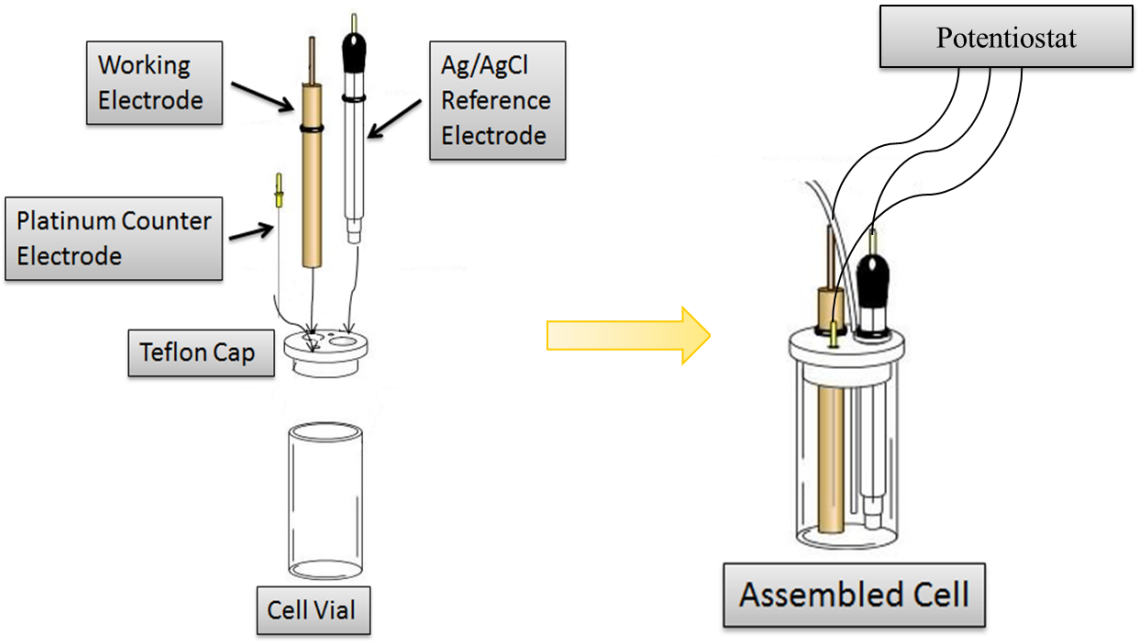

Figure 2: Schematic diagram of the three electrode electrochemical cell design used for the entire electrochemical analysis in this work.

Techniques and Procedures

Electrochemical Cell: For optimum inspection of the redox phenomena at the surface of the electrode, a minimum of two electrodes are needed, a working and reference electrode. The overall chemical reaction taking place in an electrochemical cell is made up of two independent half-reactions, which describe the real chemical changes at these two electrodes. Voltammetry experiments examine these half-cell reactions at an electrode where current is monitored against the applied potential. Each half-reaction responds to the interfacial potential difference at the consequent electrode. However, most often only one of these reactions is of interest and the electrode at which it occurs is called the working (or indicator) electrode.[37]

The additional reference electrode operates to standardize and balance the overall charge. The internationally accepted primary reference is the standard hydrogen electrode (SHE), or normal hydrogen electrode (NHE).[37] Various other types of reference electrodes are also utilized depending on the experimental requirements. As the potential measured is the potential between the working and the reference electrode, it is also imperative to report any potential with respect to the reference electrode used. The reference electrode must be capable of balancing any charge variation caused by the working electrode. Other vital requirements of the reference electrode are that it must maintain a constant composition and a constant potential whether used as an anode or a cathode and be irrespective of the current, if any, which flows through it.[38] The difficulty with the two electrode electrochemical cell system is that it is extremely challenging to maintain a constant reference potential while passing the current through the same electrode.[39] For that reason, a third electrode, referred to as counter electrode, is frequently used to overcome the problem of the reference electrode

being polarized.[40] In this three electrode system, the potential is applied between the working and the reference electrode. Keeping high impedance between the working and the reference electrode ensures that the current flows between the working and the counter electrode.

Cyclic Voltammetry: Cyclic voltammetric experiments are conducted in a stationary solution and therefore rely mostly on diffusion to transport material to the electrode surface. The potential of the working electrode is swept from a value of V_1 to V_2 and once the potential reaches V_2, a reverse sweep is performed scanning the potential back to the original value, V_1, as shown in Figure 3(a). For the shape of the voltammogram on the forward sweep, at first no significant change in current is observed since the applied potential is not great enough to induce electron transfer. However as the potential is swept to higher potentials, it reaches values that are capable of inducing a redox reaction generating an increase in current. As the potential is swept back to the original value for the reverse scan, the oxidized species on the electrode surface is then reduced in the diffusion layer and reconverted to the starting compound and the current reaches zero. The resulting current versus potential, cyclic voltammetric behavior for a reversible system is illustrated in Figure 3(b). The peak potential and the peak size on the reverse scan reflect the reversibility of the redox couple. Regardless of the reversibility, the intensity of the peak current for both forward and reverse scans depends on the potential scan rate.[39] The potential range chosen for CV experiments depends completely upon the application and the nature of the redox species of interest. The applied potential occurs at the surface of the electrode. The potential then drops rapidly as it moves away from the electrode creating a varying electric field. Thus, redox processes can only happen near the electrode where the potential is sufficient enough to carry the reaction.

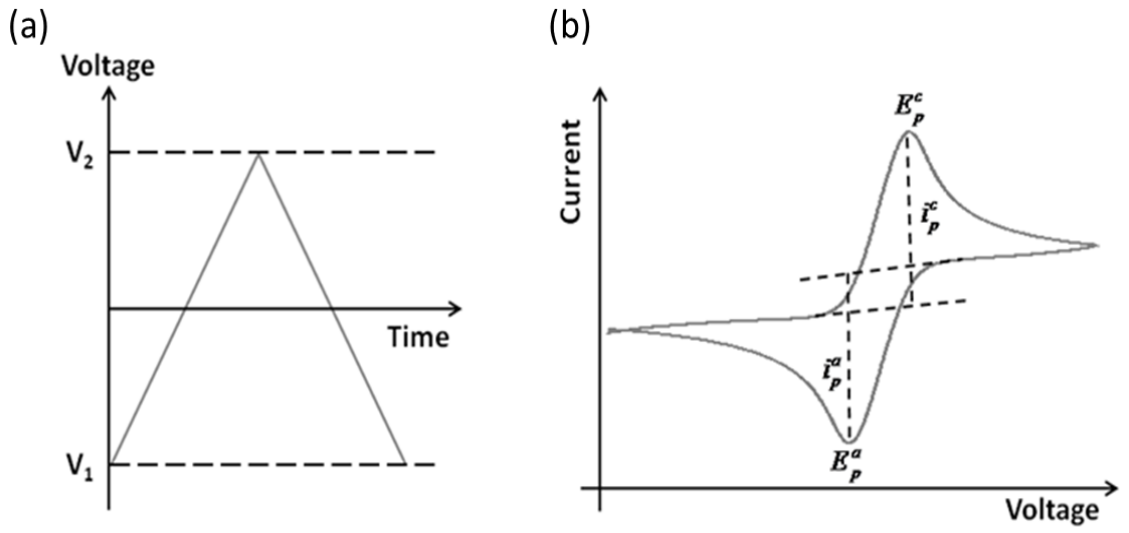

Figure 3: (a) Triangular voltage waveform applied during cyclic voltammetry (b) observed cyclic voltammogram entailing the cathodic and the anodic peak resulting from the potential scan.

Modification of Electrodes through Electrodeposition: The bimetallic-ceria composite electrodes were prepared by electrodeposition of nanoceria along with gold and platinum salts. A custom made 50-mL cell was used for all electrodeposition experiments. A 10 mM nanoceria suspension in a 1 mM K_2PtCl_6 solution was used for the Pt/ceria electrodeposition, a 1 mM $AuCl_3$ solution was used for the Au/ceria electrodeposition, and 0.5 mM K_2PtCl_6 with 0.5 mM $AuCl_3$ solution was used for the Pt/Au/ceria electrodeposition keeping a total of 1 mM concentration of the metal ions. All electrodeposition solutions were prepared in 0.5 M H_2SO_4.

The composite electrodes were prepared from polished Au and Pt electrodes whose cleanliness was verified via cyclic voltammetry. These electrodes were then placed in a three-electrode apparatus in the deposition solution of interest. The electrodeposition was carried out by holding the potential at -0.200 V for 600 seconds. This resulting current was

then plotted as a function of time. All Pt/ceria, Au/ceria, and Pt/Au/ceria composite electrodes were prepared by holding the electrode potential at -0.200 V vs. the Ag/AgCl reference electrode for a total of 600 seconds (10 minutes) while stirring the solution at rotations close to 200 rpm using a magnetic stir bar in order to keep the deposition current constant at 1 x 10^{-4} A. The cleanliness and the electrochemically active area (ECA) of all the modified electrodes were determined immediately after the deposition procedure by observing the CV of a 0.1 M PBS solution. All hydrogen peroxide solutions were bubbled with nitrogen gas for approximately five minutes to purge the solution of oxygen immediately before running.

Previous studies have shown that the electrodeposition of the metal ions in the presence of a higher concentration of nanoscale ceria particles causes the occlusion of ceria in the growing metallic film onto the surface of the electrode.[41] These ceria particles are trapped on the surface of the electrode resulting in a metal/ceria composite modified electrode.[42] When these ceria particles are "trapped" on the working electrode surface, the procedure yields Au/ceria, Pt/ceria, and Pt/Au/ceria composite electrodes. Once these composite electrodes were fabricated, their catalytic ability was then assessed for the electrooxidation of glucose and hydrogen peroxide.

Determination of Total Active Electrode Surface Area via Copper Underpotential Deposition: There exist various methods to obtain the electrochemical active area (ECA) of modified electrodes, such as adsorption/stripping of adsorbed probe species. Conventionally, the hydrogen adsorption method in acidic media is used to determine the ECA of various platinum electrodes. As platinum is reduced, the protons from the acid are adsorbed at the surface of the electrode. Similarly, during the oxidation, these hydrogen

atoms are desorbed from the electrodes surface. The number of electrons liberated during the oxidation of platinum for low potentials give the number of hydrogen atoms desorbed and thus, the number of adsorption sites present on the electrodes surface. The area occupied by the adsorbed hydrogen reflects the actual surface area of the electrode, and it is defined as the electrochemical active surface area of the electrode. However the introduction of bi- or tri-metallic catalysts can alter the activity of the Pt electrode and the hydrogen adsorption is not particularly useful to determine the surface area of metals on which it does not adsorb, such as Au. Therefore, in cases like these a different method must be utilized to determine the total surface area of the electrode. Underpotential deposition (UPD) is a technique that has been extensively used in electro-analytical chemistry for this purpose, to determine the surface area of conductive electrodes such as Au.[43] UPD is a phenomenon where the electrochemical reduction of a metal cation onto a substrate occurs at a higher (more oxidative) potential than the calculated Nernst potential. This is attributed to the strong interaction between the electrodeposited metal with the electrode substrate on which it is being deposited. In order for UPD to occur, the metal-substrate interaction must be more energetically favorable than the metal-metal interaction in the crystal lattice of that pure metal. The result of UPD is the adsorption of a single monolayer of that metal deposited at the electrodes surface as illustrated in Figure 4. Of the catalytic electrodes in electrochemical sensor research, copper has shown to be an excellent choice for UPD. Based on the Nernst equation the potential for bulk Cu deposition is -0.20 V vs. Ag/AgCl reference in 0.5 M supporting electrolyte solution. The UPD for Cu (Cu-UPD) occurred at -0.10 V vs. Ag/AgCl on the Pt and Au electrodes.

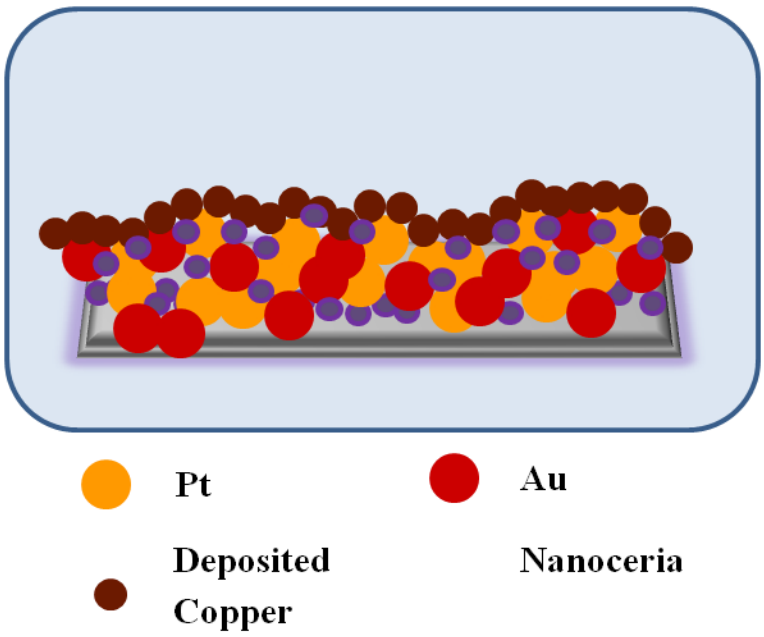

Figure 4: Illustration of copper underpotential deposition on the surface of an electrode. Presented is the confinement of nanoceria within the bi-metallic composite modification along with a monolayer of copper deposition on the surface of the electrode.

Cu-UPD was used as the surface area calculation technique during this study. Each of the composite electrodes was first submerged in a 0.001 M $CuSO_4$ solution with 0.5 H_2SO_4 as support electrolyte. Then, linear sweep voltammetry was performed by scanning in the potential region between 0.30 to -0.10 V in order to deposit a monolayer of Cu^{+2} ions. Subsequently another linear sweep voltammetry was performed in 0.5 M H_2SO_4 supporting electrolyte solution. The resulting voltammogram curves show the potential region between 0.00 to 0.60 V in the forward scan where the Cu monolayer (formed from Cu-UPD) is stripped from the surface of a composite electrode (Figure 5). As additional sweeps are completed, the Cu stripping peak goes away indicating that only a monolayer was formed on the modified electrode.

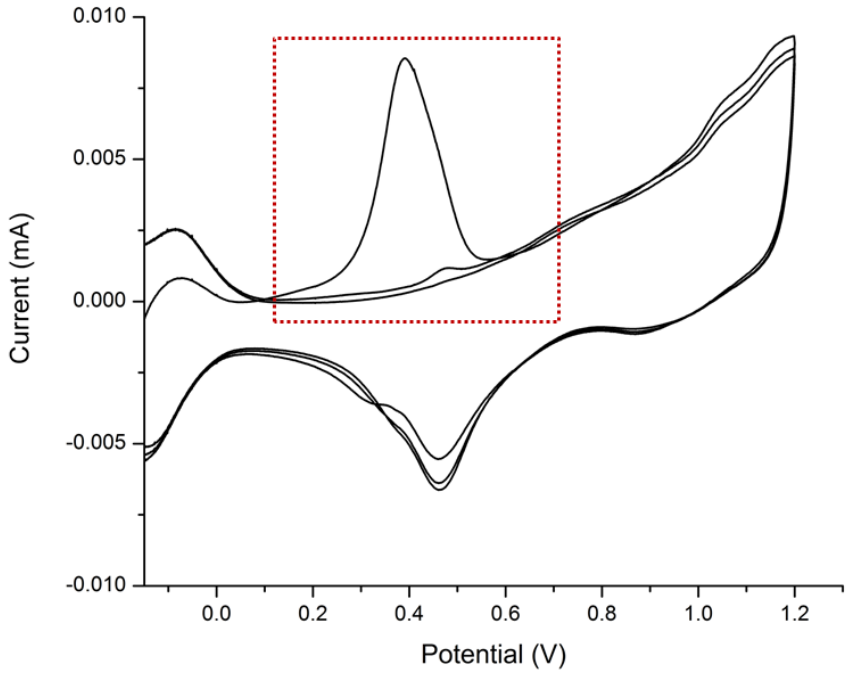

Figure 5: Cyclic voltammogram after Cu-UPD on the surface of Pt/Au modified Pt electrode. The copper stripping peak (E = 0.4 V) is illustrated in the red box displaying a diminishing trend for this peak as futher cycles are performed.

The total charge corresponding to desorption of copper can be related to the integral of the potential region where the Cu-stripping occurs as follows:

$$I = \frac{dQ}{dt} \tag{2}$$

where Q is the charge associated with the oxidation peak. In a linear sweep the potential, E, can be directly related to time, t, given the scan rate yielding:

$$Q = \int_{t_1}^{t_2} i\, dt \tag{3}$$

Upon integrating the Cu-stripping (oxidation) peak it yields the charge generated from the oxidation of Cu monolayer according to the following equation:

$$Cu_{upd} \rightarrow Cu^{2+} + 2e^{-} \quad \textbf{(4)}$$

From this two electron process, the ECA can be calculated using:

$$ECA = (Q_m) / (420\ \mu C\ cm^{-2}) \quad \textbf{(5)}$$

where Q_m corresponds to the charge obtained from the integrated Cu-stripping peak and 420 $\mu C\ cm^{-2}$ is calculated from the density of Cu, number of moles, and Avogadro's number.[43] The technique of Cu-UPD was used in this study to calculate the surface area of bare Au and Pt electrodes, Au and Pt modified with Pt/Au and Au and Pt modified with Pt/Au/ceria.

Results and Discussion

Characterization of Modified Electrodes

Thin glass Au and Pt film electrodes were modified in the same manner as the planar electrodes for characterization purposes. Thin film electrodes were used due to the sample size and shape restrictions of the instruments used for analysis. Figure 6 displays the two sets of electrodes used for surface characterization. A visual change in the color is observed for both Au and Pt electrodes as they are modified using different composite suggesting a change in the surface morphology of these electrodes upon modification. These electrodes were then characterized via scanning electron microscopy (SEM) and atomic force microscopy (AFM).

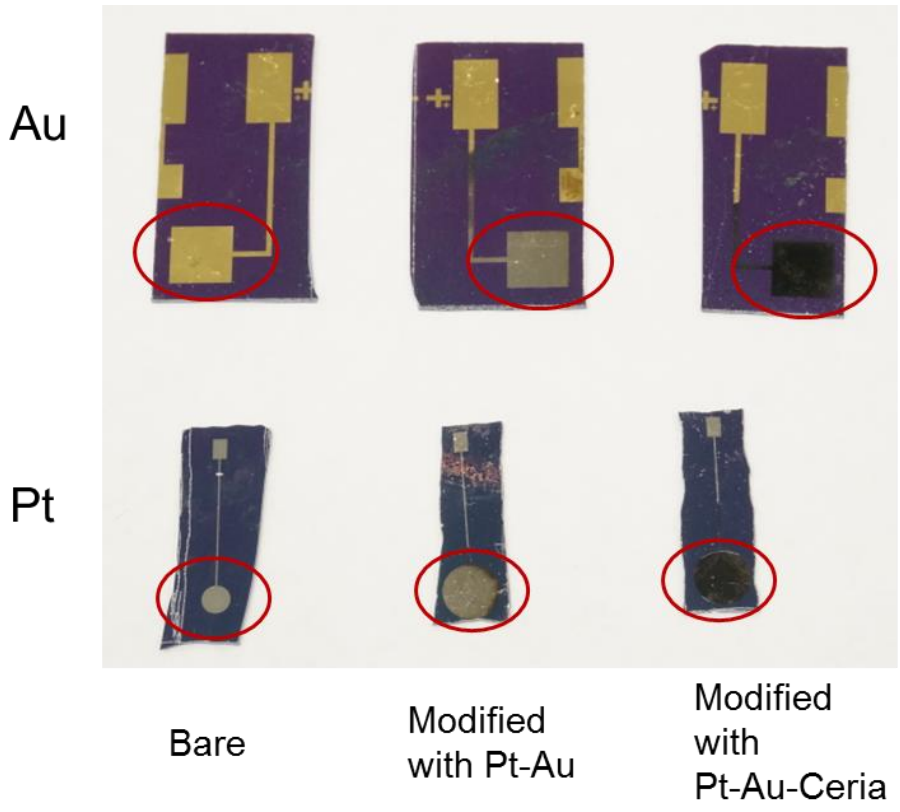

Figure 6: Thin glass Au and Pt film electrodes used for SEM and AFM analysis. The active electrode is shown in red circles. A visual change in color can be observed as the electrodes are modified with Pt-Au and then with the ceria composite showing the darkest color.

Figure 7 shows the surface morphology of the Au and Pt film electrodes as evaluated via SEM. It can be noted that not only does the roughness of the electrode's surface increases but there is also a change in the structure relating to the modification of the electrode. Dendrite like structures are observed when the Pt electrode is modified with the ceria composite which produces an increase in the surface area of the electrode. AFM analysis was also performed on all six electrodes in order to calculate the estimated roughness of theses electrodes as the surface area plays an important role on the amperometric detection of compounds.

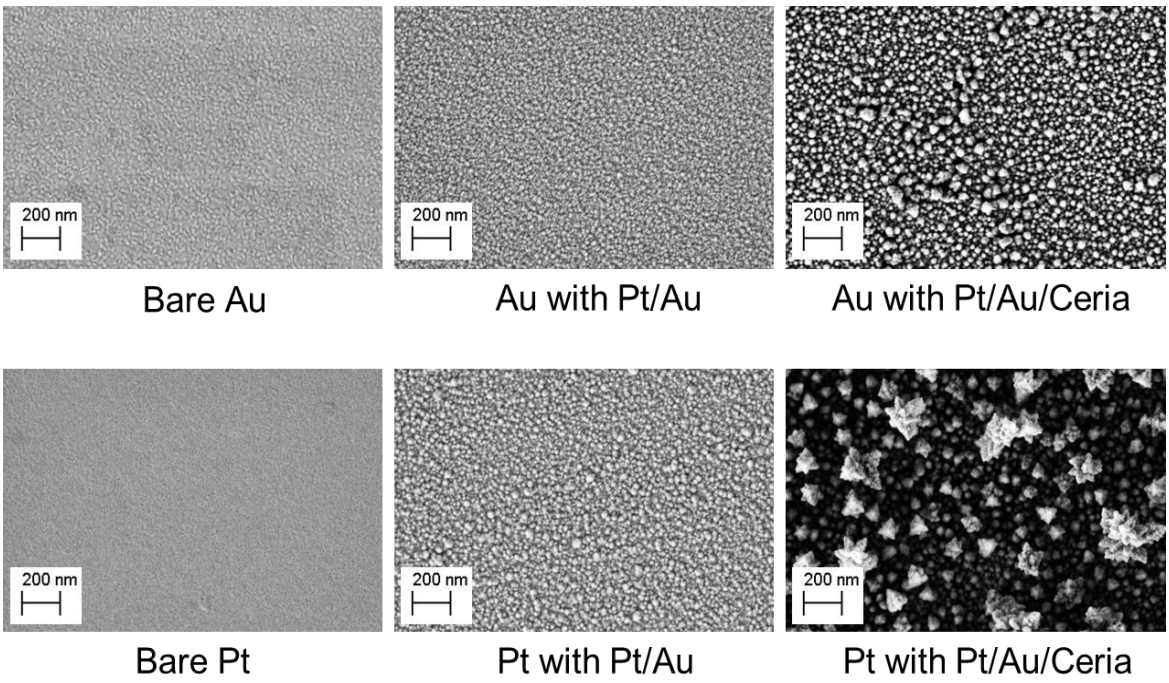

Figure 7: SEM images of the six electrodes. All images portrayed are at the same magnification and scale for comparison. A significant change in the surface morphology is observed as the electrodes are modified with the bi-metallic salt and also with the presence of ceria for both Au and Pt electrodes. When Pt electrode is modified with the ceria composite, dendrite like structures are observed causing increase in the surface area of the electrode.

The AFM results for the six electrodes are shown in Figure 8. All images are shown on a 3D plot. The AFM images of the bare Au and Pt electrodes portray a relatively smooth surface whereas the Pt/Au modified electrodes show a few crystallites and small peaks. The highest peaks and valley formation is seen in the ceria modified Au and Pt electrode. A significant change in the surface area of these electrodes can be concluded based on these results.

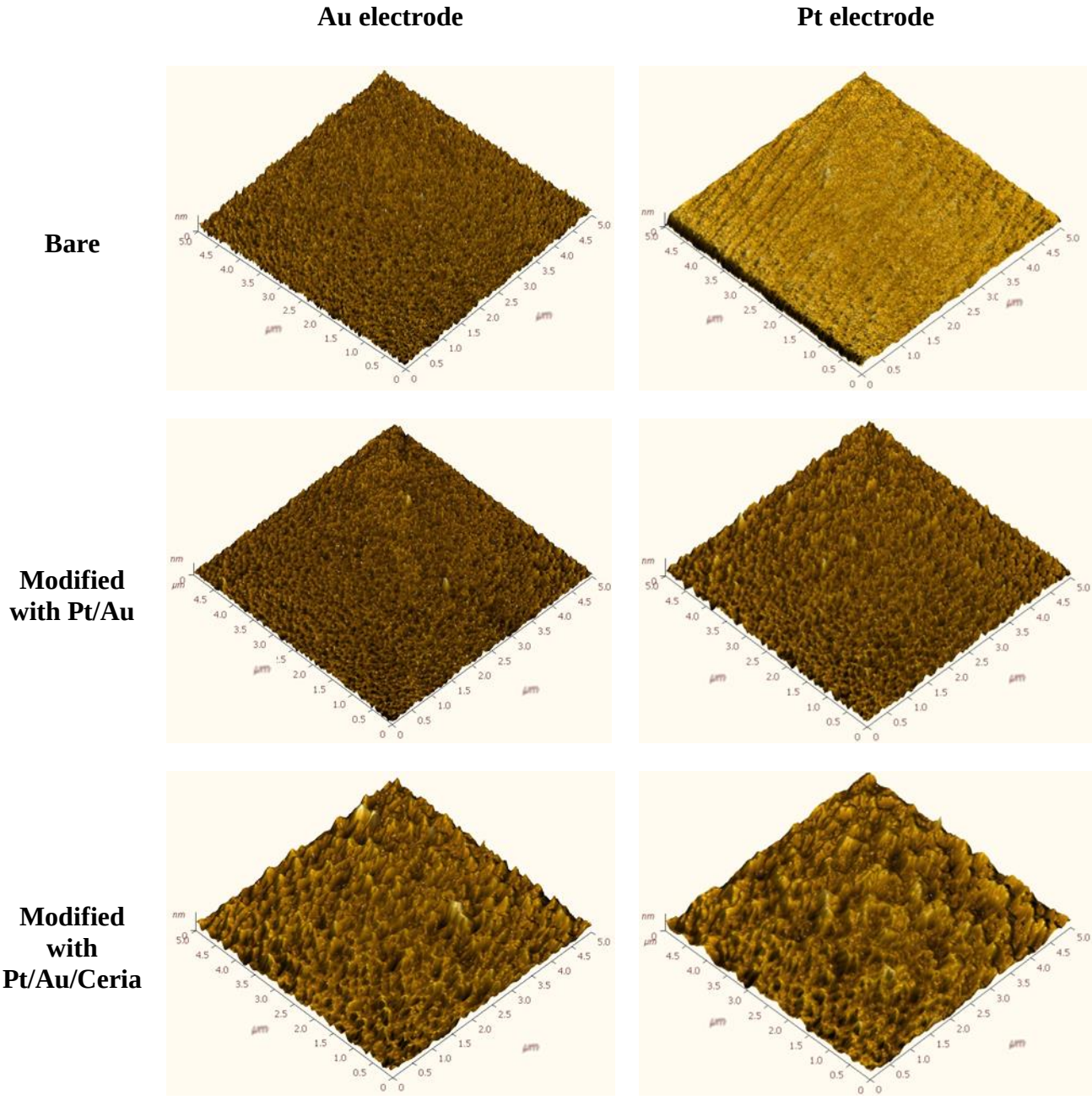

Figure 8: AFM images (3D) of Au and Pt electrodes. Visual change in the surface of the electrodes is observed when the electrodes are modified with Pt/Au. Higher peaks and valley formation can be observed on the ceria modified electrodes.

The root mean square roughness (RMS), an approximated roughness values, of the electrodes are displayed in Table 2. There is a significant increase in the roughness of the ceria composite modified electrodes compared to the bare metal electrode for both Au and Pt. The highest roughness is observed for the ceria modified Pt electrodes which can be attributed to the formation of the dendrite like structure observed in the SEM images. These results also support the previous characterization findings of these electrodes via the same electrodeposition method.

Table 2: AFM results for the six electrodes presenting the root mean square roughness values of each. A significant increase in the roughness of the ceria composite modified electrodes is observed when compared to the bare metal electrode for both Au and Pt.

Electrode	Root mean square roughness (RMS) (nm)
Bare Au	1.329
Au with Pt/Au	6.262
Au with Pt/Au/Ceria	15.421
Bare Pt	0.585
Pt with Pt/Au	6.160
Pt with Pt/Au/Ceria	30.407

Electrochemical Oxidation of Glucose on Au Electrodes

A characteristic current response from the oxidation of glucose on Au working electrode can be seen in Figure 9. Numerous peaks and curves can be observed due to complex redox process of glucose as many byproducts and intermediates are formed.

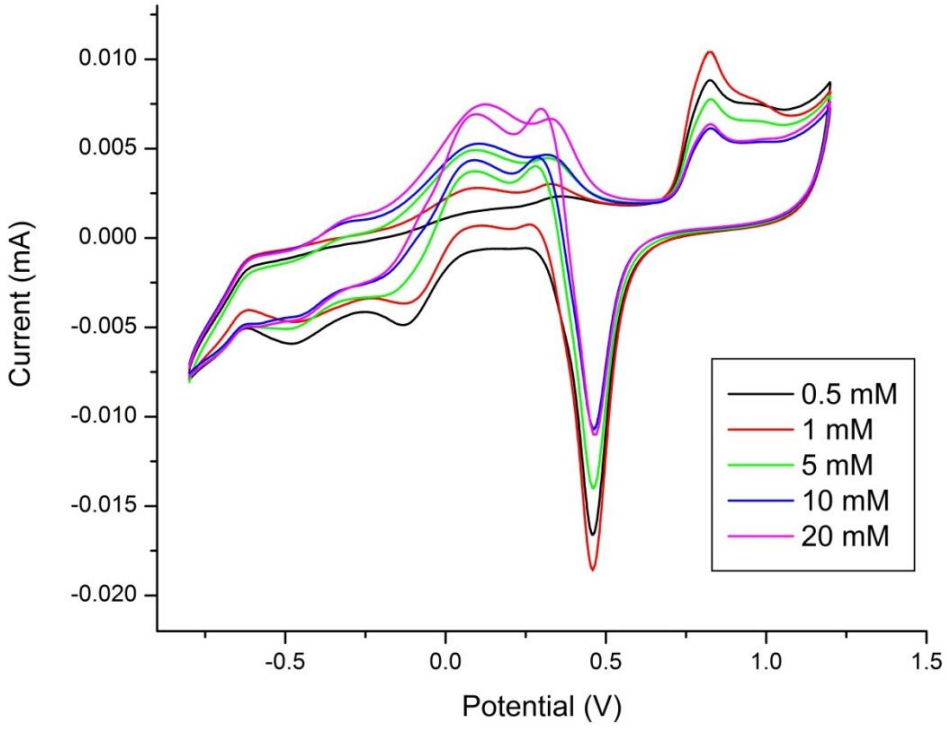

Figure 9: Superimposed cyclic voltammograms of various glucose solutions in 0.1 M PBS at the surface of a bare Au electrode vs. Ag/AgCl and at a scan rate of 100 mV/s. The electrochemical oxidation of glucose is observed at a potential of 0.27 V.

The electrochemical oxidation of glucose on a bare Au electrode in neutral phosphate buffer solution (PBS) was observed at 0.27 V and 0.05 V vs. Ag/AgCl (100 mV/s scan rate) as shown in Figure 9. Previous studies have shown ascorbic acid as a major interference for glucose detection on bare Au and Pt electrodes as it is also electroactive in the glucose oxidation potential region.[17] Thus, the interference of ascorbic acid (AA) was studied using the same parameters as for glucose CV and the oxidation of AA in PBS was found to occur at

approximately 0.20 V and 0.87 V vs. Ag/AgCl. The cyclic voltammograms of glucose solutions combined with various concentrations of ascorbic acid showed oxidation in the potential range of 0.10 V to 0.60 V. This suggests that this electrode would yield an inaccurate measurement of glucose concentration if ascorbic acid was present in the tested matrix. This overlaps partially with the oxidation region of glucose, indicating the need for modification of the electrode. Analysis of the Au electrode modified with Pt/Au (in the absence of ceria) shows a significant enhancement in the glucose oxidation current as compared to a clean Au (Figure 10). The overlay of various glucose solutions as shown in Figure 10, give three major oxidation peaks at -0.58 V, -0.28 V, and at 0.25 V.

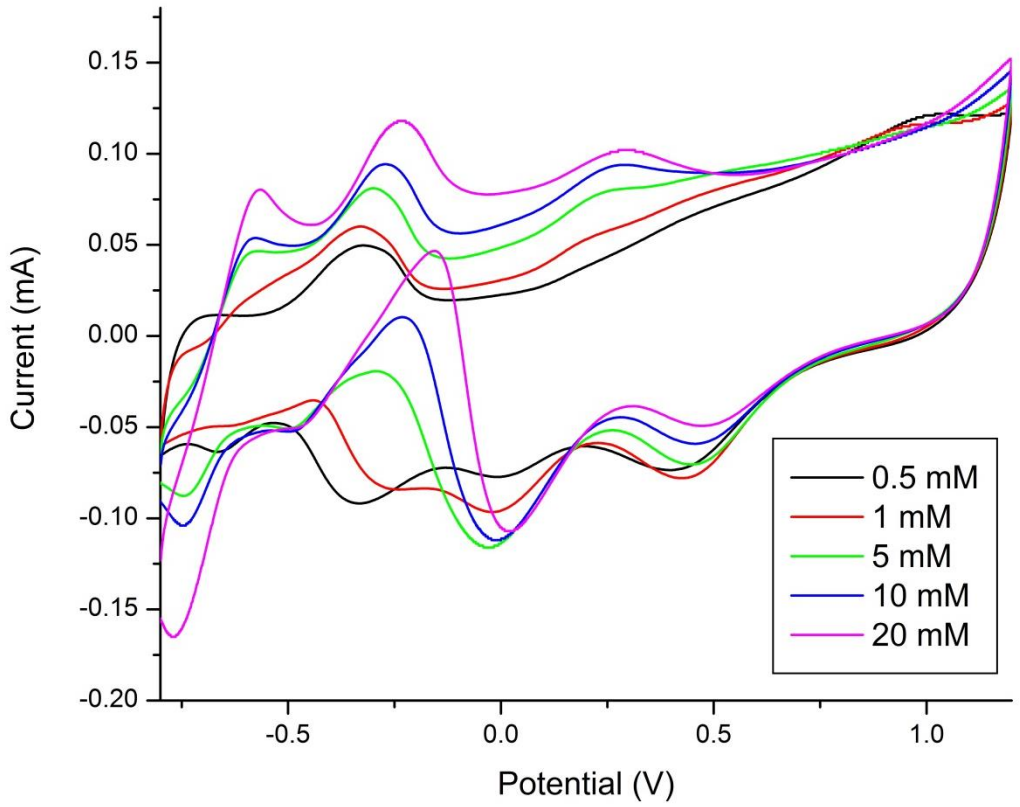

Figure 10: Compilation of the cyclic voltammograms representing the electrochemical oxidation of glucose solutions on a Au electrode modified with Pt/Au salts vs. Ag/AgCl at scan rate of 100 mV/s. An increase in the oxidation current is observed compared to the bare Au electrode.

Cyclic voltammograms of various glucose solutions using a gold electrode modified with potassium hexachloroplatinate (K_2PtCl_6), auric chloride ($AuCl_3$), and nanoceria show a shift in the oxidation of glucose into the negative potential region. Two distinct peaks were detected at -0.28 V and 0.25 V showing a significant shift from the bare Au electrode as seen in Figure 11. An order of magnitude increase in the glucose oxidation current was also observed versus the bare gold electrode (Figure 12).

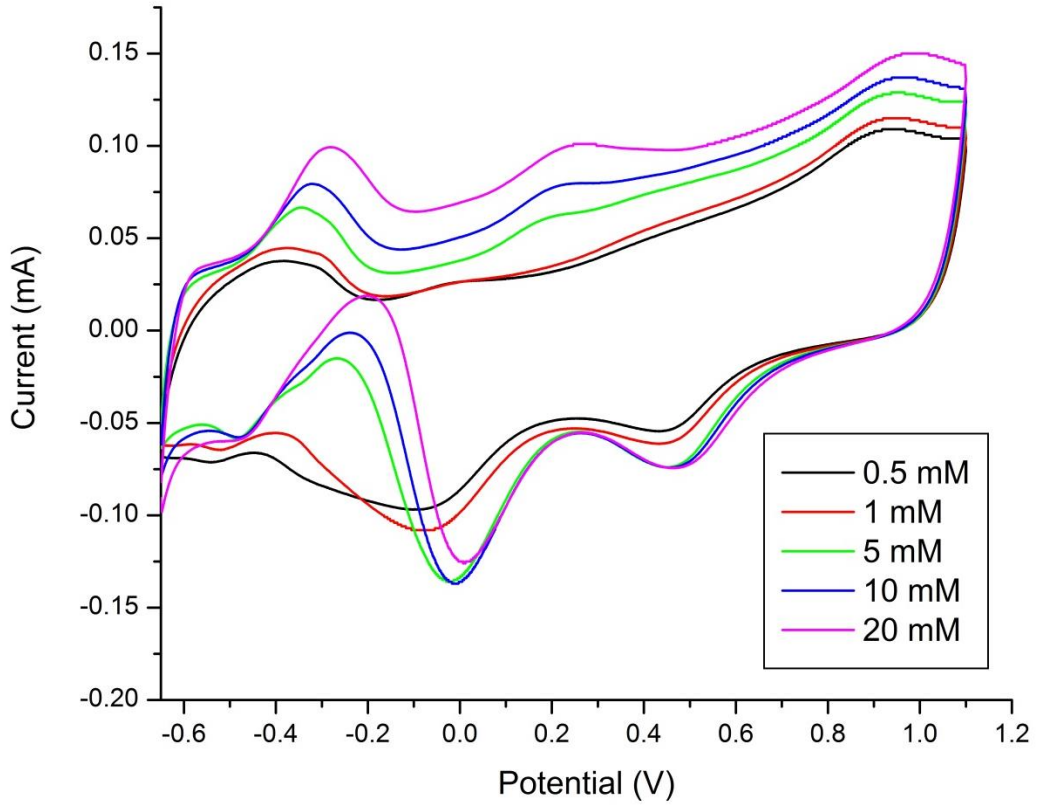

Figure 11: Compiled cyclic voltammograms of various glucose solutions on Au electrode modified with Pt/Au/ceria vs. Ag/AgCl at scan rate of 100 mV/s. The greatest oxidation current (an order of magnitude) is observed in the presence of the bi-metallic nanoceria modified electrode.

A distinct linear correlation between the glucose concentration and the oxidation current was also obtained. There was a significant increase in the current as compared to a bare Au electrode when the gold electrode was modified with a combination of Pt, Au, and nanoceria composite (Pt/Au/ceria). The voltammograms show characteristics of both Au and Pt electrodes as presumed due to the presence of Au and Pt ions onto the electrode. The glucose oxidation peak at -0.28 V demonstrates a potential for glucose oxidation free of interferences while also providing an increase in the current intensity.

Figure 12 and Figure 13 present a typical calibration plot for the amperometric detection of glucose at 0.27 V vs. Ag/AgCl. Glucose concentration versus the observed oxidation current linear plot for Au electrodes is as shown in Figure 12. Based on these oxidation current intensities, it can be presumed that incorporating nanoceria into the bi-metallic composite gives an improvement in the current intensity when compared to bare Au and Au modified with Pt/Au. For the Au electrode modified with Pt/Au, there is pronounced (an order of magnitude) increase in current intensity when compared to clean Au electrode. However, when nanoceria is incorporated into this composite, there is yet another increase observed in the oxidation current, but less prominent when compared to Au modified with Pt/Au (Figure 12).

Cu-UPD was performed in order to determine the current density of the modified and the unmodified Au electrodes. The observed oxidation currents were then corrected for the active electrochemical surface area on each of the modified and unmodified electrodes. The observed enhancement in the initial oxidation current was shown to be attributed to the increase in roughness of the electrode due to the presence of the bi-metallic/ceria composite. The plot of glucose concentration versus current density is as shown in Figure 13. It can be

perceived that the clean Au and both of the modified Au electrodes demonstrate a similar behavior relatively.

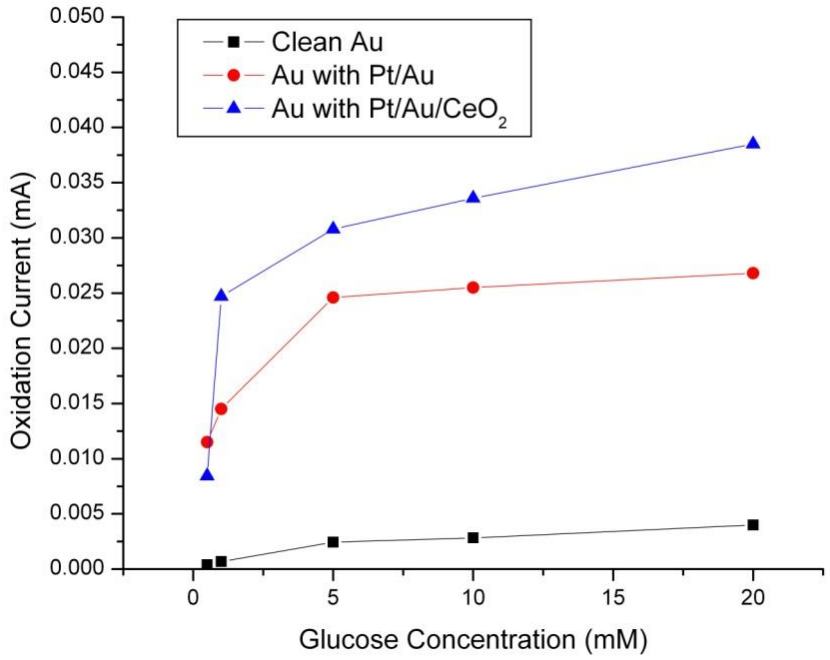

Figure 12: The electrochemical oxidation current versus glucose concentration on clean Au, Au modified with Pt/Au, and Au modified with Au/Pt/ceria electrode. A significant increase is observed when on the bi-metallic modified Au electrodes and another current increase is observed when nanoceria is incorporated into the composite.

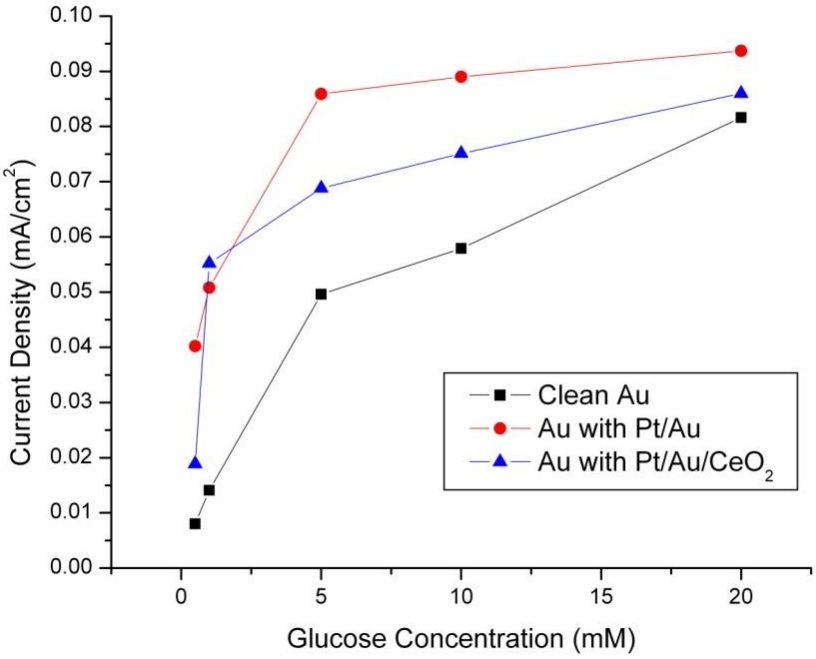

Figure 13: Normalized glucose oxidation current (current density) vs. glucose concentration for the various Au electrodes. The calculated current density suggested that the initial increase in the current was observed due to the increase in the overall surface area of the electrodes.

Electrochemical Oxidation of Glucose on Pt Electrodes

Numerous studies have been performed to overcome the limitations of an enzyme based glucose sensor for their lack of stability due to the intrinsic nature of enzymes. One of the promising approaches is the use of a Pt surface which allows for the electrochemical oxidation of glucose by amperometric measurements.[44] However, bare Pt electrodes often have low sensitivity and poor selectivity in glucose detection and occasionally are not free from poisoning by adsorbed intermediates.[45] Such disadvantages have been partly overcome by bi-metallic alloy electrodes or through the use of mesoporous or nanoporous metal film electrodes.[23a, 46] Numerous studies have been reported on significant enhanced amperometric

responses to glucose oxidation based on these porous Pt structures. The key idea is based on the fact that the roughness of the porous electrodes greatly enhances the oxidation response due to the higher surface area. For that reason, one of the goals of this study is to develop a nonenzymatic glucose sensor based on Pt electrode modified by nanoceria composite.

The electrochemical oxidation of glucose on a clean Pt electrode in neutral phosphate buffer solution (pH = 7.4) was examined over a wide range of potentials from -0.40 V to 0.80 V. The cyclic voltammograms in Figure 14 show two key potential regions at 0.22 V and at -0.37 V vs. Ag/AgCl. The oxidation of various concentrations of ascorbic acid solutions on clean Pt was investigated and was found to oxidize at 0.43 V. A direct relationship of current versus concentration was observed for both glucose and ascorbic acid on clean Pt. cyclic voltammograms of glucose solutions combined with 1 mM ascorbic acid showed that the oxidation occurs in the potential region of -0.10 V to 0.60 V vs. Ag/AgCl. Since glucose oxidation occurs at -0.45 V and ascorbic acid oxidation peak gets shifted to 0.60 V, it can be concluded that ascorbic acid is not of concern as an interferent for glucose detection on the Pt electrode.

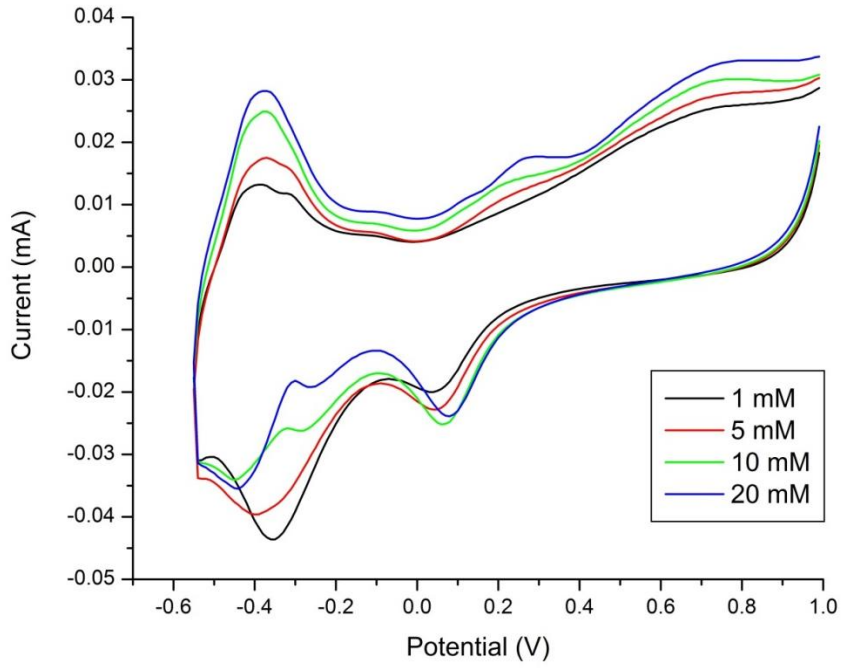

Figure 14: Cyclic voltammograms of glucose solutions on bare Pt electrode vs. Ag/AgCl at scan rate of 100 mV/s. The glucose oxidation is examined to occur at 0.22 V.

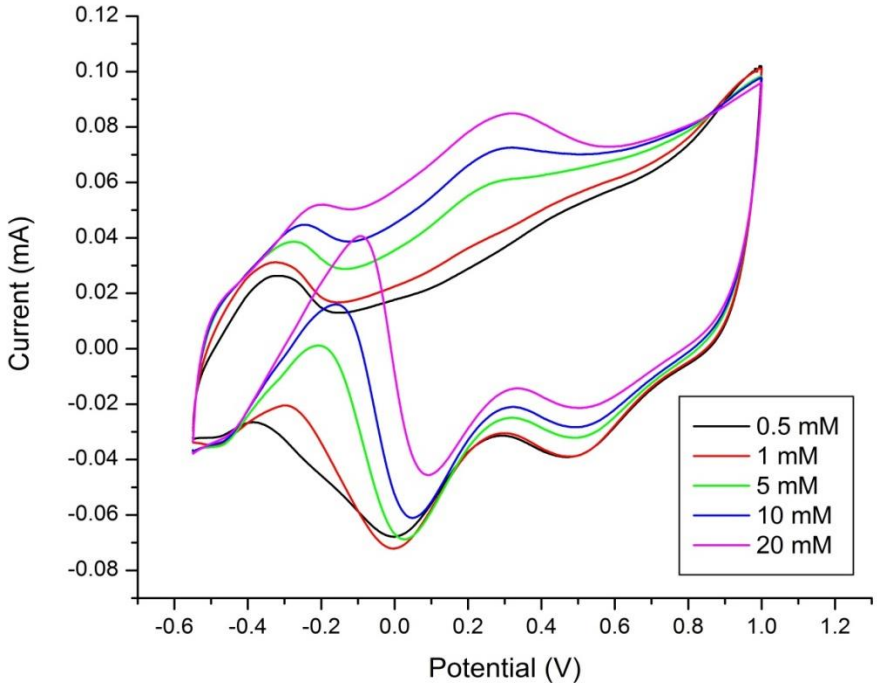

Figure 15: Cyclic voltammograms of glucose oxidation on Pt electrode modified with Pt/Au vs. Ag/AgCl and at a scan rate of 100 mV/s. A significant increase in the oxidation current is examined when compared to the bare Pt electrode.

Three potential regions can be distinguished in the cyclic voltammogram of glucose solutions on Pt electrode modified with Pt/Au (Figure 15). The oxidation of ascorbic acid does not interfere in the region of glucose oxidation as it occurs at a different potential of 0.35 V. The modified electrode shows a desirable improvement in the selectivity of glucose oxidation. Also, as expected, an increase in glucose concentrations leads to a proportional increase in the current, and the Pt electrode modified with Pt/Au/ceria composite showed the largest enhancement in the oxidation current (Figure 16). This is also demonstrated in the current vs. concentration curve as shown in Figure 17.

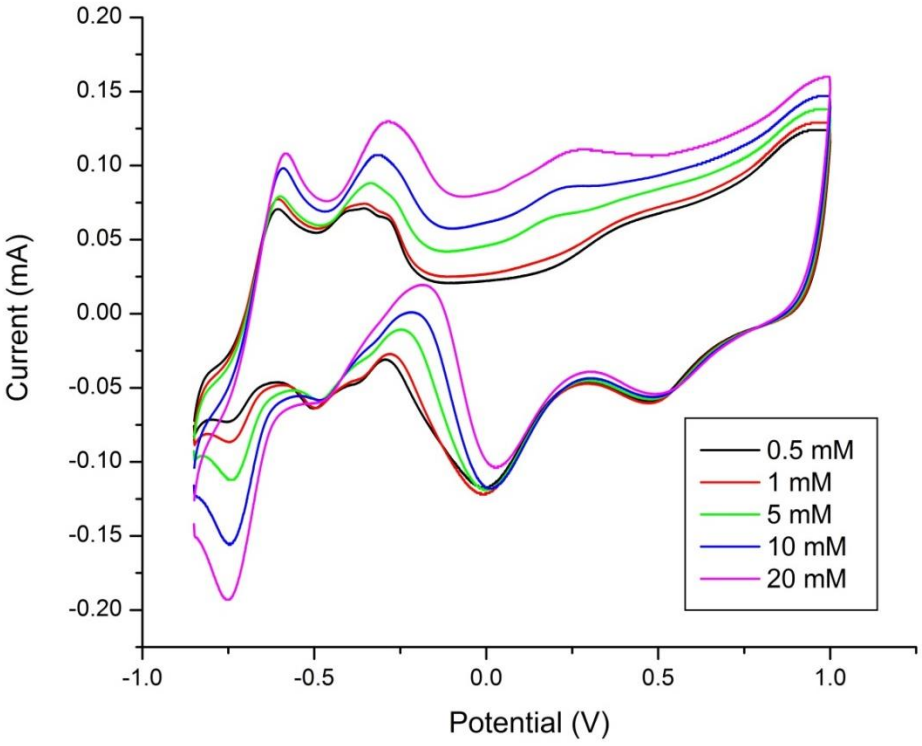

Figure 16: Cyclic voltammograms of glucose oxidation on Pt electrode modified with Pt/Au/ceria vs. Ag/AgCl atscan rate of 100 mV/s. The glucose oxidation peaks not only increase in current but are also well defined and the various concentrations can be differentiated better due to the peak separations leading to a higher sensitivity of the sensor.

The typical calibration curve for the amperometric detection of glucose on Pt electrodes is shown in Figure 17 and Figure 18. Glucose concentration versus the observed oxidation current linear plot for Pt electrodes is as shown in Figure 17. Based on these oxidation current intensities, it can be presumed that incorporating nanoceria into the bi-metallic composite gives an improvement in the current intensity when compared to bare Pt and Pt modified with Pt/Au. For the Pt electrode modified with Pt/Au/ceria, there is pronounced (an order of magnitude) increase in current intensity when compared to clean Pt or Pt with Pt/Au electrode suggesting catalytic effects of nanoceria.

Once again, Cu-UPD was performed in order to determine the current density of the modified and the unmodified Pt electrodes. The observed oxidation currents were then normalized for the active electrochemical surface area on each of the modified and unmodified Pt electrodes. As in the case of Au electrodes, the observed enhancement in the initial oxidation current was shown to be attributed to the increase in roughness of the electrode due to the presence of the bi-metallic/ceria composite. The plot of glucose concentration versus current density is as shown in Figure 18. Although bare Pt yields the optimum results, upon comparing the Pt with Pt/Au and Pt with Pt/Au/ceria, it can be concluded that nanoceria does in fact enhance the sensitivity and the selectivity of the sensor.

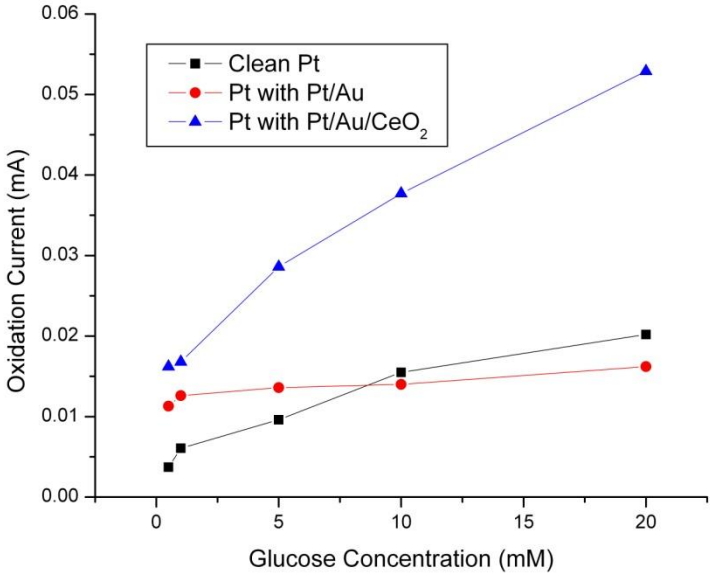

Figure 17: Glucose oxidation current vs. concentration on the various Pt electrodes. There is insignificant change in the observed current for the clean Pt and the Pt electrode modified with Pt/Au salts. However, a significant current increase occurs when nanoceria is incorporated into the bi-metallic composite.

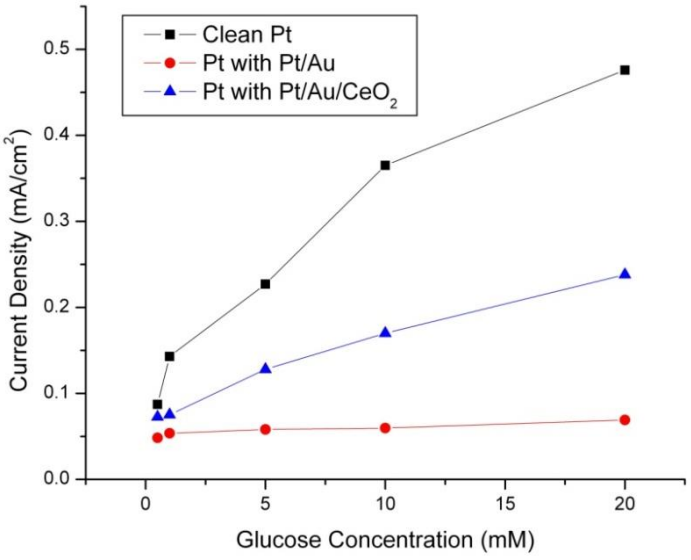

Figure 18: Current density vs. glucose concentration for the three Pt electrodes. Upon normalization of the initial oxidation currents, an enhancement in the current per surface area is examined when the electrode is modified with nanoceria however; this enhancement is not as significant as that observed for the bare Pt electrode.

pH Study on Ceria Modified Pt Electrode

The Pt electrode alone modified with Pt/ceria composite was used for the pH study, as it gave the optimal results from the prior cyclic voltammetry experiments. $HClO_4$ was used as the electrolyte to produce a 0.1 M solution with a pH of 0.23. Under these acidic conditions, the highest glucose oxidation takes place at approximately 0.50 V and with the addition of ascorbic acid as shown in Figure 19(a); the glucose oxidation overlaps with ascorbic acid oxidation causing interference. Also, the oxidative peaks in the cyclic voltammograms are rather small compared with those appearing under neutral or basic conditions. Previous studies have indicated that glucose is not very reactive in acidic media on a bare Pt electrode whereas similar behavior is observed with the nanoceria modified Pt electrode.[47] Figure 19(b) shows that similar interference is observed at a pH of 5.97 and as expected within the same region. Nonetheless, under basic conditions at a pH of 13.23, the glucose oxidation occurs at a potential of -0.20V and at 0.10 V as seen in Figure 19(c). When ascorbic acid is present in the glucose solution, the glucose oxidation peak at -0.20 V is separated by approximately 0.70 V from the ascorbic acid interfering current as observed in Figure 19(d). A significant increase in the glucose oxidation current is also observed under the basic conditions at the nanoceria modified Pt electrode.

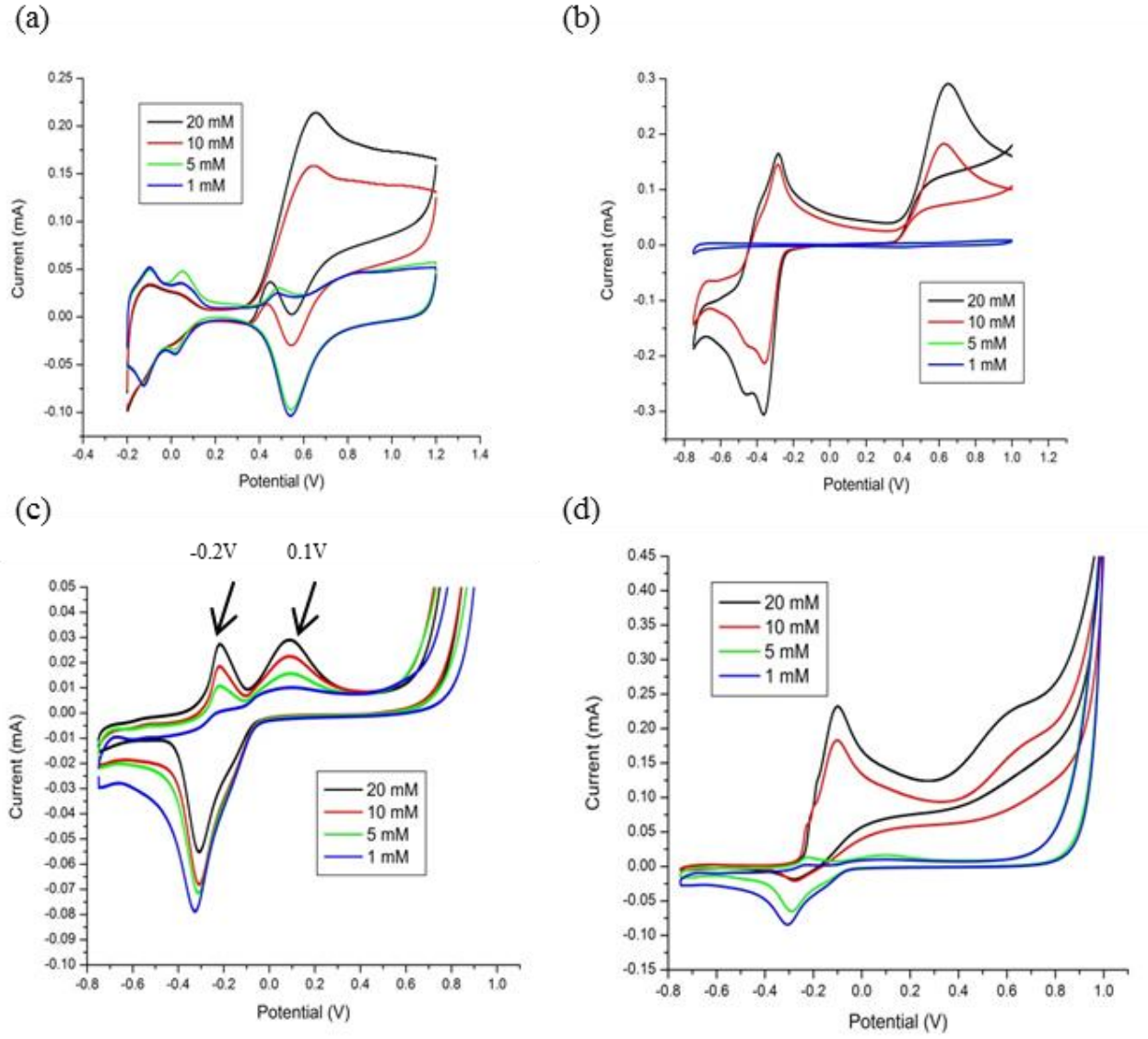

Figure 19: Cyclic voltammogram on nanoceria midified Pt electrode of (a) glucose with ascorbic acid at pH of 0.23 (b) glucose with ascorbic acid at pH of 5.97 (c) just glucose at pH of 13.23 (d) glucose with ascorbic acid at pH of 13.23. The least interference of ascorbic acid is observed at neutral or basic pH levels.

Conclusions

To mimic the physiological conditions required by most practical glucose sensor applications, all of the electrodes were studied in 0.1 M phosphate buffer solution. Cyclic voltammograms for the electrochemical oxidation of glucose on Pt and Au electrodes were compared to the voltammograms for the Pt/Au and Pt/Au/ceria electrode. Overall, an increase in the glucose concentration leads to a relative increase in the current. The platinum electrode was more effective in providing higher sensitivity and selectivity than gold. However, the highest current intensity was achieved when the Pt electrode was modified with Pt/Au/ceria, indicating certain catalytic activity due to the presence of nanoceria. Both Au and Pt electrodes modified with ceria composite were examined at various pH levels. The results of this study indicated a possible use of the ceria composite modified electrodes under relatively neutral or basic conditions.

Since avoiding the interfering species is one of the biggest challenges in non-enzymatic glucose detection, the interference of ascorbic acid was also studied under these conditions. As the results show, the peak potential for glucose oxidation and ascorbic acid oxidation are remote to each other, indicating that sensing glucose on an electrode modified with Pt/Au/ceria would successfully avoid the interfering current signal contributed by ascorbic acid. The interference of ascorbic acid was also studied at various pH levels on the ceria modified Pt electrode and it can be concluded that the best detection of glucose oxidation is observed under basic conditions which has the potential for applications in non-physiological environments.

CHAPTER 3: NON-ENZYMATIC HYDROGEN PEROXIDE SENSOR BASED ON NANOCERIA MODIFIED GOLD AND PLATINUM ELECTRODES AND ITS KINETIC STUDY

Background

ROS Overview

Reactive oxygen species (ROS) are highly reactive forms of oxygen and are usually radical in nature.[48] As a result, these species are highly capable of oxidizing other atoms and molecules. The primary reactive oxygen species are the superoxide (O_2^-), hydrogen peroxide (H_2O_2) and the hydroxyl radical ($^{\cdot}OH$).[10, 49] Such species are inevitable byproducts of aerobic metabolism. These radicals are biologically produced in cells by electron transfer reactions, and serve as signaling and messenger molecules.[49] Oxidative stress caused by ROS may be one of the greatest biological problems as it derives from the least-specific type of reaction, univalent electron transfer.[50] Oxygen species are relatively small molecules that can easily bind to enzymes active site. If they contact redox cofactors of a lower potential then electron transfer can take place. Reactions of this type are responsible for the formation of ROS and for their inactivation of enzymes. Oxygen toxicity is largely facilitated by partially reduced oxygen species that are more reactive than molecular oxygen itself. Figure 20 elucidates the redox states of various ROS with standard reduction potentials.[50]

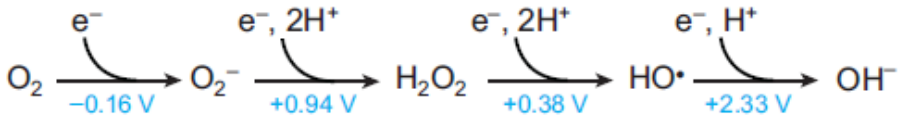

Figure 20: Redox states of oxygen with standard reduction potentials of the various ROS species[50]

Several natural sources of oxidative stress for bacteria have been identified which include intracelluar enzyme autooxidation, environmental redox reactions, H_2O_2 released by competing microbes, phagosomal NADPH oxidase, and redox-cycling antibiotics.[50] The natural vulnerability of organisms to ROS is utilized by plants and microbes that try to dominate the growth of their competitors. Hydrogen peroxide, unlike O_2^-, is an uncharged species that infiltrates membranes. Therefore, H_2O_2 stress arises inside cells whenever it is present in their extracellular environment.

Hydrogen peroxide also plays an important role in many chemical, biological, pharmaceutical, clinical, environmental, and food processes.[51] Hydrogen peroxide and other reactive oxygen species are also linked to the defense mechanisms of plants, oxidative damage to the human brain in Parkinson's disease and other stress related signals in eukaryotic organisms.[52] Known mechanisms by which H_2O_2 and O_2^- injure cells are portrayed in Figure 21. Of these pathways, the detailed mechanisms of the inactivation of transketolase and of sulfur metabolism remain unclear.

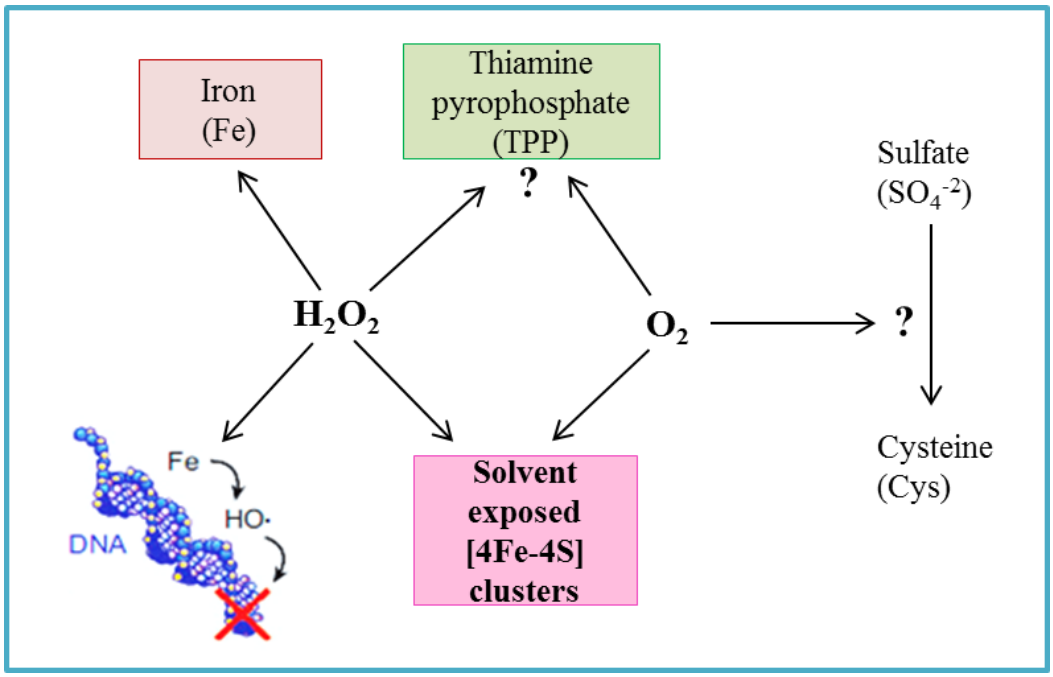

Figure 21: Recognized reactions by which H_2O_2 and O_2^- injure cells include Fenton-mediated damage to proteins *(rectangles)* and DNA, the oxidation of solvent-exposed [4Fe-4S] clusters, apparent inhibition of transketolase, and disruption of the sulfur assimilatory pathway.[50]

Furthermore, H_2O_2 is the by-product of many enzymatic reactions and its detection represents the basis of numerous enzyme biosensors.[53] Both O_2^- and H_2O_2 are known to have mutagenic properties.[54] Due to its role as a harbinger of oxidative damage, early, in-vivo detection of hydrogen peroxide and other reactive oxygen species is essential. In order to have in-vivo aqueous hydrogen peroxide detection, the electrode must be non-toxic and non-enzymatic to ensure electrode stability while still maintaining sensitivity to physiologically relevant peroxide levels and demonstrating a linear relationship between current and hydrogen peroxide concentration within the range of interest.

H_2O_2 Detection

Current H_2O_2 detection techniques include: electrochemical oxidation/reduction, electron spin resonance (electron paramagnetic resonance) spectroscopy, optical detection through reaction with suitable dyes or molecules, and biochemical assays monitoring reactions upstream or downstream of ROS.[55] Among these methods, electrochemical detection methods offer reliable stability, sensitivity, label-free detections, and operate in real time. Electrochemical methods based on direct reduction or oxidation of H_2O_2 represent an effective and inexpensive methods for its detection. However, the use of bare electrodes exhibits slow electrode kinetics, low sensitivity, and high overpotentials and therefore it is not suitable for analytical applications.[53] To overcome these limitations, different strategies and materials have been used to modify the surface of the working electrode. Polymers such as polypyrrole, polyvinylpyridine, polysiloxane, and polyethylene oxide are commonly used due to them being permselective to small neutral molecules such as H_2O_2, while polyoxomtalate or metal-hexacyanoferrate compounds are used to reduce the overpotential of the redox reaction.[56] Many enzyme immobilized electrodes are also utilized but they have many limitations such as low stability and sensitivity in micro-molar range, high cost, restricted specificity, and short shelf life.[57] Consequently, an enzymeless detection is often preferred. Recently, many metallic and inorganic nanoparticles such as silver, platinum, gold rhodium, indium-tin oxide, iridium and nanocomposites have been exploited as electrode materials for this application.[58] Current literature studies have shown that Co_3O_4, MnO_2, Fe_2O_3, and TiO_2 metal oxides have excellent catalytic properties making them suitable for an enzymeless sensor.[59] Ceria has been significantly popular as well due to its catalytic and free radical scavenging properties, yielding a potential for multiple applications in biology,

medicine, and catalysis.[60] Typical biosensor designs employed for the quantification of ROS are illustrated in Figure 22.[55]

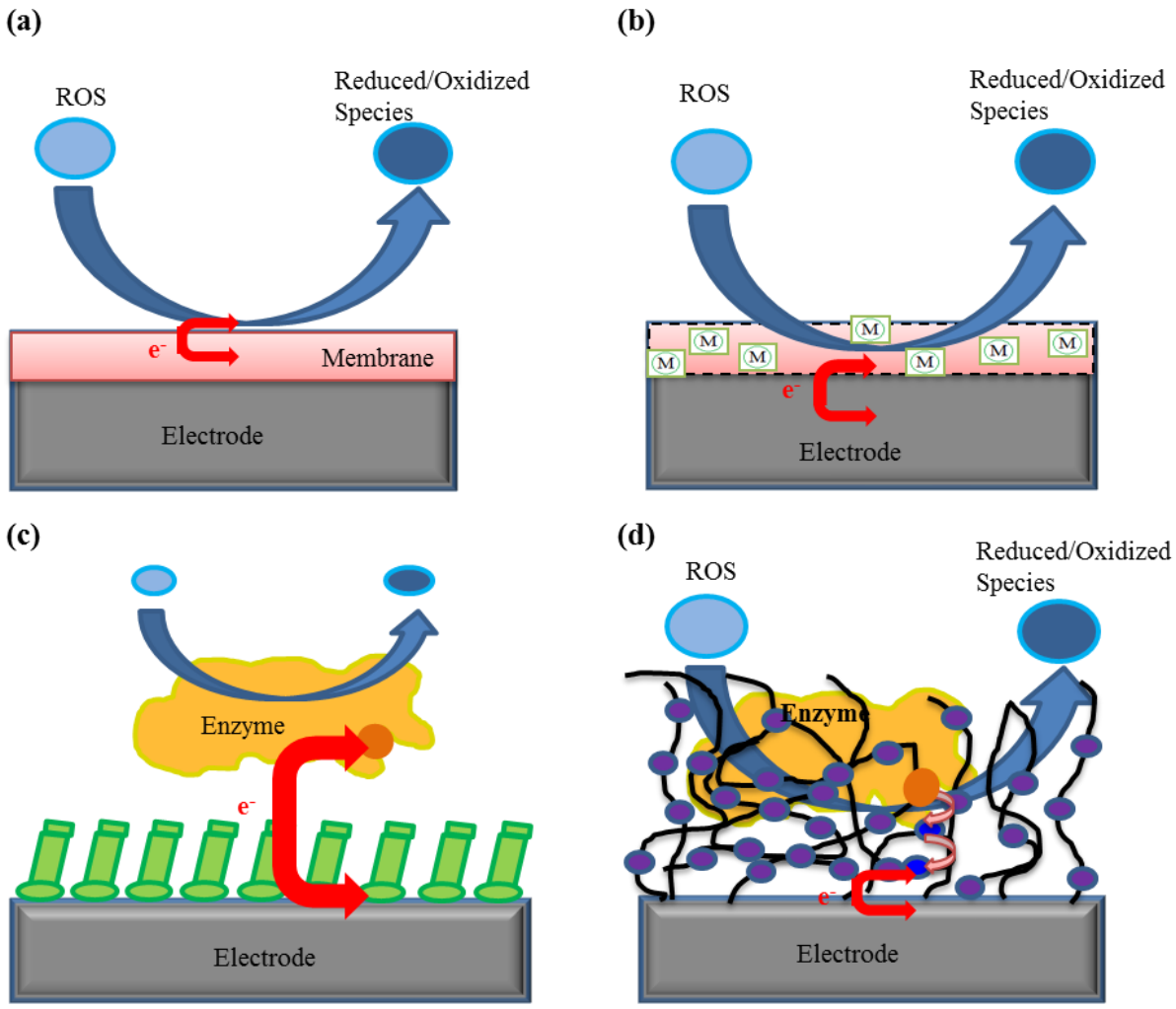

Figure 22: Common biosensor designs employed for the quantification of ROS. (a) Direct oxidation or reduction at the electrode surface, which is covered with an additional membrane. (b) A modified electrode surface with metal (M) complexes which facilitate the electrocatalytic oxidation or reduction of the analyte. (c) Direct electron transfer of the active site of a selective enzyme for ROS towards the electrode; the protein is immobilized on a self-assembled monolayer. (d) Mediated electron transfer from the biological recognition element for ROS via a redox hydrogel modified with redox relays.[55]

In order to eliminate the need for enzyme and mediator, the approach to integrate regenerative ceria nanoparticles as a sensor transduction mediator was undertaken. During this study the electrocatalytic effect of ceria toward H_2O_2 was explored for potential use in the development of an enzymeless hydrogen peroxide sensor for biological applications. By depositing gold and platinum salts onto the electrode's surface, the electrode surface area is effectively increased, allowing for a potential increase in the active sites for redox reactions to take place. Ceria is used as a catalyst due to the ease with which it can switch between its III and IV oxidation states, depending upon the environment. This ability enables ceria to be a potent free radical scavenger, and has been shown to impart protection from reactive oxygen species. The surface area of nanoceria particles is dramatically increased for greater oxygen exchange and redox reactions when compared to cerium oxide.[61]

In this work, Au and Pt electrodes modified with various nanoceria composites were used to measure the electron transfer kinetics and the oxidation potential of the hydrogen peroxide redox process. The electrodes were modified with salts of gold and platinum as well as ceria (cerium oxide) nanoparticles via electrodeposition. A thorough electrochemical study to characterize both mass transport and kinetic components was executed via cyclic voltammetry and rotating disk electrochemisty (RDE). Additionally, the selectivity, sensitivity, long-term stability, and the electrode-fouling processes of the sensor will be addressed.

Experimental

Materials and Reagents

All aqueous solutions were prepared with triply distilled water with 18 MΩ·cm resistivity (Barnstead B-Pure). New solutions were prepared before each run. A 0.1 M phosphate buffer solution (PBS) was prepared using 0.0226 M ACS reagent grade sodium phosphate monohydrate (Ricca) and 0.0774 M ACS reagent grade sodium phosphate monohydrate (Ricca). A 30% hydrogen peroxide aqueous stock solution (Fisher Scientific) was used to prepare 30 mM, 20 mM, 10 mM, 5 mM, 1 mM, 0.5 mM and 0.25 mM hydrogen peroxide solutions in phosphate buffer solution (PBS). The sulfuric acid used in all solutions was supplied by Fisher Scientific. High-purity nitrogen gas (N_2) was obtained from Air Liquide and was bubbled through all solutions to remove dissolved oxygen. High purity, 40% Pt, potassium hexachloroplatinate (K_2PtCl_6, Aldrich), auric chrloride, 64.4 % Au, ($AuCl_3$, Alfa Aesar), and cerium (IV) oxide (Aldrich or as prepared by previously published results)[9b] were used for preparation of the composite electrodes deposition. Sulfuric acid (Fisher) was used as the supporting electrolyte for the deposition. All chemicals were ACS reagent grade or better and used as received unless specified otherwise.

Methods and Apparatus

A three electrode apparatus was used for all cyclic voltammetry and electrodeposition procedures without regard to liquid junction potentials. The working electrodes consisted of 2 mm diameter platinum and gold electrodes (CH Instruments, Inc) with an Ag/AgCl electrode (CH Instruments, Inc) used as the reference electrode, and a platinum wire electrode (CH Instruments, Inc) used as the counter electrode. Cyclic voltammetry and

chronoamperometry experiments were run using CH Instruments (Austin, TX) potentiostats. Rotating disk electrode (RDE) experiments were performed using a PINE (Pine Instruments Co., Grove City, PA) analytical rotator. Cyclic voltammetry experiments were run at scan rates ranging from 0.05 V/s to 0.25 V/s. The platinum and gold working electrodes were polished by circular rotation on a diamond lapidary machine (Hi-Tech), using 1 micron diamond polishing fluid (Buehler) combined with fluid extender (Buehler). Once polished, the cleanliness of the surfaces of the platinum and gold work electrodes was assessed through analysis of the cyclic voltammogram of each electrode in 0.5 M H_2SO_4. A custom made 50.0- mL electrochemical cell was used for the electrodeposition experiments and a 20.0-mL electrochemical cell (CH Instruments) was used for all CV experiments..

Procedures

Cyclic voltammetry experiments were performed starting with a negative scan polarity for six sweep segments, a high and initial potential of 1.20 V relative to Ag/AgCl reference, and a low potential of -0.6 V. All CV experiments were performed at scan rates of 200, 100, and 50 mV/s. RDE experiments were performed using a low and initial potential of 0.0 V, and a high potential of 0.70 V. The RDE electrodes consisted of polycrystalline 5 mm diameter gold or platinum and were polished using 0.3 micron alumina powder obtained from CH Instruments, Inc and a microcloth obtained from Buehler. The cleanliness of the RDE electrodes was assessed in similar behavior as the 2 mm planar electrodes. Rotating speed was varied from 0 to 4,000 revolutions per minute (rpm). A schematic diagram of an RDE experimental setup is illustrated in Figure 23.

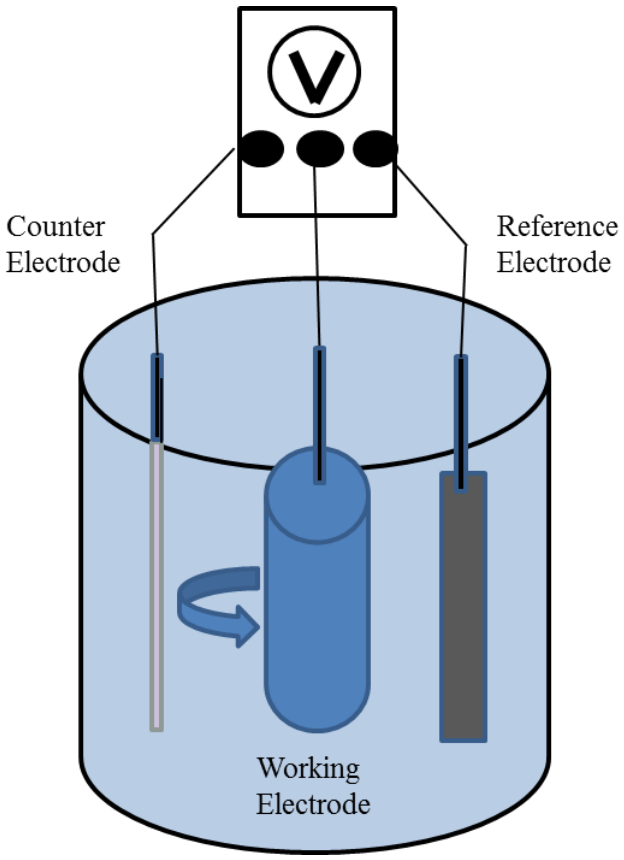

Figure 23: Schematic diagram of the electrochemical cell design for RDE experiments. The working is rotated at a chosen speed to eliminate any mass transport issue in order to investigate the kinetic parameters of the redox reaction taking place.

Results and Discussion

Electrochemical Studies of H_2O_2 on Ceria Modified Au Electrode

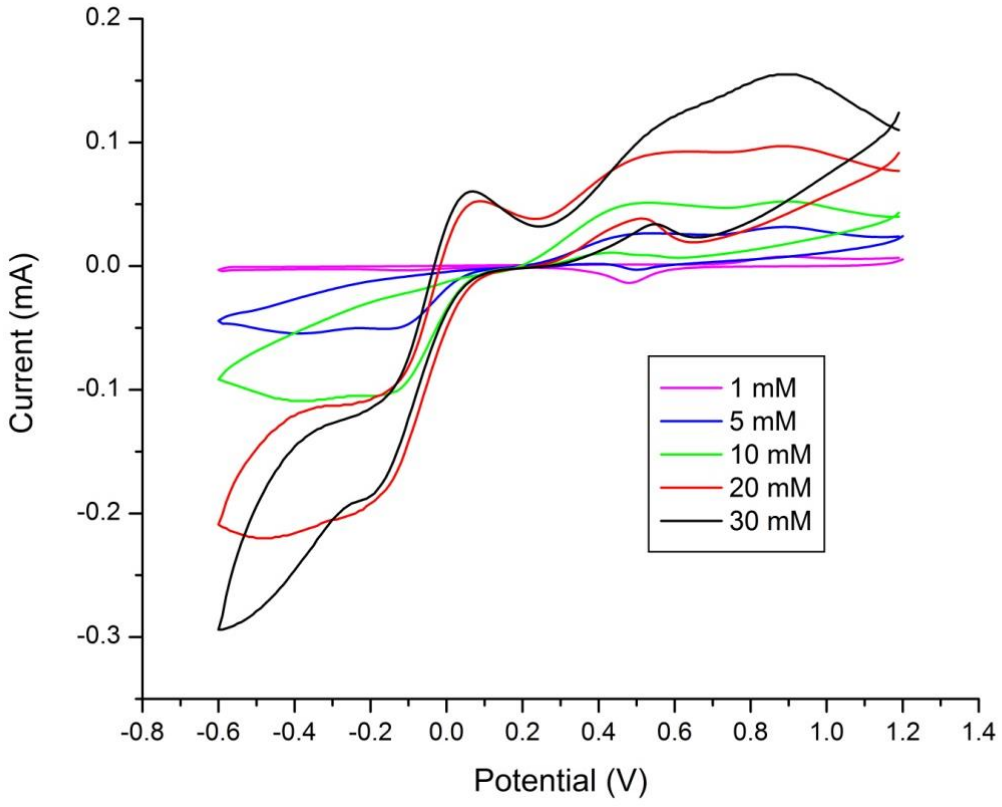

Figure 24: An overlay of cyclic voltammograms of various H_2O_2 solutions on bare Au electrode vs. Ag/AgCl and at scan rate of 100 mV/s. The electrochemical oxidation is analyzed at 0.20 V.

In order to evaluate the catalytic role of ceria, CV experiments were first performed on bare Au electrode. Figure 24 shows that the oxidation of H_2O_2 occurs at approximately 0.20 V and in the range of 0.50 to 1.20 V while a reduction wave is also observed within the applied potential range (-0.60 to 1.20 V vs Ag/AgCl) ranging from 0.10 to -0.60 V. A variety of experiments with different concentrations of H_2O_2 with both ceria-modifed and

unmodified electrodes were performed to further evaluate the potential of ceria as an electrode material for H_2O_2 detection.

As ceria is known to have weak capability to bind to Au and Pt electrodes, a composite of platinum and gold salts were used to electrochemically capture ceria onto the electrode. Figure 25 shows an overlay of various H_2O_2 solutions cyclic voltammograms on Pt/Au modified Au electrode. There is a slight increase in current due to the increase in the surface area. However, the greatest enhancement in the current intensity is observed in the presence of ceria as shown in Figure 26. Figure 27 shows the linear plots of the current vs. H_2O_2 concentration of clean Au, Au modified with Pt/Au, and Au modified with Pt/Au/Ceria. Figure 28 shows the linear plots of current density vs. H_2O_2 concentration. An increase in current with relative increase in H_2O_2 concentration is observed for all electrodes. The electrochemical results demonstrate the catalytic effect of nanoceria towards H_2O_2 detection.

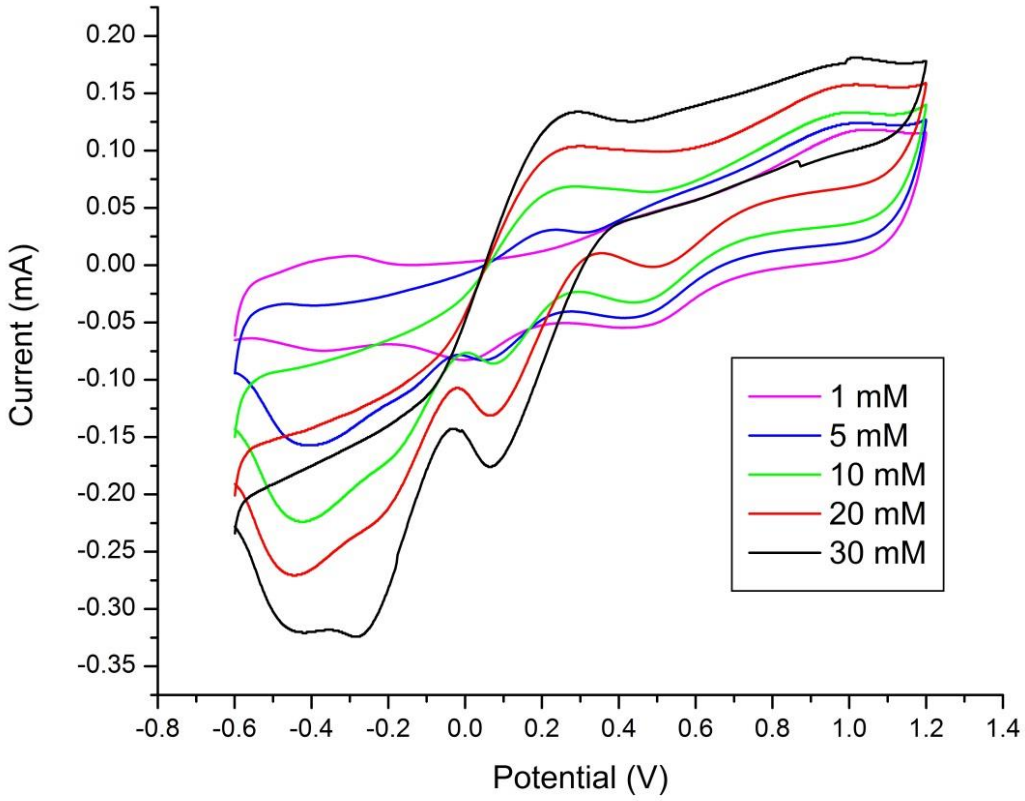

Figure 25: Superimposed cyclic voltammogram curves for the various H_2O_2 on Au electrode modified with Pt/Au vs. Ag/AgCl and at scan rate of 100 mV/s. The electrochemical oxidation current is higher compared to bare Pt electrode along with better peak separations.

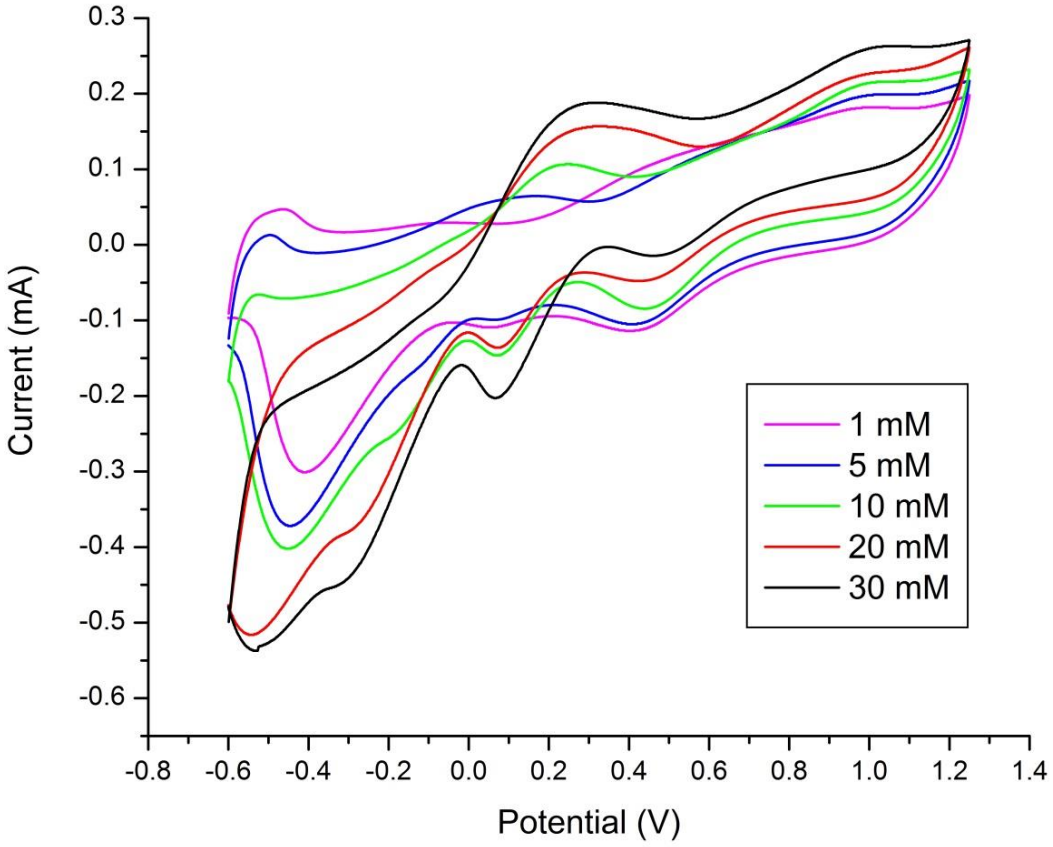

Figure 26: Cyclic volatmmograms of the electrochemical oxidation of various H_2O_2 on Au electrode modified with Pt/Au/ceria vs. Ag/AgCl and at scan rate of 100 mV/s. The highest currents are obtained for this modification of the electrode yielding an order of magnitude increase.

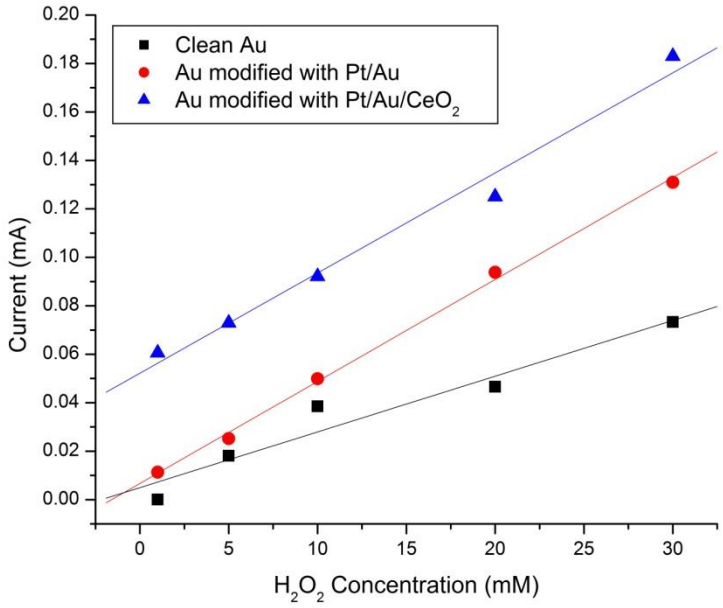

Figure 27: Oxidation current (E = 0.2 V) vs. concentration linear plot showing the catalytic enhancement in the oxidation current for the detection of H_2O_2 vs. Ag/AgCl for the three modifications of the Au electrode. The highest increase in current is examined for the Au electrode modified with the nanoceria composite.

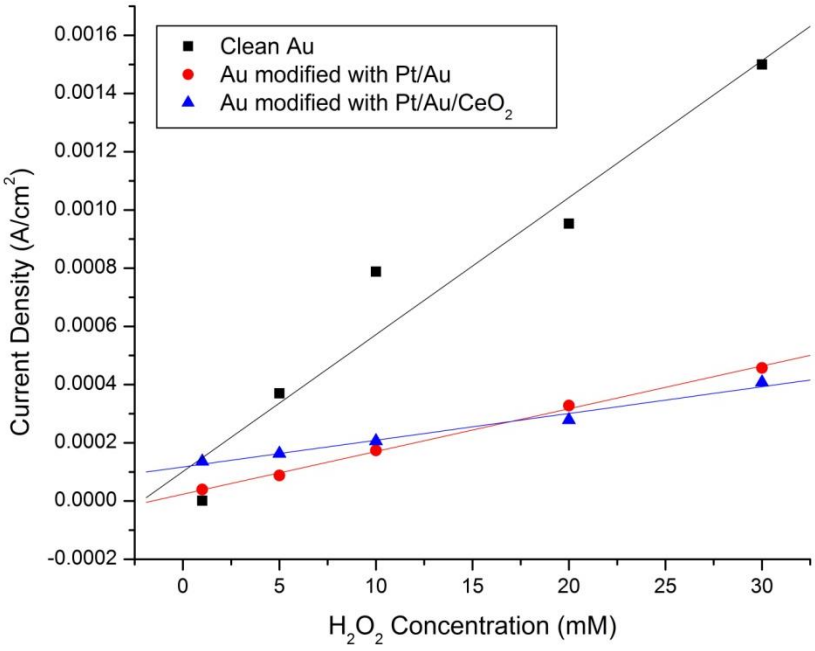

Figure 28: Current density vs. H_2O_2 concentration on the Au electrodes vs. Ag/AgCl. Modification of the Au electrodes does not show optimum results for H_2O_2 detection. The initial current increase was observed due to the increase in the active surface area of the electrode.

Electrochemical Studies of H_2O_2 on Ceria Modified Pt Electrode

Cyclic voltammetry experiments were performed on several Pt electrodes with similar modification as those of Au electrode. Figure 29 shows an overlay of voltammograms for various H_2O_2 solutions with a bare Pt electrode where the electrochemical oxidation of H_2O_2 is observed at about 0.20 V and a reduction wave in the region of 0.00 V and -0.20 V vs. Ag/AgCl. When the Pt electrode is modified with just the binary salts, Pt^{+4} and Au^{+3}, there is significant reduction in the current intensity when compared to bare Pt as shown in Figure 30. However, the current increases when ceria is incorporated onto the electrode in contrast to both the bare Pt and Pt modified with Pt/Au as observed in Figure 31.

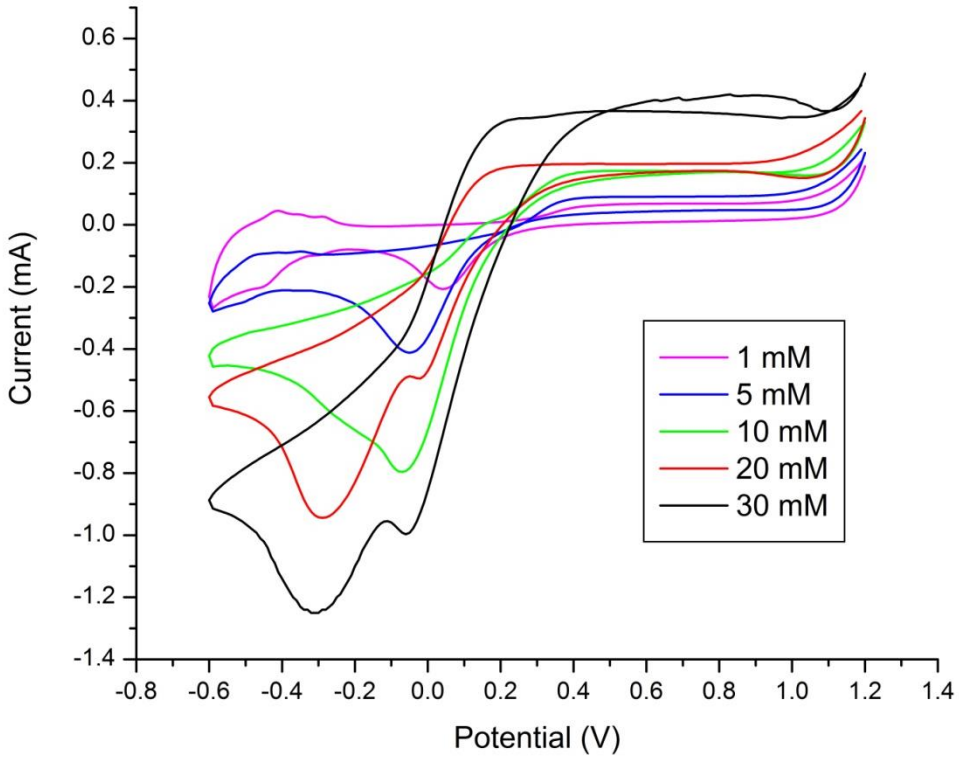

Figure 29: Cyclic voltammogram emphasizing the electrochemical oxidation of behavior of H_2O_2 on bare Pt electrode vs. Ag/AgCl and at scan rate of 100 mV/s. The oxidation peaks are ambiguous whereas the reduction peaks are much more apparent.

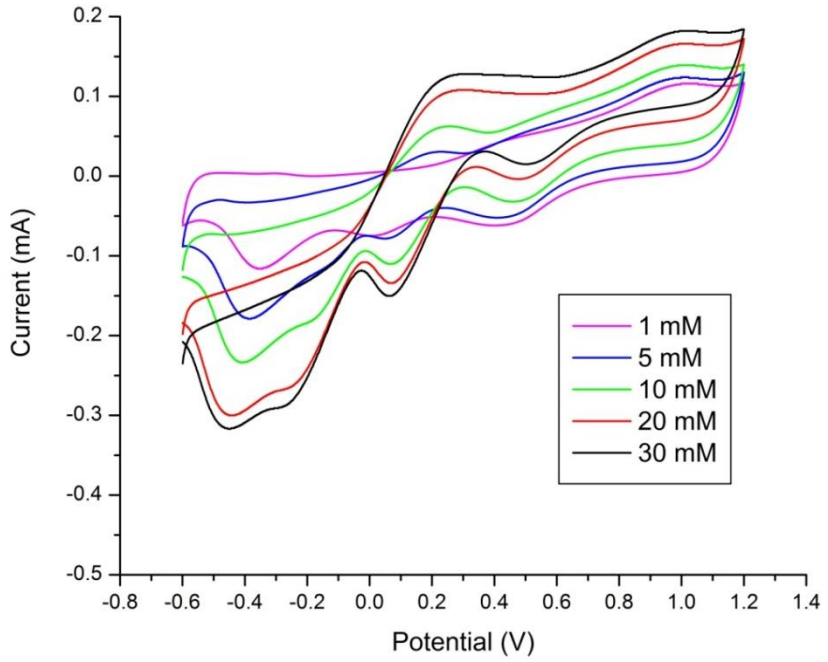

Figure 30: Cyclic voltammogram overlay of various H_2O_2 on Pt electrode modified with Pt/Au at scan rate of 100 mV/s vs. Ag/AgCl. The H_2O_2 oxidation peaks are well defined and an apparent trend in the current increase with concentration can be observed.

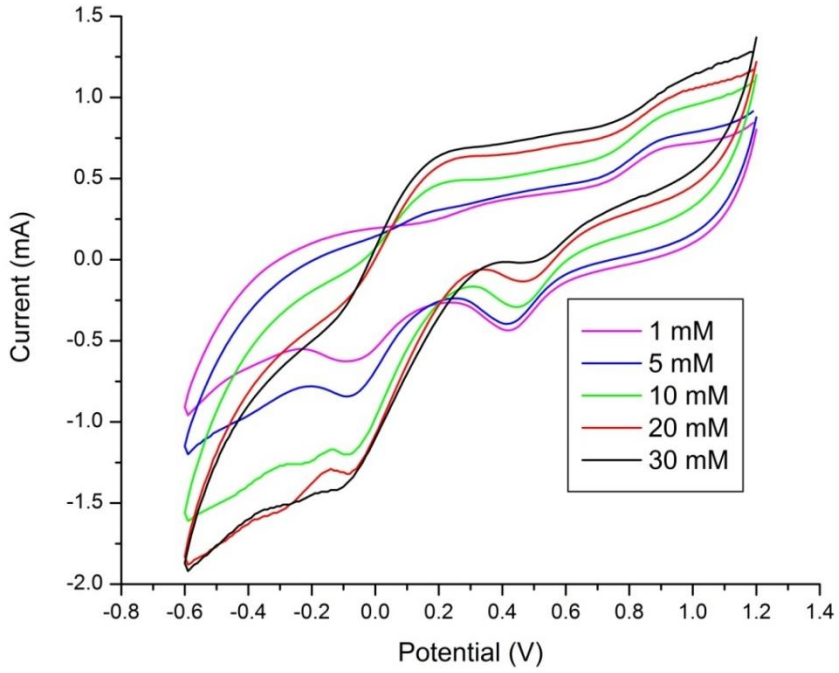

Figure 31: Cyclic voltammogram overlay of various H_2O_2 solutions on Pt electrode modified with Pt/Au/ceria at scan rate of 100 mV/s vs. Ag/AgCl. Modification of the electrode with the bi-metallic nanoceria complex gave the highest oxidation current suggesting the catalytic effect of nanoceria towards H_2O_2 detection.

Figure 32 shows the current vs. concentration plot of these Pt electrodes where the highest current is obtained in the presence of ceria. Also, the amplitude of the current is proportional with the H_2O_2 concentration. For unknown reason, incorporating Au onto the surface of Pt electrode seems to inhibit the oxidation of H_2O_2. Nonetheless, these electrochemical studies initially implied that ceria has both catalytic oxidation and reduction ability towards the detection of H_2O_2. The Pt/Au/ceria modified Pt electrode showed the highest current when compared to other Pt electrodes and all of the studied Au electrodes. Upon normalization of these electrodes, it was found that the presence of ceria does yield a higher current per unit area when compared to Pt with Pt/Au. Nevertheless, the bare Pt electrode yielded the optimum current per surface area as illustrated in Figure 33.

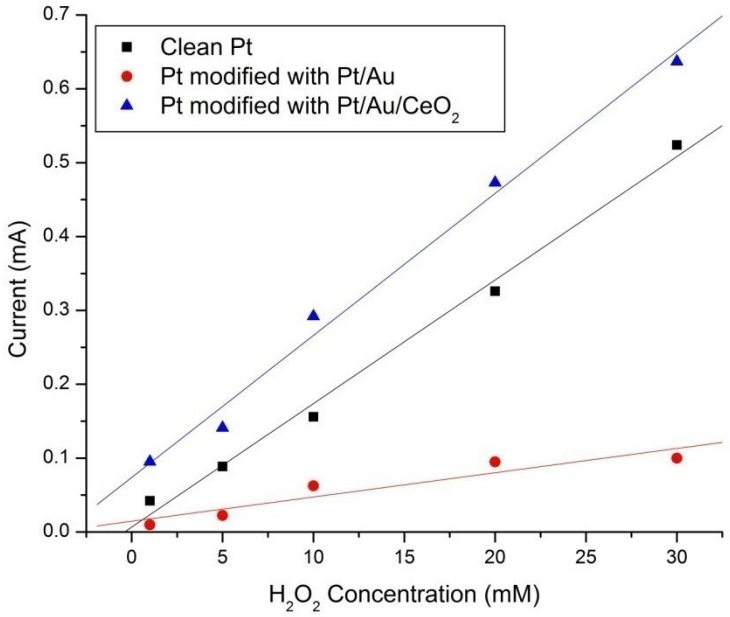

Figure 32: Oxidation current (E = 0.4 V) vs. H_2O_2 concentration linear plot showing the catalytic enhancement in the oxidation current for the detection of H_2O_2 on Pt electrode modified with nanoceria composite.

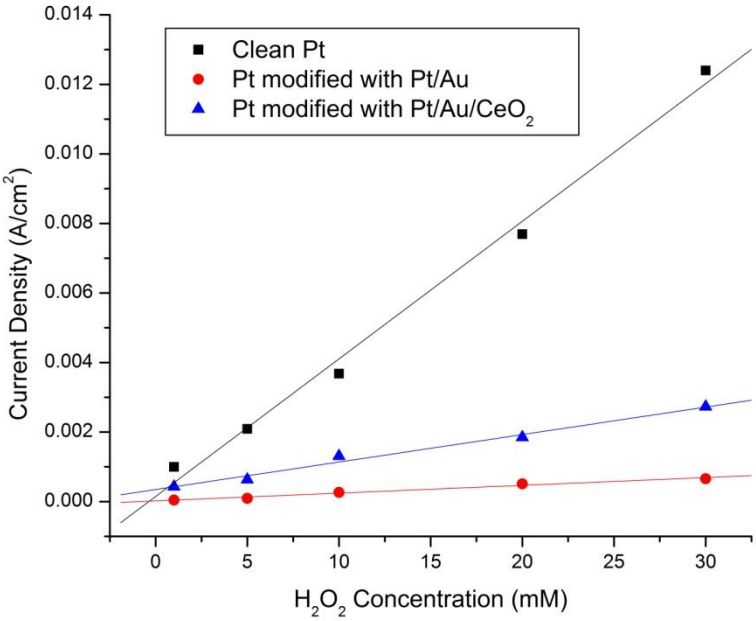

Figure 33: Current density vs. H_2O_2 concentration for the three Pt electrodes vs. Ag/AgCl. An increase in the current per surface area is observed upon incorporation of nanoceria, but is not significant when compared to a bare Pt electrode suggesting a need for an electron transfer mediator.

Koutecky-Levich Study of Electron Transfer Kinetics

Previous investigations have shown that the kinetics of the electrochemical oxidation of H_2O_2 in phosphate buffer solution (pH = 7.4) can be studied via rotating disk electrochemistry by treating the electrode reaction as a process involving both kinetic and mass transfer components.[62] In this case, the electrode is rotated and mass transport to the electrode is generated. This allows us to eliminate mass transport limitations and to measure the electron transfer kinetics. Advantages of utilizing RDE are that the rate of mass transport of reactants to the RDE surface is controlled precisely by fixing the rotational velocity of the electrode and the electrode currents quickly achieve steady-state values.[63]

In this study, the oxidation of H_2O_2 on solid gold and platinum rotating disk electrodes over a range of concentrations and rotation rates was investigated so that the extent of diffusion control and nature of the surface kinetics could be evaluated. All RDE measurements were made in H_2O_2 solution (in 0.1 M PBS) while using the three electrode system. Chronoamperometric measurements for the oxidation of H_2O_2 were made by stepping the potential of the working electrode of choice from 200 mV to 600 mV vs Ag/AgCl. This potential was selected for maximum oxidation rate of H_2O_2 and is consistent with previously reported values.[64] The Au and Pt rotating disk electrodes were cleaned and modified using the procedure described previously. Chronoamperometry experiments were performed on each electrode in a various hydrogen peroxide solutions with a rotation speed of 0, 100, 200, 300, 400, 500, 600, 700, 800, 900, 100, 1585, 2500, and 4000 revolutions per minute (rpm) for a run time of 60 seconds. These rotation speeds were selected so that they were evenly space in $\omega^{-1/2}$. The currents obtained from these chronoamperometry experiments were used to determine the k_f values via Koutecky-Levich (KL) plots.

The resulting data was analyzed using KL plots, which plots $1/i$ vs $1/\omega^{1/2}$ where ω is the angular speed and ω = (rpm x 2π)/60, plus the electrode reaction is treated as an irreversible process involving both kinetic and mass transfer components. The general relationship for this process is given by:

$$\frac{1}{i} = \frac{1}{i_k} + \frac{1}{i_d} \quad \textbf{(6)}$$

The kinetic current, i_k, is given by:

$$i_k = nFk_f[H_2O_2]_{bulk} \quad \textbf{(7)}$$

where k_f is the heterogeneous electron transfer rate constant and $[H_2O_2]$ is the bulk concentration in mM. The diffusion current, i_d, is given by:

$$i_d = 0.620nF[H_2O_2]_{bulk}D_{H_2O_2}^{2/3}v^{-1/6}\omega^{1/2} \quad \textbf{(8)}$$

where D_{H2O2} is the diffusion coefficient, υ is the kinematic viscosity (taken to be 1.00 x 10^{-6} m^2 s^{-1}) and ω is the rotation speed in rad s^{-1}.[62] Figure 34 and Figure 35 show the KL plot for the Pt/Au/ceria modified Au and Pt electrodes, respectively. A plot of $1/i$ vs $1/\omega^{1/2}$ gave an intercept which is equal to i/i_k, which is the kinetic limit for the current at infinitely large speed of rotation, eliminating all mass transport limitations. Since the y-intercept converts to $1/i_k$ and using this y-intercept along with the Faraday's constant and the concentration of H_2O_2 for the given electrode, the k_f value can be determined. Using this analysis method, the k_f values were calculated for both Au and Pt electrodes and their several modifications. Table 3 shows the k_f values for the various electrodes. The results show that for the rate constant, k_f, values range in the order of 10^{-8} to 10^{-10}, implying that the two electron process

of hydrogen peroxide is kinetically limited. Even though, ceria enhances the H_2O_2 oxidation current response at the electrode, it does not properly catalyze the electron transfer process due to kinetic limitations. In order to speed up the reaction to a practical degree, an electron transfer mediator is needed.

Table 3: Calculated rate constant, k_f, values for various H_2O_2 solutions on Au and Pt electrodes with and without modification with the bi-metallic nanoceria composite.

$[H_2O_2]$ (mM)	**Bare Au k_f (cm s^{-1})**	**Au modified with Pt/Au/ceria k_f (cm s^{-1})**	**Bare Pt k_f (cm s^{-1})**	**Pt modified with Pt/Au/ceria k_f (cm s^{-1})**
0.25	3.17E-10	2.09E-11	1.91E-10	5.73E-11
0.5	1.65E-10	1.26E-8	4.58E-9	7.44E-9
1	2.12E-10	1.76E-8	2.62E-9	1.23E-8
5	1.30E-10	3.40E-8	6.22E-9	1.56E-8
10	5.71E-10	5.83E-9	2.86E-9	1.07E-9
20	1.78E-10	1.60E-9	1.32E-9	6.06E-10
30	7.21E-11	1.01E-9	1.02E-9	4.25E-10
Average	**2.35E-10**	**1.04E-8**	**2.69E-9**	**5..36E-9**
Standard Deviation	**1.66E-10**	**1.23E-8**	**2.12E-9**	**6.47E-9**

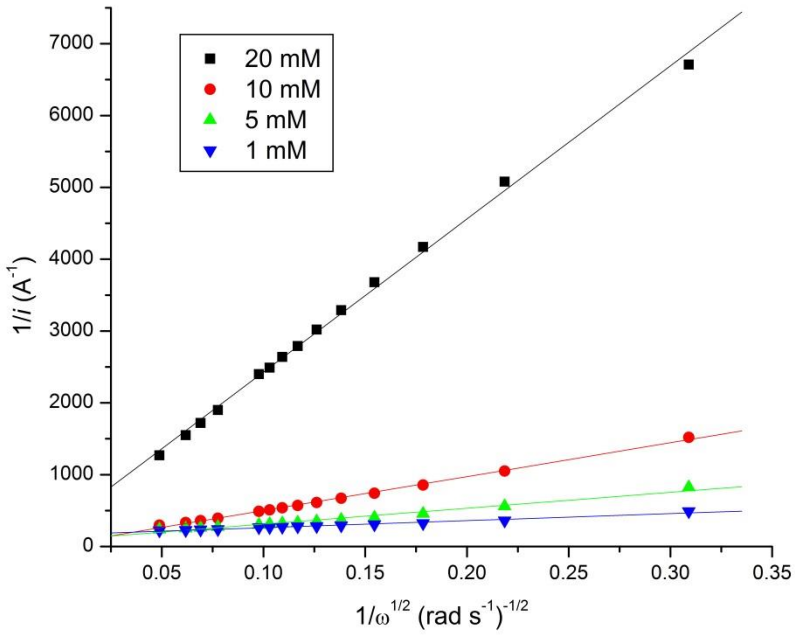

Figure 34: Koutecky-Levich plot of H_2O_2 oxidation vs Ag/AgCl on Au electrode modified with Pt/Au/ceria.

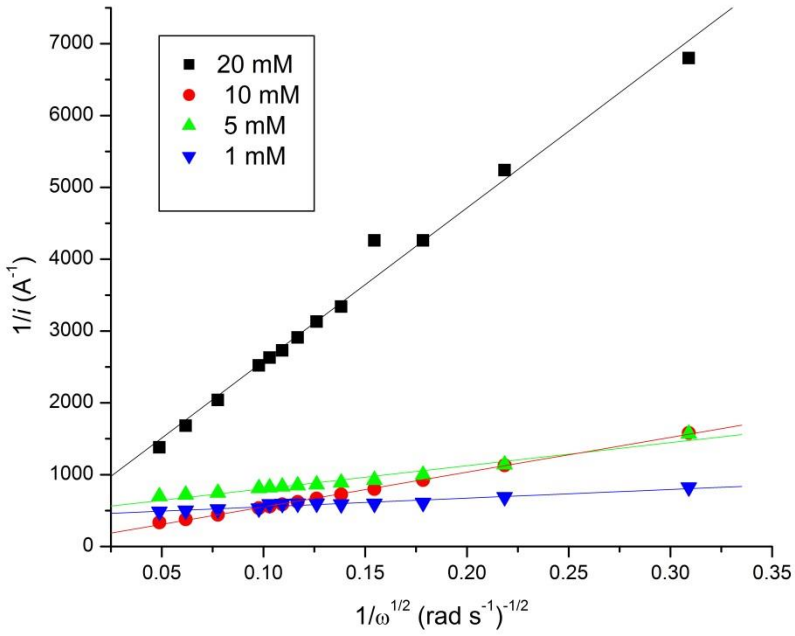

Figure 35: Koutecky-Levich plot of H_2O_2 oxidation vs Ag/AgCl on Pt electrode modified with Pt/Au/ceria.

Ce^{+3} vs. Ce^{+4} Study

The effect of Ce^{+3} vs. Ce^{+4} on the electrochemical oxidation of H_2O_2 was investigated. Ceria coexists in both (III) and (IV) oxidation state in the synthesized nanoparticle solution. For all the prior studies, Ce^{+3} was in a higher ratio than Ce^{+4}, however for this study, both the Au and Pt electrode were modified using Ce^{+4}composite and the electrochemical performance was analyzed towards H_2O_2. Figure 36 and Figure 37 show the H_2O_2 concentration vs. the oxidation current plot for both Au and Pt electrodes, respectively modified with Ce^{+3} and Ce^{+4} composite. Au electrode modified with Pt/Au/Ce^{+3} show greater enhancement in the H_2O_2 oxidation current than Au electrode modified with Pt/Au/Ce^{+4}. Similar results were found for the Pt electrode except the enhancement in the H_2O_2 oxidation current was significantly larger when compared to the Au electrode.

In general, the higher oxidation state of Ce^{+3}(Ce^{+4}) nanoceria does not have a significant effect on the Au electrode modified with the composite. However, for the Pt electrode, there is a noteworthy difference between the Ce^{+3} and Ce^{+4} modified electrode. When the Pt electrode is modified with Pt/Au/Ce^{+3} there is a considerable increase in the oxidation current. There is also a higher linear correlation for the Pt/Au/Ce^{+3} modified Pt electrode. The higher linear correlation and a higher slope correspond to higher sensitivity of the sensor.

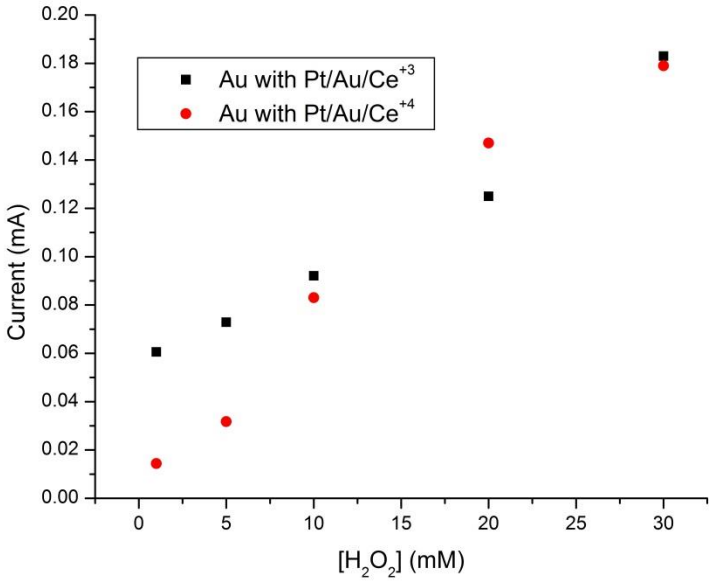

Figure 36: Effect of Ce^{+3} and Ce^{+4} composite modified Au electrode towards H_2O_2 oxidation at 100 mV/s vs. Ag/AgCl.

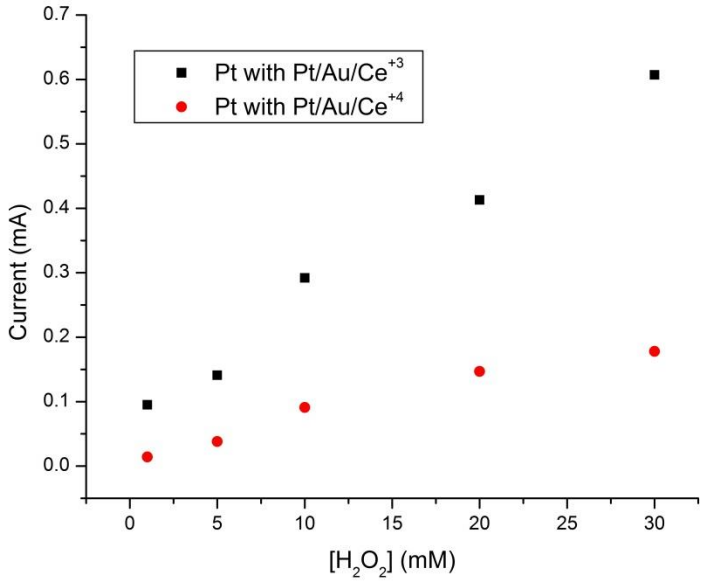

Figure 37: Effect of Ce^{+3} and Ce^{+4} composite modified Pt electrode towards H_2O_2 oxidation at 100 mV/s vs. Ag/AgCl. The Pt electrode modified with the Ce^{+3} composite yields the optimum current for H_2O_2 detection.

Stability of Ce^{+3} and Ce^{+4} Modified Au and Pt Electrodes

The performance of both Au and Pt modified with Pt/Au/Ce^{+3} and Pt/Au/Ce^{+4} was tested by performing CV in a hydrogen peroxide solution. Each of the modified electrodes was placed in a 10 mM H_2O_2 in 0.1 M PBS and six cycles of cyclic voltammetry were performed every 24 hours over a period of nine days. The electrodes were stored in 0.1 M PBS when not in use. Figure 38 and Figure 39 show the observed trend in 10 mM H_2O_2 oxidation current over the period of nine days for the Ce^{+3} and Ce^{+4} modified Au and Pt electrodes, respectively.

The Au electrode modified with Pt/Au/Ce^{+3} showed higher deviation in the oxidation current for 10 mM H_2O_2 solution when compared to Pt/Au/Ce^{+4}. When the Au electrode was modified with Pt/Au/Ce^{+3} the current stabilized relatively after three days. However, for the Au electrode modified with Pt/Au/Ce^{+4} there was a continuous increase in the current until the sixth day and from there on, it stabilized for four days. On the other hand, the Ce^{+3} and Ce^{+4} modified Pt electrodes did not deviate much from each other for the oxidation current. Overall, the Au electrode modified with Pt/Au/Ce^{+3} had higher stability than the Pt/Au/Ce^{+4} modified electrode, while for the Pt electrodes, Ce^{+3} and Ce^{+4} modified electrodes showed reasonably similar behavior.

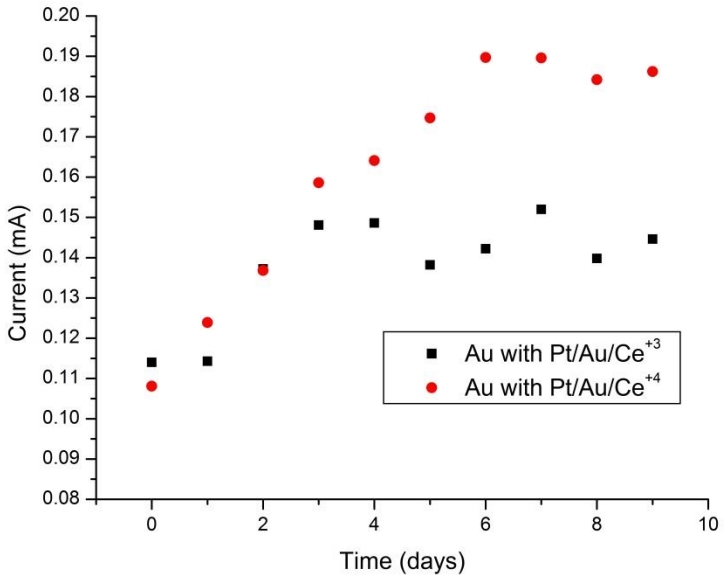

Figure 38: Oxidation current of 10 mM H_2O_2 vs. time on Ce^{+3} and Ce^{+4} composite modified Pt vs. Ag/AgCl. Over the period of nine days, Au electrode modified with Ce^{+4} gives the highest current indicating long term stability of the sensor.

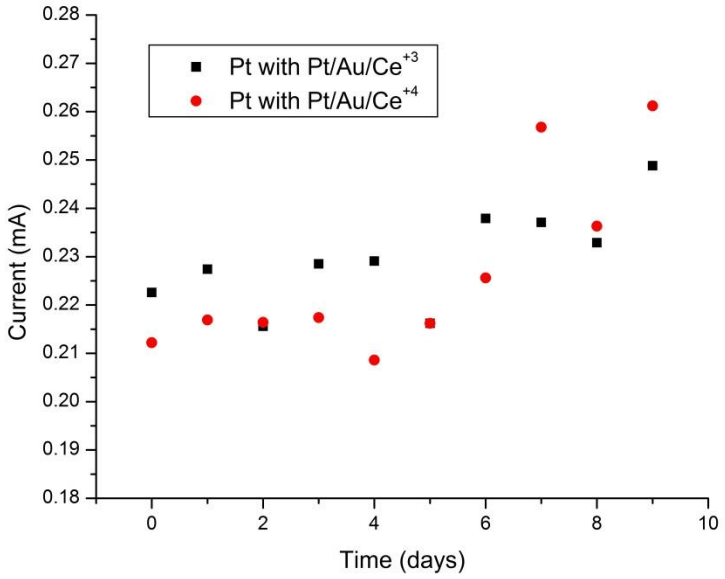

Figure 39: Oxidation current of 10 mM H_2O_2 vs. time on Ce^{+3} and Ce^{+4} composite modified Pt vs. Ag/AgCl. No significant change is observed in the performance of the two modified Pt electrodes suggesting the same stability of each of the electrodes.

Conclusion

The electrochemical oxidation of H_2O_2 on Au and Pt electrodes modified with nanoceria composite were studied to examine the catalytic ability of nanoceria. The cyclic voltammogram results demonstrated that the Pt/Au/Ceria modified electrodes gave the highest oxidation/reduction current for H_2O_2 when compared to bare metal electrodes and in the absence of ceria. A linear increase in the oxidation current was also observed as the H_2O_2 concentration increased for both Au and Pt electrodes and its modifications. A slight increase in the current intensity is observed when the electrodes are modified with the Au^{+3} and Pt^{+4} salts due to the increase in the surface area of the electrode. However, the increase in the electrochemical H_2O_2 oxidation current observed in the presence of ceria particles is larger than what can be attributed to changes in the morphology and the active electrochemical surface area of the electrode. Although the Koutecky-Levich study verified a slow kinetic process for H_2O_2 on the surface the electrode, it can be concluded that nanoceria has a perceptible catalytic effect for the electrochemical oxidation of H_2O_2. Different ratios of Ce^{+3} and Ce^{+4} composite modified electrodes and the stability of these electrodes were also investigated towards H_2O_2 sensing. The analysis of these experiments confirmed that the Ce^{+3} complex modified electrodes gave the most favorable results for H_2O_2 detection. Initial studies of nanoporous gold electrodes towards bio-fouling of the electrode have displayed promising results in the presence of bovine serum albumin (BSA).

CHAPTER 4: INDIRECT DETERMINATION OF HYDROXYL RADICALS GENERATED BY AN ODOR CONTROL TECHNOLOGY

Background

Reactive Oxygen Species

The hydroxyl radical, •OH, is one of the most reactive species belonging to the reactive oxygen species family, ROS. Hydroxyl radicals are generated by several methods such as the decomposition of hydrogen peroxides by photolysis or in atmospheric chemistry by the reaction of water with excited atomic oxygen.[65] Hydroxyl radicals have been shown to enhance corrosion due to their reaction with water and oxygen, and are also highly reactive with pollutants and can cause cellular damage.[66] Hydroxyl radicals hold a very high electronic potential making them one of the most powerful known oxidative reactants. For this reason, they are widely used in the treatment of drinking, industrial, and wastewater due to their effectiveness in destroying organic chemicals, as they are electrophiles that react rapidly and non-selectively with nearly all electron-rich compounds.[67] The instability of these hydroxyl radicals makes their direct detection difficult as they react rapidly with their surroundings.[68] Since the direct detection of hydroxyl radicals is rather complex, several indirect determination methods have been studied including the direct hydroxylation from benzene to phenol,[69] a time gated luminescence detection,[66] monitoring of photo production rates,[70] trace determination,[71] photochemical production,[72] advanced oxidation with salicylic acid trapping with liquid chromatography,[73] and photolysis of Fe(III) pyruvate complexes among others.[68a, 74] A widely used indirect technique involves the reaction of hydroxyl radicals with benzene resulting in the formation of phenol. The reaction mechanism is

stoichiometric, where one molecule of phenol is generated per each hydroxyl radical reacting with one molecule of benzene.[74f, 75]

Indirect Detection of •OH Generated by Fine Particle Mist

During this study, the indirect determination of the hydroxyl radical by its reaction with benzene was applied to aid in the determination of the chemical mechanism of the OHxyPhogg® process. This odor control technology, OHxyPhogg®, utilizes an air, ozone, and water mixture to generate a hydroxyl radical fine particle mist which oxidizes hydrogen sulfide and other odorous compounds such as mercaptans and amines, as stated by the patent (US patent No. 6076748). This system utilizes a 3-fluid nozzle patented by Vapex Environmental Technologies. This nozzle combines water, air and ozone molecules to generate micro-sized water particles with hydroxyl radicals in them. The generated hydroxyl radicals are then reacted with benzene to form phenol as the major product as shown in (9). The 1:1 stoichiometry of hydroxyl radical to phenol allows a straightforward quantitation of the generated hydroxyl radicals.

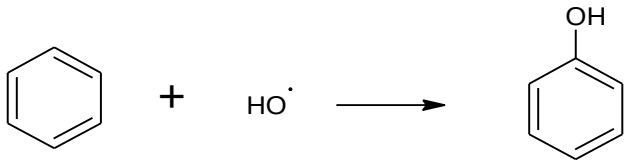

(9)

In recent years, microbubble and nanobubble technologies have gained significant attention due to their applications in a variety of fields of science and technology such as water treatment, biomedical engineering, and nanomaterials. Microbubbles are defined as miniscule bubbles with a diameter of 10-50 μm while nanobubbles are usually less than 200

nm in diameter.[76] A key difference between microbubbles and nanobubbles is that microbubbles tend to decrease in size and subsequently collapse due to long stagnation and dissolution of interior gases into the surrounding water whereas nanobubbles remain as such for a long period of time (months) and do not burst at once.[77] This phenomenon is portrayed in Figure 40.

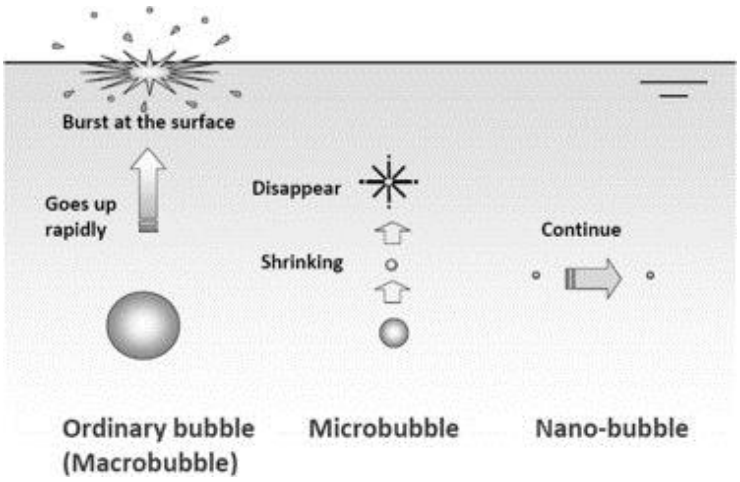

Figure 40: Schematic diagram depicting the behavior of macro, micro, and nanobubbles illustrating the behavior of each.[76, 77b]

Decrease in the size of microbubbles below the water surface results in a high internal pressure inside the microbubbles which is directly proportional to the bubble's diameter. The pressure and diameter relationship is given by the Young-Laplace equation:

$$P = PI + \frac{4\sigma}{d_b} \quad \textbf{(10)}$$

Where P is the gas pressure, PI is the liquid pressure, σ is the surface tension of the liquid and d_b is the bubble diameter.[76] Previous studies show that the micro-sized water particles provide large surface areas for both adsorption and reaction of pollutants in the atmosphere. It has been observed that organic solutes such as polycyclic aromatic hydrocarbons,

pesticides, and alkanes are found at concentrations higher than that expected from their corresponding gas-liquid-phase equilibria,[78] which were hypothesized to result from surface adsorption onto fog droplets.[79] Recent work on naphthalene vapors also showed that small water droplets in the micrometer range had higher concentrations of these vapors than the large droplets.[80] Furthermore, it is recognized that the smaller the size of droplets the higher the internal pressure. According to the Young-Laplace equation, for a bubble with a diameter 1 μm at 298 K, the internal pressure is about 390 kPa.[76] A high pressure region is eventually created at the final stage of the microbubble collapse due to the rate of increase in the internal pressure being inversely proportional to its size as represented in Figure 41.

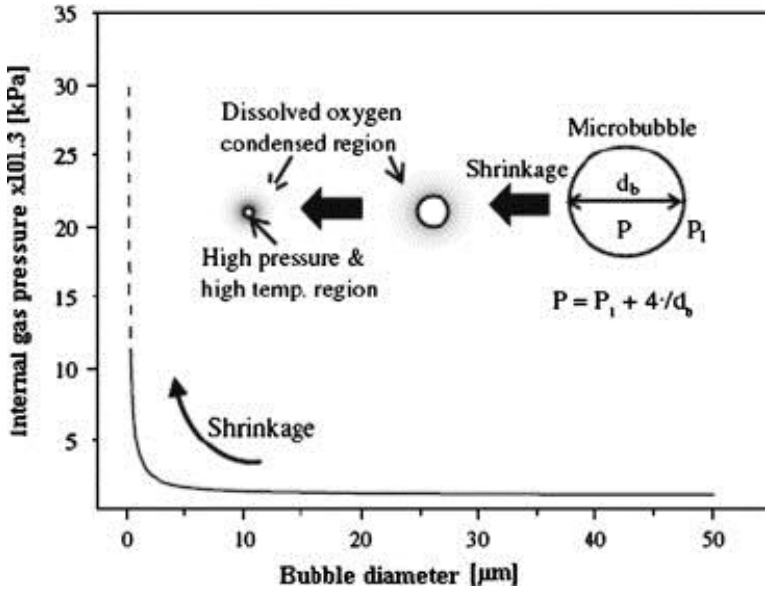

Figure 41: Increase in the interior gas pressure of microbubbles during shrinkage at T = 298 K, P = 100 kPa. The rate of increase of the interior gas pressure was inversely proportional to the bubble size.[81]

Hydroxyl radicals and shock waves can be generated at the gas–liquid interface due to pyrolytic decomposition that takes place within the collapsing micro-size water particles.[82] Consequently, the decomposition of ozone to produce hydroxyl radicals is accelerated in the

case of ozonated water micro-bubbles.[77a] Due to this phenomenon, micro-size mists of gases with oxidizing ability, such as ozone, have been applied to various water treatment processes since the ozone micro-bubbles have high solubility and improved disinfection ability due to the generation of hydroxyl radicals and/or pressure waves.[83]

During this investigation, the analysis of droplet size created from the fine particle mist was studied to corroborate the claim that the OHxyPhogg® technology can indeed produce micron-sized water particles. Further studies were performed to verify and quantify the presence of hydroxyl radicals via HPLC and UV-Vis spectrophotometry. For this study, the analyzed samples were collections of the resulting hydroxyl radical fine particle mist after a mixture of saturated aqueous benzene, ozone, and air was sprayed through the nozzle. Phenol is formed as a stable product of this reaction and thus the quantification of hydroxyl radical formation could be performed. Therefore, the purpose of this study was to apply an indirect method for the detection of hydroxyl radicals generated in the fine, micro-sized water mist.

Experimental

Materials and Reagents

Phenol (Fisher Scientific, 99%) was used to prepare standard phenol solutions using saturated aqueous benzene as the solvent. The saturated aqueous benzene solution with a concentration of 2.23×10^{-2} M was prepared using benzene obtained from Sigma Aldrich (99%). All aqueous solutions of phenol and benzene were prepared using triple-distilled water with 18 ΩM resistivity (Barnstead B-Pure). Acetonitrile (Fisher Scientific, HPLC grade) and triple-distilled water from a B-Pure Barnstead purification system producing ~18

ΩM cm water were used as the eluent solutions for HPLC. Water samples collected from the experimental setup were analyzed as received. All chemicals and solvents used were of reagent grade and were used without further purification unless specified. A DC-III droplet measurement technology (KLDLABS incorporated) was used to measure the droplet size distribution of the generated mist in the reactor.

Methods

UV-Vis spectrophotometry was performed using a Varian Cary 50 spectrophotometer. The data interval was set under a minimum ratio of a spectral band width (SBW) of 3:1. A quartz cuvette with dimensions of 10 mm path length and 4 mm path width was used for all UV-Vis experiments.

The HPLC experiments were performed using a Perkin-Elmer series 200 HPLC, consisting of a series 200 binary pump, a series 200 UV-Vis detector with deuterium lamp set at a maximum wavelength of 273 nm, a series 200 autosampler, and a series 200 vacuum degasser. The analytical column used was a Zorbax (Agilent) SB-C18 column. The mobile phase was $CH_3CN:H_2O$ = 50:50 (v/v) with a flow rate of 1 cm^3/ min. A 50 µdm^3 portion of the sample was injected with a 50 µdm^3 gas-tight syringe.

Determination of Phenol in Standard Solutions

Ten concentrations of aqueous phenol in saturated aqueous benzene solution (2.23 x 10^{-2} M) were prepared via serial dilution,[84] over a range of 5.00 x 10^{-5} M to1.00 x 10^{-7} M. These solutions were used as HPLC standards. These standards were then analyzed on HPLC after conditioning the column for 60 minutes. The solvent, 2.23 x 10^{-2} M aqueous benzene was also analyzed via HPLC to determine its elution time. A calibration curve was

constructed using the ten standard solutions of phenol in order to indirectly quantify the hydroxyl radicals present in the water samples collected from the reactor.

Apparatus and Sampling

The experimental apparatus was designed as shown in Figure 42. The water collection apparatus was a steady-state flow-through system which consisted of a black, thick polyethylene cylinder which was divided into four chambers designated C-1, C-2, C-3, and C-4, respectively. Each of the chambers was separated by an acrylic disk with an 8.5-inch diameter opening in the middle to allow the passage of the fine particle mist. Each chamber had a condenser designed to condense the mist particles for easier sample collection and a valve which allowed for the collection of these samples. At the head of the cylinder, the odor control technology generated a mist which was injected into the space with the patented 3-fluid nozzle (US patent No. 6076748).[85] This nozzle combines ozone with a rapid application of micro-sized water particles that generates a mist of hydroxyl radicals. This mist was then dispersed through the open space with subsequent passage through the 8.5-inch disk holes for complete dispersion into the entire reactor. For experimental purposes, the water line was replaced with a line containing a saturated aqueous benzene solution with a fluid flow rate of about two gallons per hour. The saturated aqueous benzene solution was sprayed through the nozzle to create the mist and was allowed to react with ozone and air in the first reaction chamber. The reaction time was measured from the point when the ozone reached a steady concentration of approximately 13,000 ppm. The resulting mixture consisting of micro-sized water particle mist then traveled through the four chambers as the bigger droplets collapsed at the bottom of the reactor. The reaction was allowed to take place for two hours before the condensed samples from each of the four chambers were collected as illustrated in Figure 42.

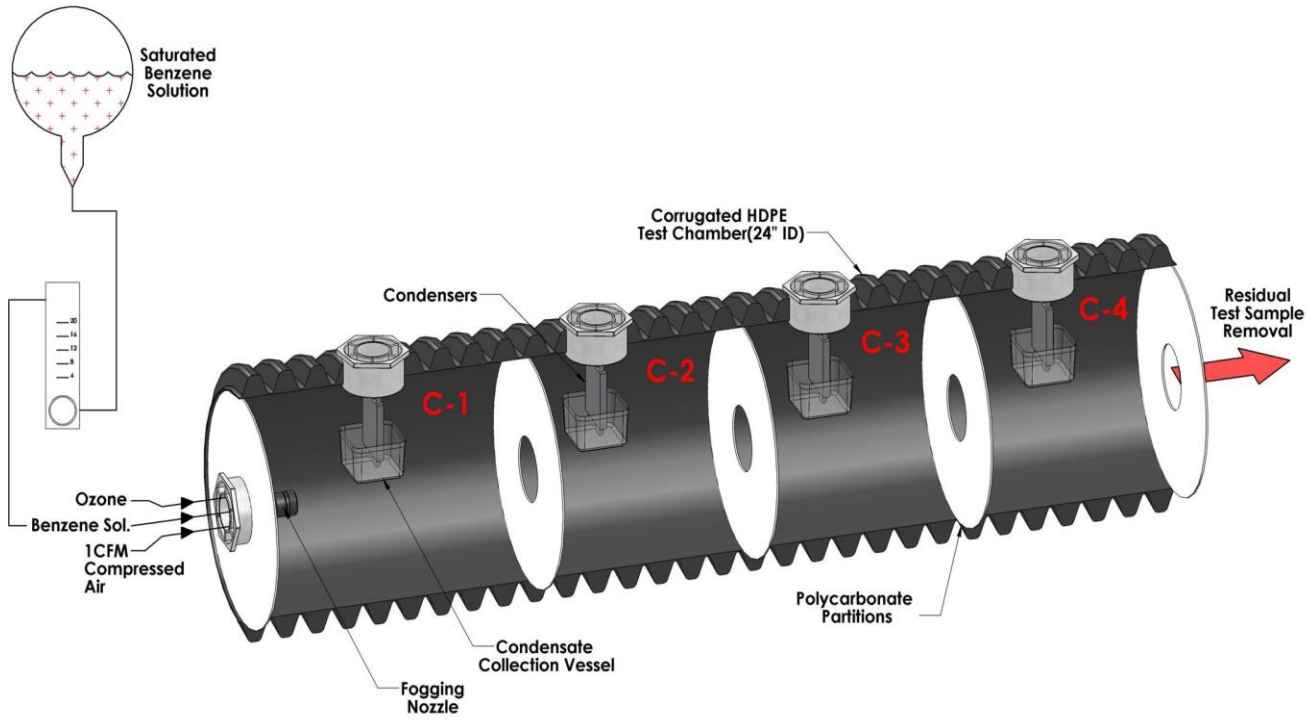

Figure 42: Diagram of the experimental system showing the patented nozzle connected to a cylindrical collection unit divided into four chambers; chamber 1 being closest to the nozzle. Each chamber has a condenser unit and the water samples were collected and analyzed by HPLC.

Results and Discussion

Droplet Size Analysis

The DC-III probe was inserted in the headspace in each of the four chambers to obtain the size distribution of the micro-sized water droplets in the fine particle mist. **Error! eference source not found.** illustrates the observed volume mean diameter and the size of the particles in the headspace of each of the chambers. Over 90 percent of these particles are in the range of 10-60 micrometers. The largest particles were observed in chamber 1 and were found to have an average diameter of 55.22 microns whereas the smallest particles with an average diameter of 13.90 microns were observed in chamber 4 as shown in Figure 43.

The size of these droplets demonstrated a decreasing trend going from chamber 1 (closest to the nozzle) to chamber 4 (furthest from the nozzle), as only the smaller droplets travel through the reactor unit whereas the bigger droplets condense out at the bottom of each chamber. Based on this analysis, it can be concluded that the odor control technology does indeed produce a fine micro-size particle mist.

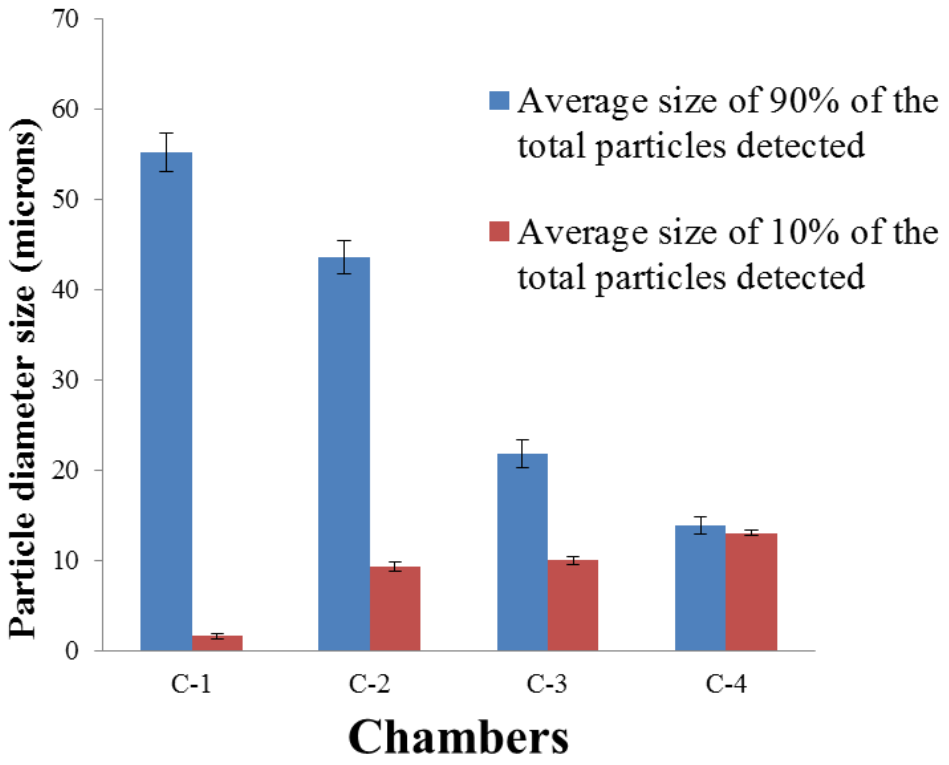

Figure 43: Size distribution of the micro-sized fine particle mist in the four reaction chambers showing the generation of micro-size particle mist via the nozzle.

UV-Vis Results

A UV-Visible spectrograph was used for the identification of the phenol generated by the reaction of benzene and hydroxyl radicals. For this experiment, standard solutions with

various concentrations of phenol in aqueous benzene were prepared in the range of 50-500 parts-per-million (ppm). The saturated benzene concentration utilized was $5.0x10^{-3}$ M and it was used as the solvent for the preparation of the standard mixtures. The maximum absorption wavelengths recorded were 270 nm for phenol and 250 nm for benzene which when compared to literature, were very similar with values of 270.75 nm or 273.75 nm for phenol and 254.75 nm for benzene.[86] These wavelengths were also utilized for the initial parameters in the HPLC analysis. The UV-Vis absorbance spectrum of a standard solution is shown in Figure 44(a) while Figure 44(b) shows the absorbance spectra of the samples collected from the reactor.

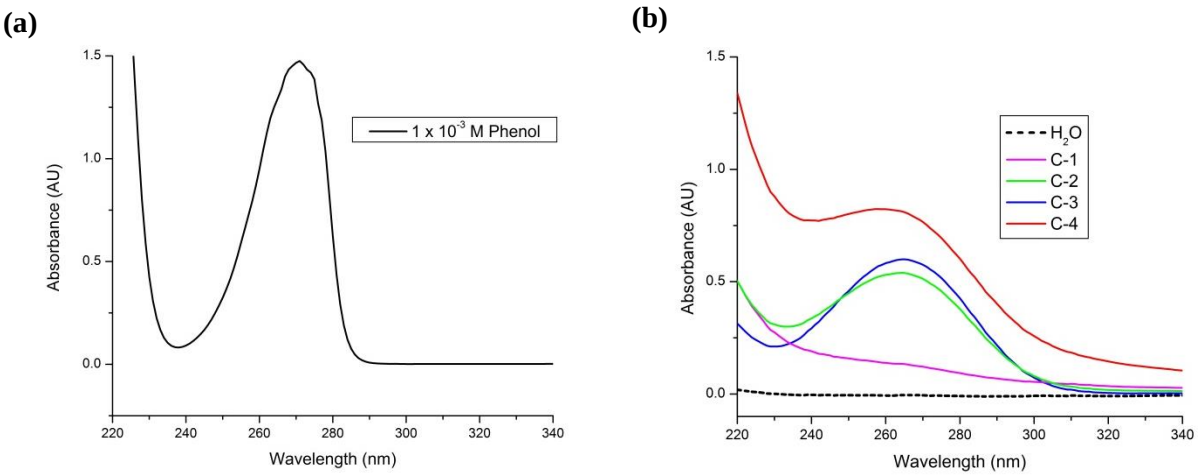

Figure 44: UV-Vis spectrum of (a) standard phenol solution observed at 270 nm and (b) blank and water samples from each of the four reaction chambers illustrating an increasing trend from chamber 1 to chamber 4.

HPLC Results of the Standard Solutions

The first step in the quantification of the amount of hydroxyl radicals produced was to generate a calibration curve using known standard solutions. Ten different solutions of

phenol in saturated benzene were used as the standard solutions and were analyzed via HPLC. Retention times of 2.6 minutes and 4.4 minutes were observed for phenol and benzene, respectively.

Figure 45 shows the chromatograms of the standard solutions used for the calibration curve. The area of the peak associated with phenol was analyzed for each solution and a plot of phenol concentration versus peak area was constructed. A best fit line was plotted through the data points resulting in R^2 value of 0.99998. The line equation:

$$A = 5.32\ x\ 10^{-9} \times\ C - 29.07 \quad \textbf{(11)}$$

where A is the peak area in µV*sec and C is the concentration in molarity, was then used to determine the phenol concentration in the various fine particle mist samples from the reactor. Figure 46 shows the phenol concentration versus the peak area for each one of the standard solutions representing a calibration curve.

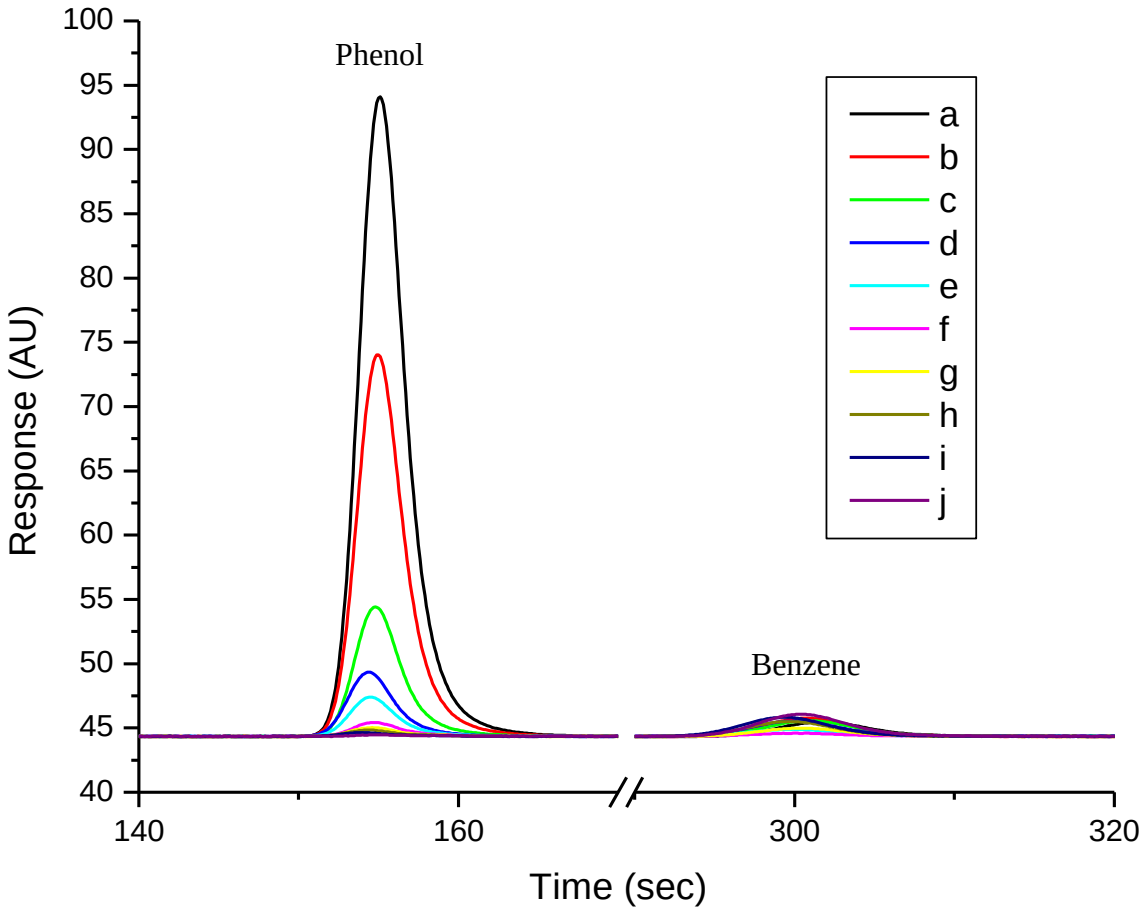

Figure 45: HPLC chromatograms of the standard phenol solutions: (a) 5.00 x 10^{-5} M, (b) 3.00 x10^{-5} M, (c) 1.00 x 10^{-5} M, (d) 5.00 x 10^{-6}M, and (e) 3.00 x 10^{-6} M (f) 1.00 x 10^{-6} M, (g) 7.00 x 10^{-7} M, (h) 5.00 x 10^{-7} M, (i) 3.00 x 10^{-7} M, (j) 1.00 x 10^{-7} M.

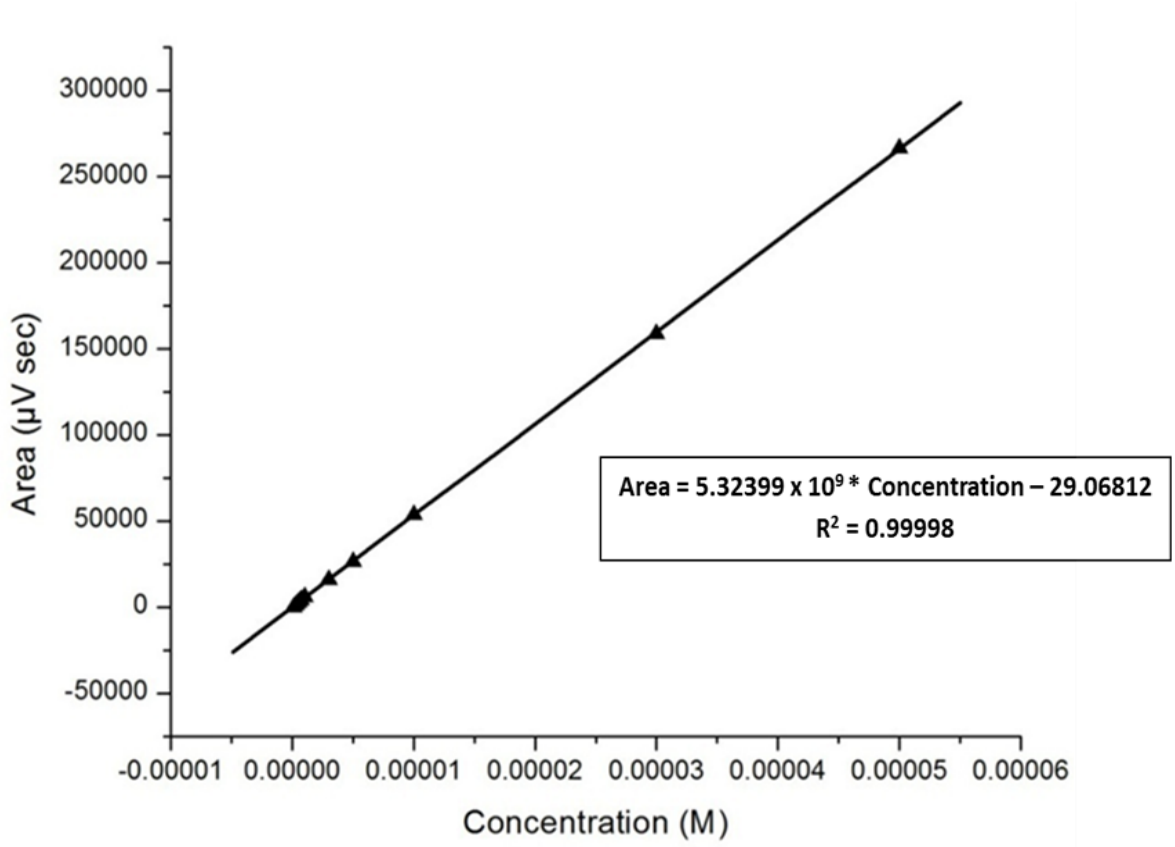

Figure 46: Constructed calibration curve of standard phenol solutions based on HPLC analysis. The linear equation was used for the analysis of the phenol concentrations in the reaction chamber samples.

HPLC of the Reactor Samples

The four experimental samples collected, one from each chamber, were examined via HPLC using the same parameters as those for the standard solutions. Phenol was observed to have a retention time of 2.6 minutes as shown in Figure 47 while the retention time of benzene was observed to be approximately 4.5 minutes. The area under the phenol peak was substituted into the linear equation from the calibration curve to solve for the phenol concentration in each of the four reactor samples. Chamber three, C-3, had the highest concentration of phenol followed by C-4, C-2, and C-1, respectively, as shown in Table 4. All four samples were within the linear dynamic range of the calibration curve. The

calculated hydroxyl radical concentrations in terms of molarity and parts per million are as shown in Table 4. As expected, chamber 4 showed the least variability due to it being farthest away from the injecting nozzle since most of the bigger particles condensed to the bottom.

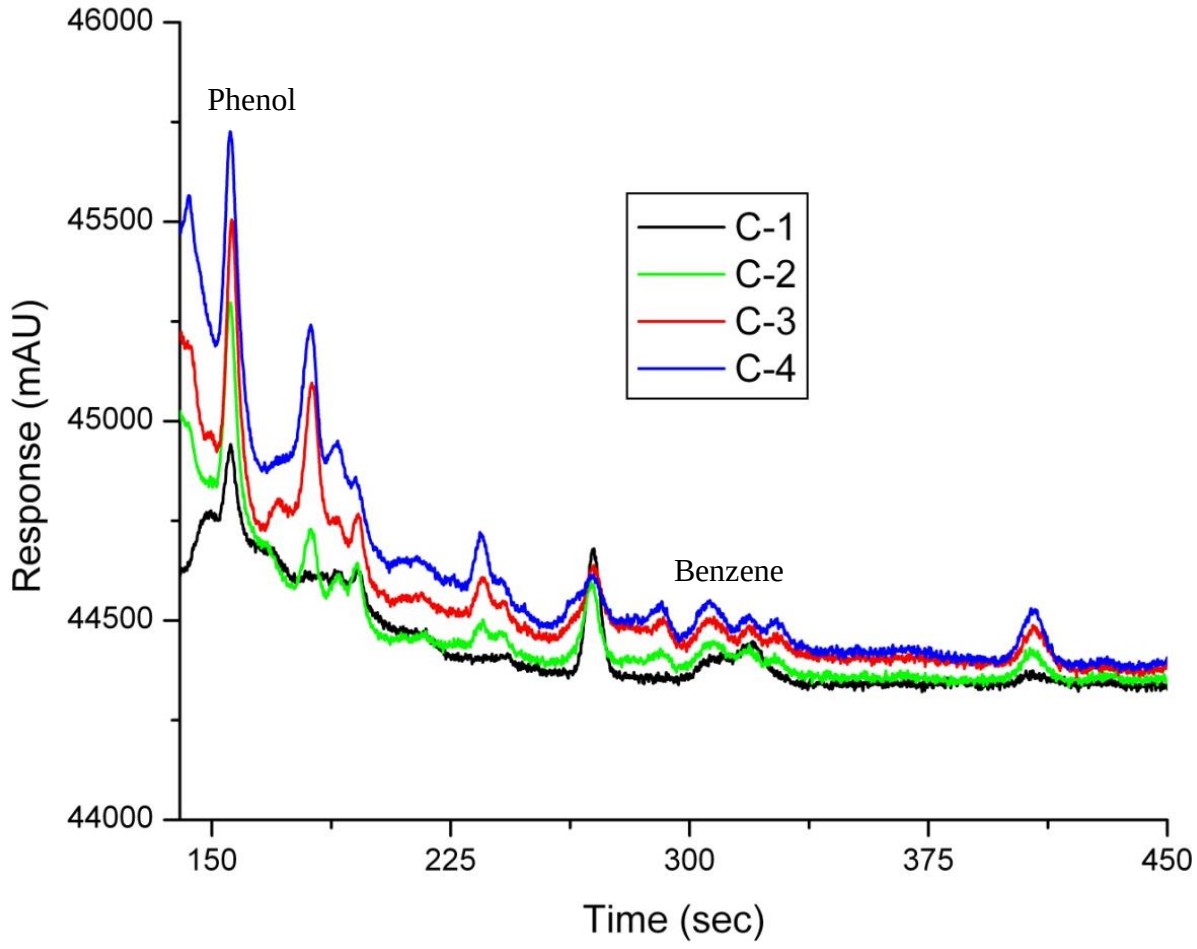

Figure 47: HPLC chromatogram overlay of the experimental samples collected from each of the four chambers showing the retention time of phenol along with aqueous saturated benzene solution.

Table 4: Calculated concentrations of hydroxyl radicals in each of the four reaction chambers based on HPLC analysis. Chamber 3 and chamber 4 gave the highest hydroxyl radical concentrations as expected.

Reaction Chamber	Peak area (µV*sec)	Peak height (µV)	[Phenol] (µM)
C-1	1281.83	316.59	0.26 ± 0.22
C-2	2766.35	698.85	0.56 ± 0.13
C-3	3758.30	888.12	0.76 ± 0.10
C-4	4085.23	939.48	0.83 ± 0.08

Conclusions

The first set of experiments for this study was to perform droplet size analysis. This was performed by inserting a probe into each of the four chambers. The resulting data from this study confirmed that the odor control technology, OHxyPhogg®, does indeed generate a fine micro-size particle mist. The hydroxyl radicals generated from this odor control technology were then verified using UV-Vis and quantified via HPLC. The generated hydroxyl radicals reacted with benzene to form phenol as the major product. The 1:1 stoichiometry of hydroxyl radical to phenol allowed for a direct quantification of the hydroxyl radicals formed in the fine particle mist. The resulting hydroxyl radical concentrations ranged from 0.0247 to 0.774 ppm.

Although ozone is also known to react with benzene, the reaction kinetics are considerably slower than the reaction of benzene with the hydroxyl radicals.[87] These reactions are reported to have reaction rates of 12 M^{-1} sec^{-1} and 41 M^{-1} sec^{-1}, respectively.[87-88]

Moreover, the ozone concentration was monitored in all chambers during the collection of samples and the generation of the fine particle mist remained constant. In that regard, we are confident that the phenol concentration determined can be attributed to the reaction with hydroxyl radicals and not with ozone. In general, the hydroxyl radical concentrations were observed to be in the low parts per million range. As expected, C-3 and C-4 showed the highest radical concentrations since the smallest micro-sized water droplets were present in those chambers because the larger particulates could not pass across the holes in the separation disks. Based on these findings, it can be concluded that this technology is effective in producing hydroxyl radicals which would be available for reaction with odor producing species.

CHAPTER 5: MONITORING THE DEGRADATION OF HYDROGEN SULFIDE GAS UPON ITS REACTION WITH FINE PARTICLE MIST CONTAINING OZONE AND HYDROXYL RADICALS

Background

H_2S Odor Control Using Ozone

When sewage and industrial plants produce high levels of unpleasant odors near residential areas, they can be subject to political and legal problems. Chemicals or enzymes may be added to the liquid phase to aid in preventing odors in wastewater plants and the connected collection system. Mechanical changes to the sewage pump stations may also be made to reduce the odor. However these methods are not always sufficient to control the odor, in which case some other form of odor control in the vapor phase may need to be applied. The substances responsible for the diffusion of odors into the atmosphere in the surrounding area of treatment plants are generally gaseous inorganic products or highly volatile organic compounds. The former are mainly the result of biological activity in the sewage, the latter are often caused by the presence in the sewer of industrial wastes. Compounds such as mercaptans, indoles, inorganic acids, aldehydes, ketones and organic compounds containing nitrogen or sulfur atoms are usually associated with these odors. These are recognized as being among the causes of bad-smelling odors at the outlet of sewer lines and in treatment plants in general. Ammonia and hydrogen sulfide inorganic compounds are considered to be the main causes of odor when the sewage comes primarily from households.[89]

Hydrogen sulfide has the odor of rotten eggs and has a threshold value of 0.0011 mg/L.[89] It can cause water to have characteristic and unpleasant tastes. Hydrogen sulfide is

formed by sulfur bacteria that may occur naturally in water. These bacteria use the sulfur in decaying plants, rocks, or soil as their food or energy source and as a by-product produce hydrogen sulfide. The sulfur bacteria do not cause disease, but their presence in water can cause a bad taste or odor. Since small amounts of hydrogen sulfide can be detected in water by smell and taste, laboratory testing is not needed to detect its presence. While aeration can be used to strip some of the hydrogen sulfide from the water, this can convert a water problem to an air pollution problem if further treatment is not applied.[89]

Chemical oxidation, thermal oxidation, and biological treatments are the most common treatments for vapor phase control of odors. Ozone is considered an alternative oxidant-disinfectant agent with multiple possible applications in water, air pollution, medicine, and many others. In wastewater treatment plants, in particular, ozone has the ability to disinfect, oxidize, or be used in combinations with other technologies and reagents. Gregor and Martin found that sulfur dioxide and water were formed in equal amounts by the reaction of ozone and hydrogen sulfide and postulated the stoichiometry as shown in the reaction below.[90]

$$O_3 + H_2S \rightarrow H_2O + SO_2 \quad \textbf{(12)}$$

Hydrogen sulfide is easily oxidized by ozone, ultimately to form sulfate. The initial oxidation is to form elemental sulfur which is seen as a light colored colloidal suspension. Further oxidation dissolves the elemental sulfur to sulfite and continued oxidation produces sulfate. As a result, more ozone than sulfur is required to produce sulfate from hydrogen sulfide. The theoretical dose to oxidize ozone to sulfate is 3:1, but in practice the ratio used is 4:1. This will leave a small ozone residual in the water, 0.2-0.3 ppm which is used to ensure that the

hydrogen sulfide is fully removed.[89] The OHxyPhogg® technology utilizes a patented nozzle which combines ozone, water, and air to produce micro-size water mists which generate hydroxyl radical mist to treat hydrogen sulfide odors in wastewater plants. All of the application sites have H_2S gasses which are buildup in the sewer tank due to the confined space. Any hazards from the radical mist itself are minimal as the sewer tank has a hatch/cover restraining leakage into the environment. Due to the highly reactive nature of the radicals, they are consumed in the redox reactions almost instantaneously. In this study, the effectiveness of this technology is examined by obtaining the optimum degradation efficiency of hydrogen sulfide via the fine particle mist.

Methodology for the Reaction Ratio of Ozone to Hydrogen Sulfide

Materials and Reagents

A low density polyethylene plastic bag (U.S. Plastic Corp.) with a diameter of 45.72 cm and total length of 6.10 m. was used as the reaction chamber and triple-distilled water with 18 ΩM resistivity (Barnstead B-Pure) was used as the water source. Ozone concentrations were measured using an InDevR 2B Technologies, Model 202 monitor while a Vapex Sentinel, Model S4 was used to determine the concentration of hydrogen sulfide. A Tedlar gas bag (10 dm^3 by Zefron International Inc.) was filled using a 99% pure hydrogen sulfide gas cylinder (air gas) and was used as needed. All chemicals and solvents used were of reagent grade and were used without further purification unless specified.

Apparatus and Sampling

After the verification and the quantification of the hydroxyl radicals, the next step was to study the optimum ratio of ozone needed to oxidize a specified amount of hydrogen sulfide gas. This was performed through injecting ozone with air into the reaction chamber and measuring its stabilized concentration. Then a specific amount of the hydrogen sulfide gas was added and its degradation was monitored for a period of time. In order to study the gas-to-gas and gas-to-liquid phase reactions, the accurate concentration of ozone had to be confirmed first. This was performed by filling the initial 3.05 m (5 ft.) of the reaction bag with ambient air using a smaller 316 stainless steel nozzle that was embedded inside a plastic case. The reaction bag was sealed tightly over the case ensuring that no gas escapes. The clamp was opened letting the air distribute itself throughout the full 6.10 m. Then a mixture of air and ozone was injected via the same nozzle until an inch of water pressure was observed. After three minutes to allow for stabilization, the ozone concentration readings were collected.

A similar procedure was repeated using an ozone and water mixture. Approximately 30 cm^3 of hydrogen sulfide was also added to the reaction bag manually using a syringe, until a hydrogen sulfide concentration of 180-200 ppm was reached, and then the bag was sealed immediately. Two hydrogen sulfide probes were inserted in the reaction bag, at 1.52 and 4.57 m. A schematic diagram of the experimental setup is shown in Figure 48 and Figure 49.

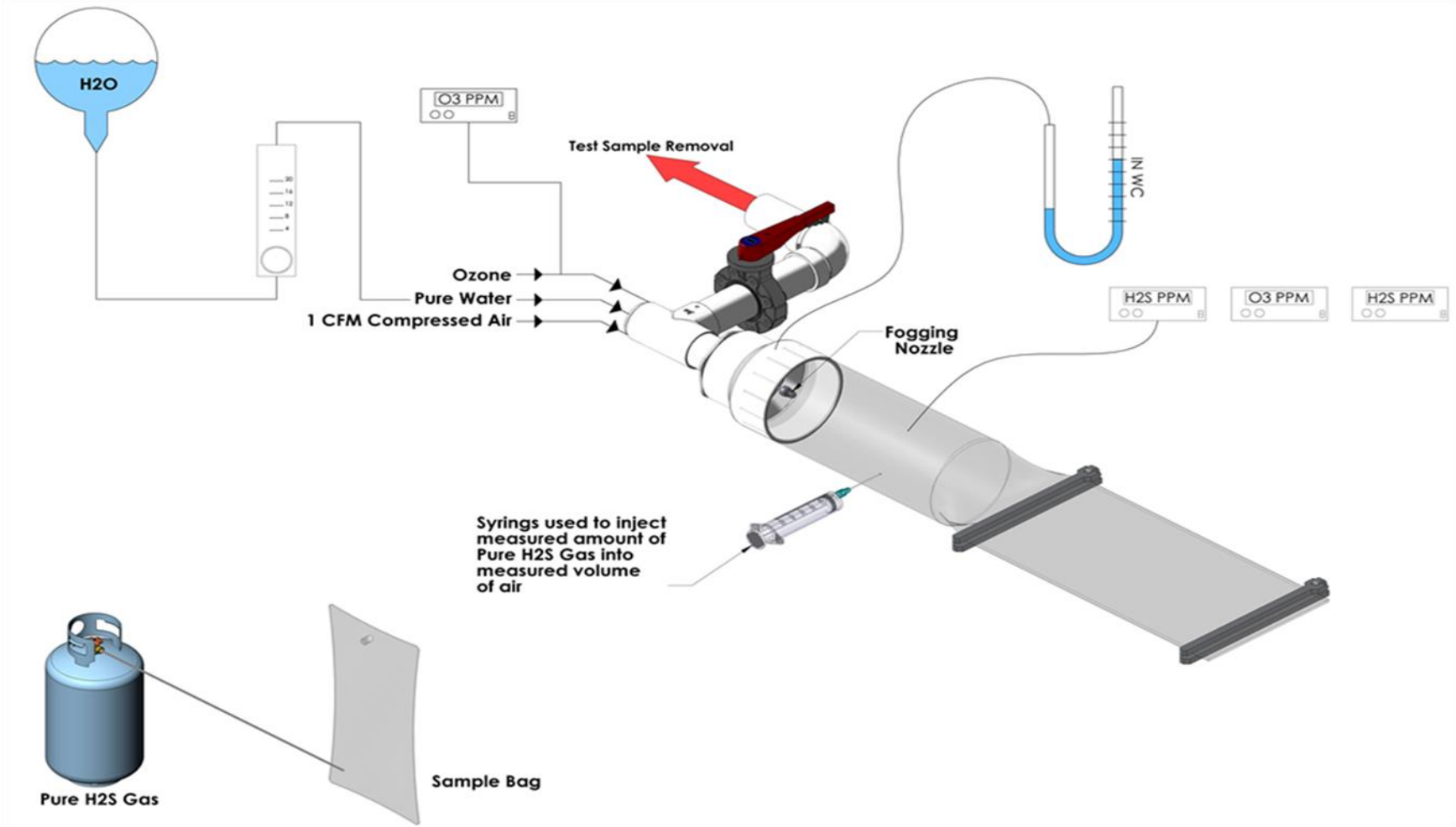

Figure 48: Schematic diagram of the experimental setup for monitoring the degradation of hydrogen sulfide using ozone and a water mist illustrating the initial filling of the first 3.05 m of the reaction bag with 30 cm^3 hydrogen sulfide gas and air.

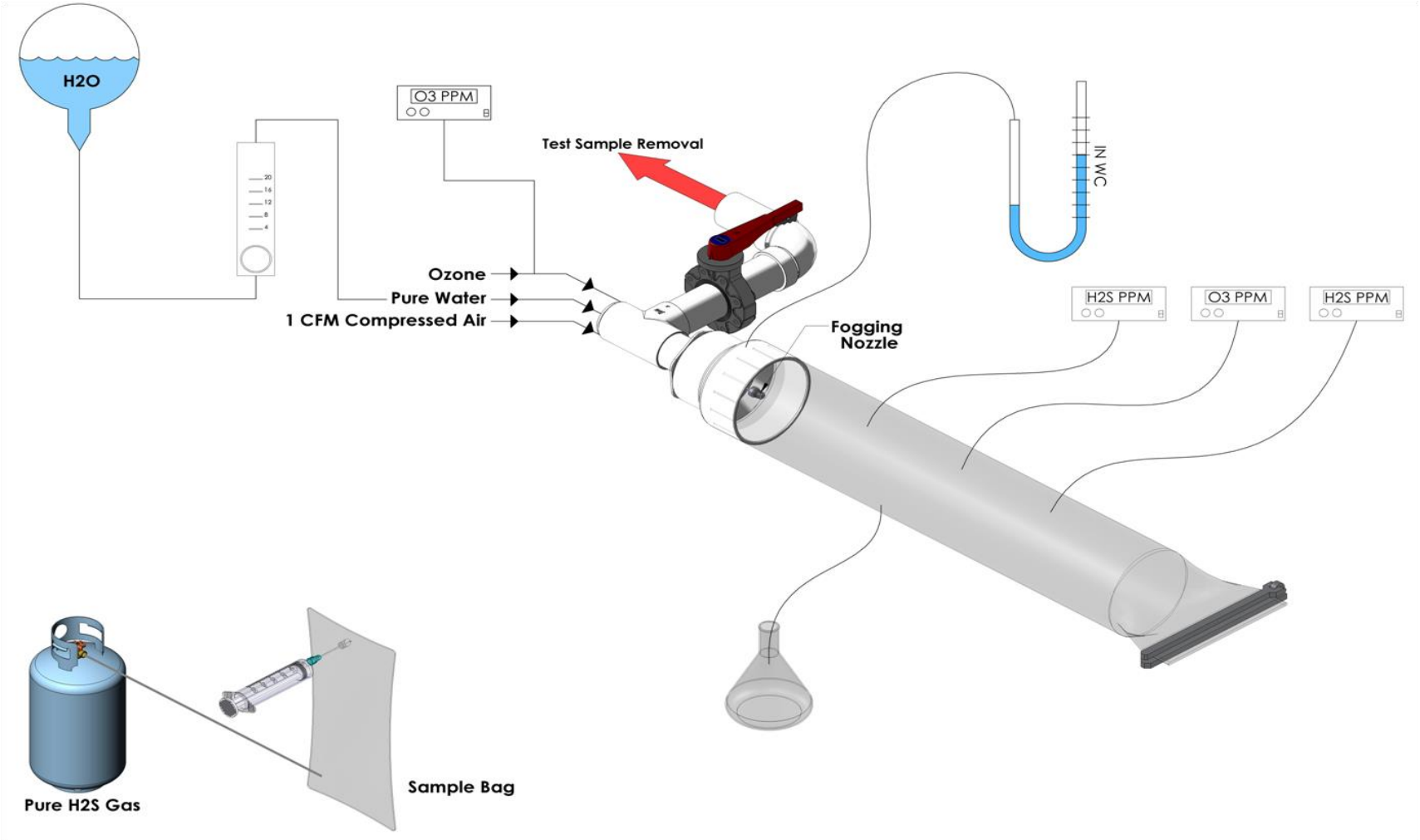

Figure 49: Schematic diagram of the experimental setup for monitoring the degradation of hydrogen sulfide using ozone and a water mist after the entire reaction chamber is filled. Various reaction parameters such as ozone and H_2S concentration along with sample collection were measured as illustrated.

Results and Discussion

Obtaining Initial Ozone Concentration

Five trials were performed to obtain an accurate concentration of ozone before its reaction with hydrogen sulfide. The ozone concentration readings varied slightly as shown in Table 5. Following the same procedure as mentioned earlier, a second set of trials were performed injecting an ozone and water mixture through the nozzle. The results show a minor deviation in the ozone and water reading when compared to just ozone by itself.

Table 5: Calculated average ozone concentrations in the presence and absence of the micro-size water mist.

Trial	$[O_3]$ (ppm)	$[O_3]$ + micro-size water mist (ppm)
1	85.8	74.1
2	86.6	69.2
3	87.9	66.3
4	92.5	60.0
5	88.9	65.9
Average	**88.4 ± 2.3**	**67.1 ± 4.6**

Monitoring the Degradation of Hydrogen Sulfide

The third set of experiments were performed using the same procedure as above except this time, H_2S gas was added with just ozone and then to the ozone and water mixture. For these experiments, instead of filling the first 3.05 meters of the bag with just air, it was filled with approximately 30 cm^3 of H_2S gas and air until the H_2S concentration stabilized in the range of 180-200 ppm. Then the clamp was opened and the fine particle mist was added through the nozzle until the entire bag was filled. The H_2S concentration readings were taken at two locations in the reaction bag; at 1.52 m and 4.57 m from the nozzle. The resulting concentrations of ozone and hydrogen sulfide in the presence of water are shown in Table 6 whereas Table 7 shows the resulting values in the absence of water. The amount of H_2S degradation was taken from the sensor readings at 4.57 m since it gave the more stable concentration readings versus the sensor at 1.52 m. When water was present, higher and steady H_2S degradation was observed due to the appropriate conditions needed for the reaction. However, when the reaction was performed with only H_2S and O_3, the degradation was very inconsistent. It can be concluded that degradation approached approximately 70% when the reaction occurred in the presence of water. As water is needed to generate the hydroxyl radicals in the fine particle mist, we hypothesize that this aids in further and better degradation of H_2S as opposed to the degradation without water.

Table 6: Experimental degradation range of hydrogen sulfide in the presence of ozone and fine particle water mist showing the different experimental parameters.

Run	Pressure (torr)	Temperature (K)	$[H_2S]$ before rxn (ppm)	$[H_2S]$ at 5 ft. after rxn (ppm)	$[H_2S]$ at 15 ft. after rxn (ppm)	H_2S Volume (L)	H_2S Degradation (ppm)	Final $[O_3]$ (ppm)	O_3 Consumption (ppm)	O_3 Volume (L)	Bag Volume (L)
1	756.62	306.46	185.94	43.3	67.0	1.26E-4	126.1	31.8	48.2	4.82E-5	444.80
2	752.95	306.55	175.77	62.1	51.3	1.24E-4	124.5	39.4	48.95	4.90E-5	444.80
3	752.44	307.55	182.65	72.9	61.7	1.21E-4	121.0	40.3	48.05	4.81E-5	444.80
4	751.18	308.45	182.12	70.9	59.1	1.23E-4	123.0	40.1	48.25	4.83E-5	444.80
5	750.40	308.85	175.33	57.5	62.1	1.13E-4	113.2	39.6	48.75	4.88E-5	444.80
6	751.84	308.65	187.78	81.4	65.0	1.23E-4	122.8	35.3	53.05	5.31E-5	444.80
7	750.61	309.81	182.94	84.3	64.2	1.19E-4	118.7	17.5	70.85	7.09E-5	444.80
8	743.33	310.15	181.58	85.5	55.1	1.26E-4	126.5	20.1	68.25	6.83E-5	444.80

Table 7: Experimental degradation range of hydrogen sulfide by ozone only, in the absence of water.

Run	Pressure (torr)	Temperature (K)	[H_2S] before rxn (ppm)	[H_2S] at 5 ft. after rxn (ppm)	[H_2S] at 15 ft. after rxn (ppm)	H_2S Volume (L)	H_2S Degradation (ppm)	Final [O_3] (ppm)	O_3 Consumption (ppm)	O_3 Volume (L)	Bag Volume (L)
1	754.83	308.75	183.52	44.0	85.0	9.85E-5	98.52	46.9	41.45	4.15E-5	444.80
2	754.52	306.05	194.86	37.8	100.8	9.41E-5	94.06	36.3	52.05	5.21E-5	444.80
3	754.09	306.25	186.77	44.1	88.8	9.80E-5	97.97	44.8	43.55	4.36E-5	444.80
4	756.93	305.85	178.86	32.3	100.8	7.81E-5	78.06	37.9	50.45	5.05E-5	444.80
5	750.63	308.65	191.45	29.9	118.9	7.26E-5	72.55	65.6	22.75	2.28E-5	444.80
6	750.39	308.21	195.09	64.7	81.8	1.13E-4	113.29	44.1	44.25	4.43E-5	444.80
7	749.60	309.05	189.23	104.9	70.7	1.19E-4	118.53	29.3	59.05	5.91E-5	444.80
8	748.57	310.05	184.71	72.6	59.7	1.25E-4	125.01	45.7	42.65	4.27E-5	444.80

Upon analysis of the multiple sets of data, degradation parameter in the presence and absence of hydroxyl radicals are shown in Table 6 and Table 7. The percentage of H_2S degradation with and without water is shown in Figure 50. The stability and the higher percentage degradation of H_2S in the presence of the fine particle mist can be used to develop a model for an in-field treatment area. The aqueous reactor samples that were collected from the bottom of the reaction bag were externally verified for pH and sulfate concentration as shown in Table 8. An average pH of 3.74 was observed due to the formation of sulfuric acid and an average concentration of 12.8 ppm was analyzed for sulfate. The analysis of SO_2 gas was performed using a Radiello probe supplied by Columbia Analytical Services, Inc. The Radiello probe is composed of microporous polyethylene coated triethanolamine (TEA) where NO_2 and SO_2 is chemi-adsorbed onto as nitrite and sulfite or sulfate ions, respectively. Sulfur dioxide is quantified via ion chromatography in an external laboratory. The analysis concluded an average concentration of 1.83 ppm for SO_2 for the four trials.

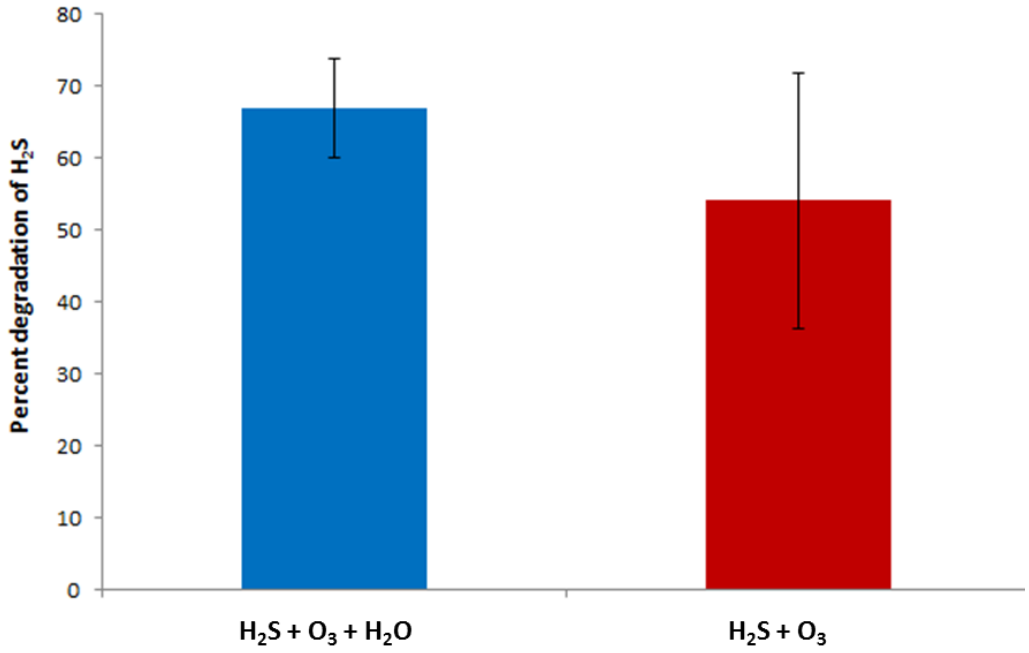

Figure 50: Percent degradation of H_2S in the presence and absence of water. A steady and higher H_2S degradation is observed at 66.9% in the presence of water compared to 54.1% in the absence of water.

Table 8: Analysis of the possible major products produced upon H_2S degradation. *Outlier removed from the data set

Run	pH	Sulfate (SO_4^{-2}) (ppm)	Sulfur Dioxide (SO_2) (ppm)
1	3.60	13.1	2.30
2	4.14	3.04*	2.90
3	3.63	12.0	0.73
4	3.58	13.3	1.40
Average	**3.74 ± 0.23**	**12.8 ± 0.6**	**1.83 ± 0.83**

Conclusions

This study investigated an odor control technology, OHxyPhogg®, which has recently been developed and is currently being used in the United States. The experimental results showed that the system does generate a micro-size hydroxyl radical mist via the patented atomizing nozzle. A successful indirect detection and quantification of the hydroxyl radicals was performed through HPLC and UV-Vis spectrophotometer. The detection limit based on the calibration curve was determined to be 1.00×10^{-7} M, which was adequate for the detection range of the collected reactor samples.

The hydroxyl radicals generated from the odor control system were verified using UV-Vis and quantified by HPLC. The generated hydroxyl radicals reacted with benzene to form phenol as the major product. The 1:1 stoichiometry of hydroxyl radical: phenol allows for quantification of hydroxyl radicals formed. Although ozone is also known to react with benzene, the reaction kinetics are considerably slower than the reaction of benzene with the hydroxyl radicals.[87] The reactions are reported to have reaction rates of 12 M^{-1} sec^{-1} and 41 M^{-1} sec^{-1}, respectively.[87-88] Moreover, the monitoring of the ozone concentration in all chambers during the collection of samples and the generation of the fog remained constant. In that regard, we are confident that the phenol concentration determined was mostly attributed to the reaction with hydroxyl radicals and not with ozone. In general, the phenol concentrations were observed to be in the low parts per million. As expected, C-3 and C-4 showed the highest phenol concentrations since the smallest fog particles were present in those chambers since the larger particulates cannot get through the holes in the separation disks.

A detailed test of the reaction conditions to examine the optimum generation and efficiency of this hydroxyl radical mist upon its reaction with hydrogen sulfide gas was also investigated. A set of experiments was performed to study the optimum reaction ratio of hydrogen sulfide to ozone; however the presence of water yielded a decrease in the concentration of gaseous ozone due to its interactions with the aqueous phase. Based on the experimental data, it can also be concluded that water is needed to achieve a higher percentage efficiency and steady oxidation of hydrogen sulfide in the presence of ozone. The experimental data suggested that by using this technology, significantly less ozone is needed to oxidize a specific amount of hydrogen sulfide when compared to the literature value.

CHAPTER 6: SUMMARY AND OUTLOOK

This work is an exploration of sensors based on redox chemistry, electrochemical sensors, for sensing applications. Today, many enzyme based sensors suffer from major obstacles such as limited sensitivity, restricted selectivity, and a short shelf life. Using this as a motivation, this dissertation explores the possibility of using nanoceria modified electrodes to overcome the complications of enzyme based sensors. In this work, various Pt and Au modified electrodes were fabricated and tested towards the electrochemical oxidation of glucose and hydrogen peroxide. One of the main goals of this work was the production and characterization of nanoceria composite materials as catalysts for glucose and hydrogen peroxide sensors. Electrochemical characterization was carried out to determine the catalytic ability of each of the composite electrode towards the oxidation of glucose and hydrogen peroxide. Due to the biological application of these sensors, all of the electrochemical tests were studied in a 0.1 M phosphate buffer solution as the electrolyte. Cyclic voltammograms for the electrochemical oxidation of glucose and hydrogen peroxide on modified Pt and Au electrodes were compared to those for the Pt/Au and Pt/Au/ceria modified electrodes.

Overall, an increase in the glucose concentration led to a relative increase in the current. The platinum electrode was more effective in providing higher sensitivity and selectivity than gold however the highest current intensity was achieved when the Pt electrode was modified with Pt/Au/ceria indicating certain catalytic activity due to the presence of nanoceria. Independently, Au and Pt electrodes modified with the nanoceria composite were also examined at various pH levels. The results of this study indicated a possible use of these composite modified electrodes under relatively neutral or basic conditions.

Since obtaining selectivity due to interfering species is one of the biggest challenges in the use of non-enzymatic glucose sensors, the interference of ascorbic acid was as well studied under these conditions. The electrochemical studies showed that the peak potential for glucose oxidation and ascorbic acid oxidation are remote to each other, indicating that sensing glucose on an electrode modified with Pt/Au/ceria would successfully avoid the interfering current signal contributed by ascorbic acid. The possible interference of ascorbic acid was also studied at various pH levels on the nanoceria modified Pt electrodes from which the results concluded that the best detection of glucose oxidation is observed under neutral or basic conditions.

The electrochemical oxidation of H_2O_2 on Au and Pt electrodes modified with nanoceria composite were also studied to examine the catalytic ability of nanoceria. The cyclic voltammetry results demonstrated that the Pt/Au/Ceria modified electrodes gave the highest oxidation/reduction current for H_2O_2 when compared to bare metal electrodes and in the absence of ceria. Although the Koutecky-Levich study verified slow kinetic processes for H_2O_2 on the surface the electrode, it can be concluded that nanoceria has a perceptible catalytic effect for the electrochemical oxidation of H_2O_2. Possible inorganic mediators could be analyzed and studied for potential kinetic improvements. Different ratio of Ce^{+3} and Ce^{+4} composite modified electrodes and the stability of these electrodes were also investigated towards H_2O_2 sensing. The analysis of these experiments confirmed that the Ce^{+3} complex modified electrodes gave the most favorable results for H_2O_2 detection.

In general, a linear increase in the oxidation current was observed as the concentration of the analyte of interest increased for both Au and Pt electrodes and its modifications. A slight increase in the current intensity is observed when the electrodes are modified with the Au^{+3} and

Pt^{+4} salts due to the increase in the surface area of the electrode. However, the increase in the electrochemical glucose and hydrogen peroxide oxidation current observed in the presence of the nanoceria particles is larger than what can be attributed to such changes in the morphology and the active electrochemical surface area of the electrode.

In this dissertation, we also investigated an odor control technology, OHxyPhogg®, which has recently been developed and is currently being used in the United States. The experimental results showed that the system does generate a micro-size hydroxyl radical mist via the patented atomizing nozzle. The generated hydroxyl radicals reacted with benzene to form phenol as the major product. The 1:1 stoichiometry of hydroxyl radical to phenol allowed for a direct quantitation of the hydroxyl radicals formed in the fine particle mist. The resulting hydroxyl radical concentrations ranged from 0.26 to 0.83 μM. A successful indirect detection and quantification of the hydroxyl radicals was performed through HPLC and UV-Vis spectrophotometer. The detection limit based on the calibration curve was determined to be 0.10 μM, which was adequate for the detection range of the collected reactor samples. In general, the phenol concentrations were observed to be in the low parts per million. As expected, C-3 and C-4 showed the highest phenol concentrations since the smallest fog particles were present in those chambers, as the larger particulates cannot get through the holes in the separation disks.

A detailed test of the reaction conditions to examine the optimum generation and efficiency of this hydroxyl radical mist upon its reaction with hydrogen sulfide gas was also investigated. A higher and steady degradation of H_2S was observed in the presence of water at 66.9% whereas it was 54.1% in the absence of water. A set of experiments was performed to study the optimum reaction ratio of hydrogen sulfide to ozone; however the presence of water

yielded a decrease in the concentration of gaseous ozone due to its interactions with the aqueous phase. Based on the experimental data, it can also be concluded that water is needed to achieve the most efficient and steady oxidation of hydrogen sulfide in the presence of ozone. The experimental H_2S degradation percentage suggested that by using this technology, less ozone is needed to oxidize a specific amount of hydrogen sulfide when compared to the literature value.

APPENDIX: COPYRIGHT PERMISSION LETTERS

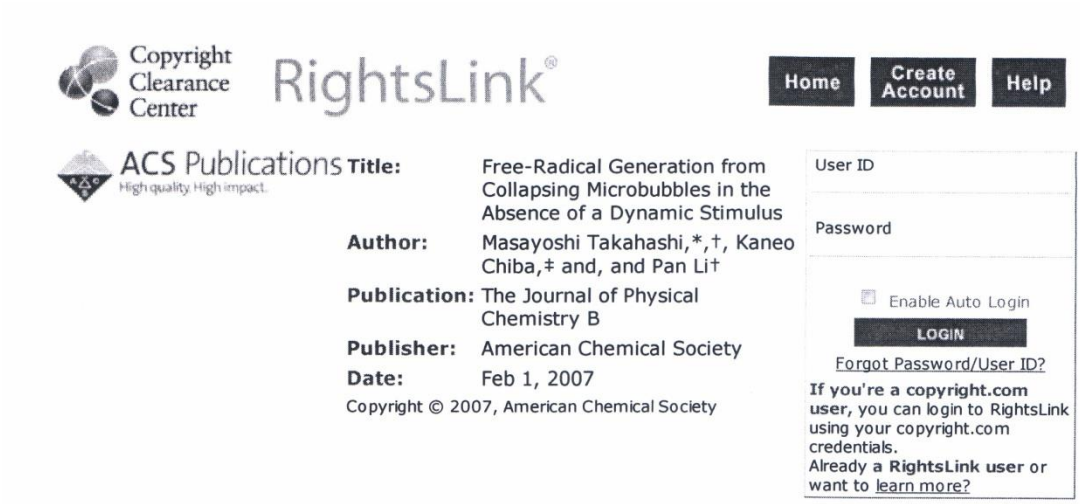

Copyright Clearance Center RightsLink®

Home | Create Account | Help

ACS Publications
High quality. High impact.

Title: Free-Radical Generation from Collapsing Microbubbles in the Absence of a Dynamic Stimulus

Author: Masayoshi Takahashi,*,†, Kaneo Chiba,‡ and, and Pan Li†

Publication: The Journal of Physical Chemistry B

Publisher: American Chemical Society

Date: Feb 1, 2007

Copyright © 2007, American Chemical Society

User ID

Password

Enable Auto Login

LOGIN

Forgot Password/User ID?

If you're a copyright.com user, you can login to RightsLink using your copyright.com credentials.
Already a **RightsLink user** or want to learn more?

PERMISSION/LICENSE IS GRANTED FOR YOUR ORDER AT NO CHARGE

This type of permission/license, instead of the standard Terms & Conditions, is sent to you because no fee is being charged for your order. Please note the following:

- Permission is granted for your request in both print and electronic formats, and translations.
- If figures and/or tables were requested, they may be adapted or used in part.
- Please print this page for your records and send a copy of it to your publisher/graduate school.
- Appropriate credit for the requested material should be given as follows: "Reprinted (adapted) with permission from (COMPLETE REFERENCE CITATION). Copyright (YEAR) American Chemical Society." Insert appropriate information in place of the capitalized words.
- One-time permission is granted only for the use specified in your request. No additional uses are granted (such as derivative works or other editions). For any other uses, please submit a new request.

If credit is given to another source for the material you requested, permission must be obtained from that source.

BACK | CLOSE WINDOW

Copyright © 2013 Copyright Clearance Center, Inc. All Rights Reserved. Privacy statement.
Comments? We would like to hear from you. E-mail us at customercare@copyright.com

Order Completed

Thank you very much for your order.

This is a License Agreement between University of Central Florida -- Jigna Patel ("You") and Elsevier ("Elsevier"). The license consists of your order details, the terms and conditions provided by Elsevier, and the payment terms and conditions.

Get the printable license.

License Number	3155000175163
License date	May 23, 2013
Licensed content publisher	Elsevier
Licensed content publication	Chemosphere
Licensed content title	Enhanced free-radical generation by shrinking microbubbles using a copper catalyst
Licensed content author	Pan Li,Masayoshi Takahashi,Kaneo Chiba
Licensed content date	November 2009
Licensed content volume number	77
Licensed content issue number	8
Number of pages	4
Type of Use	reuse in a thesis/dissertation
Portion	figures/tables/illustrations
Number of figures/tables /illustrations	1
Format	both print and electronic
Are you the author of this Elsevier article?	No
Will you be translating?	No
Order reference number	
Title of your thesis/dissertation	Development of enzymeless electrochemical redox sensors for biological applications
Expected completion date	Aug 2013
Elsevier VAT number	GB 494 6272 12
Permissions price	0.00 USD
VAT/Local Sales Tax	0.00 USD
Total	0.00 USD

Copyright Clearance Center

1 PAYMENT 2 REVIEW 3 CONFIRMATION

Step 3: Order Confirmation

Thank you for your order! A confirmation for your order will be sent to your account email address. If you have questions about your order, you can call us at 978-646-2600, M-F between 8:00 AM and 6:00 PM (Eastern), or write to us at info@copyright.com.

Confirmation Number: 11094479
Order Date: 05/23/2013

If you pay by credit card, your order will be finalized and your card will be charged within 24 hours. If you pay by invoice, you can change or cancel your order until the invoice is generated.

Payment Information

Jigna Patel
University of Central Florida
jigna@knights.ucf.edu
+1 (772)3320564
Payment Method: n/a

Order Details

Annual review of biochemistry

Order detail ID:	63698028
Order License Id:	3155001045350
ISSN:	0066-4154
Publication Type:	Journal
Volume:	
Issue:	
Start page:	
Publisher:	ANNUAL REVIEWS

Permission Status: Granted
Permission type: Republish or display content
Type of use: Republish in a thesis/dissertation

Requestor type	Government agency
Format	Print, Electronic
Portion	chart/graph/table/figure
Number of charts/graphs/tables /figures	2
Title or numeric reference of the portion(s)	Figure 1 The redox state of oxygen...oxygen was regarded as 1 M, Figure 3 Known mechanisms by which H2O2...of sulfur metabolism remain unclear.
Title of the article or chapter the portion is from	Non-enzymatic hydrogen peroxide sensor based on nanoceria modified Au and Pt electrodes and its kinetic study
Editor of portion(s)	N/A
Author of portion(s)	Jigna patel
Volume of serial or monograph	N/A

Note: This item will be invoiced or charged separately through CCC's **RightsLink** service. More info **$ 0.00**

SPRINGER LICENSE
TERMS AND CONDITIONS

May 23, 2013

This is a License Agreement between University of Central Florida ("You") and Springer ("Springer") provided by Copyright Clearance Center ("CCC"). The license consists of your order details, the terms and conditions provided by Springer, and the payment terms and conditions.

All payments must be made in full to CCC. For payment instructions, please see information listed at the bottom of this form.

License Number	3155001292422
License date	May 23, 2013
Licensed content publisher	Springer
Licensed content publication	Analytical and Bioanalytical Chemistry
Licensed content title	Electrochemical quantification of reactive oxygen and nitrogen: challenges and opportunities
Licensed content author	Sabine Borgmann
Licensed content date	Jan 1, 2009
Volume number	394
Issue number	1
Type of Use	Thesis/Dissertation
Portion	Figures
Author of this Springer article	No
Order reference number	
Title of your thesis / dissertation	Development of enzymeless electrochemical redox sensors for biological applications
Expected completion date	Aug 2013
Estimated size(pages)	130
Total	0.00 USD
Terms and Conditions	

Introduction
The publisher for this copyrighted material is Springer Science + Business Media. By clicking "accept" in connection with completing this licensing transaction, you agree that the following terms and conditions apply to this transaction (along with the Billing and Payment terms and conditions established by Copyright Clearance Center, Inc. ("CCC"), at the time that you opened your Rightslink account and that are available at any time at http://myaccount.copyright.com).

Limited License
With reference to your request to reprint in your thesis material on which Springer Science and Business Media control the copyright, permission is granted, free of charge, for the use indicated in your enquiry.

Licenses are for one-time use only with a maximum distribution equal to the number that you identified in the licensing process.

This License includes use in an electronic form, provided its password protected or on the university's intranet or repository, including UMI (according to the definition at the Sherpa website: http://www.sherpa.ac.uk/romeo/). For any other electronic use, please contact Springer at (permissions.dordrecht@springer.com or permissions.heidelberg@springer.com).

The material can only be used for the purpose of defending your thesis, and with a maximum

of 100 extra copies in paper.

Although Springer holds copyright to the material and is entitled to negotiate on rights, this license is only valid, subject to a courtesy information to the author (address is given with the article/chapter) and provided it concerns original material which does not carry references to other sources (if material in question appears with credit to another source, authorization from that source is required as well).

Permission free of charge on this occasion does not prejudice any rights we might have to charge for reproduction of our copyrighted material in the future.

Altering/Modifying Material: Not Permitted
You may not alter or modify the material in any manner. Abbreviations, additions, deletions and/or any other alterations shall be made only with prior written authorization of the author(s) and/or Springer Science + Business Media. (Please contact Springer at (permissions.dordrecht@springer.com or permissions.heidelberg@springer.com)

Reservation of Rights
Springer Science + Business Media reserves all rights not specifically granted in the combination of (i) the license details provided by you and accepted in the course of this licensing transaction, (ii) these terms and conditions and (iii) CCC's Billing and Payment terms and conditions.

Copyright Notice:Disclaimer
You must include the following copyright and permission notice in connection with any reproduction of the licensed material: "Springer and the original publisher /journal title, volume, year of publication, page, chapter/article title, name(s) of author(s), figure number(s), original copyright notice) is given to the publication in which the material was originally published, by adding; with kind permission from Springer Science and Business Media"

Warranties: None

Example 1: Springer Science + Business Media makes no representations or warranties with respect to the licensed material.

Example 2: Springer Science + Business Media makes no representations or warranties with respect to the licensed material and adopts on its own behalf the limitations and disclaimers established by CCC on its behalf in its Billing and Payment terms and conditions for this licensing transaction.

Indemnity
You hereby indemnify and agree to hold harmless Springer Science + Business Media and CCC, and their respective officers, directors, employees and agents, from and against any and all claims arising out of your use of the licensed material other than as specifically authorized pursuant to this license.

No Transfer of License
This license is personal to you and may not be sublicensed, assigned, or transferred by you to any other person without Springer Science + Business Media's written permission.

No Amendment Except in Writing
This license may not be amended except in a writing signed by both parties (or, in the case of Springer Science + Business Media, by CCC on Springer Science + Business Media's behalf).

Objection to Contrary Terms
Springer Science + Business Media hereby objects to any terms contained in any purchase order, acknowledgment, check endorsement or other writing prepared by you, which terms are inconsistent with these terms and conditions or CCC's Billing and Payment terms and conditions. These terms and conditions, together with CCC's Billing and Payment terms and conditions (which are incorporated herein), comprise the entire agreement between you and Springer Science + Business Media (and CCC) concerning this licensing transaction. In the event of any conflict between your obligations established by these terms and conditions and

those established by CCC's Billing and Payment terms and conditions, these terms and conditions shall control.

Jurisdiction
All disputes that may arise in connection with this present License, or the breach thereof, shall be settled exclusively by arbitration, to be held in The Netherlands, in accordance with Dutch law, and to be conducted under the Rules of the 'Netherlands Arbitrage Instituut' (Netherlands Institute of Arbitration).***OR:***

All disputes that may arise in connection with this present License, or the breach thereof, shall be settled exclusively by arbitration, to be held in the Federal Republic of Germany, in accordance with German law.

Other terms and conditions:

v1.3

If you would like to pay for this license now, please remit this license along with your payment made payable to "COPYRIGHT CLEARANCE CENTER" otherwise you will be invoiced within 48 hours of the license date. Payment should be in the form of a check or money order referencing your account number and this invoice number RLNK501028190.
Once you receive your invoice for this order, you may pay your invoice by credit card. Please follow instructions provided at that time.

Make Payment To:
Copyright Clearance Center
Dept 001
P.O. Box 843006
Boston, MA 02284-3006

For suggestions or comments regarding this order, contact RightsLink Customer Support: customercare@copyright.com or +1-877-622-5543 (toll free in the US) or +1-978-646-2777.

Gratis licenses (referencing $0 in the Total field) are free. Please retain this printable license for your reference. No payment is required.

REFERENCES

1. (a) Ahammad, A. J. S.; Lee, J.-J.; Rahman, M. A., Electrochemical Sensors Based on Carbon Nanotubes. *Sensors* **2009,** *9* (4), 2289-2319; (b) Huang, J. W., Q., Gas Sensors Based on Semiconducting Metal Oxide One-Dimensional Nanostructures. *Sensors* **2009,** *9*, 9903-9924; (c) Liu, A., Towards development of chemosensors and biosensors with metal-oxide-based nanowires or nanotubes. *Biosensors and Bioelectronics* **2008,** *24* (2), 167-177; (d) Zhai, T.; Fang, X.; Liao, M.; Xu, X.; Zeng, H.; Yoshio, B.; Golberg, D., A Comprehensive Review of One-Dimensional Metal-Oxide Nanostructure Photodetectors. *Sensors* **2009,** *9* (8), 6504-6529.

2. Rahman, M. M.; Ahammad, A. J. S.; Jin, J.-H.; Ahn, S. J.; Lee, J.-J., A Comprehensive Review of Glucose Biosensors Based on Nanostructured Metal-Oxides. *Sensors* **2010,** *10* (5), 4855-4886.

3. (a) Anderson, J.; Karakoti, A.; Diaz, D. J.; Seal, S., Nanoceria-Modified Platinumâˆ’Gold Composite Electrodes for the Electrochemical Oxidation of Methanol and Ethanol in Acidic Media. *The Journal of Physical Chemistry C* **2010,** *114* (10), 4595-4602; (b) Heckert, E. G.; Seal, S.; Self, W. T., Fenton-Like Reaction Catalyzed by the Rare Earth Inner Transition Metal Cerium. *Environmental Science & Technology* **2008,** *42* (13), 5014-5019.

4. (a) Heckert, E. G.; Karakoti, A. S.; Seal, S.; Self, W. T., The role of cerium redox state in the SOD mimetic activity of nanoceria. *Biomaterials* **2008,** *29* (18), 2705-2709; (b) Baer, D. R.; Amonette, J. E.; Engelhard, M. H.; Gaspar, D. J.; Karakoti, A. S.; Kuchibhatla, S.; Nachimuthu, P.; Nurmi, J. T.; Qiang, Y.; Sarathy, V.; Seal, S.; Sharma, A.; Tratnyek, P. G.; Wang, C. M., Characterization challenges for nanomaterials. *Surface and Interface Analysis* **2008,** *40* (3-4), 529-537.

5. Libby, W. F., Theory of Electron Exchange Reactions in Aqueous Solution. *Journal of Physical Chemistry* **1952,** *56,* 869-871.

6. (a) Teeguarden, J. G., Hinderliter, P. M., Orr, G., Thrall, D., Pounds, J. G., Particokinetics in vitro: Dosimetry Considerations for In Vitro Nanoparticle Toxicity Assessments. *Toxicological Sciences* **2007,** *95* (2), 300-312; (b) Esch, F., Fabris, S., Zhou, L., Montini, T., Africh, C., Fornasiero, P., Comelli, G., Rosei, R., Electron Localization Determines Defect Formation on Ceria Substrates. *Science* **2005,** *309* (5735), 752-755; (c) Campbell, C., Peden, C., Oxygen Vacancies and Catalysis on Ceria Surfaces. *Science* **2005,** *309* (5735), 713-714.

7. (a) Masui, T.; Ozaki, T.; Machida, K.-i.; Adachi, G.-y., Preparation of ceria–zirconia sub-catalysts for automotive exhaust cleaning. *Journal of Alloys and Compounds* **2000,** *303–304* (0), 49-55; (b) Martínez-Arias, A.; Hungría, A. B.; Fernández-García, M.; Conesa, J. C.; Munuera, G., Interfacial Redox Processes under CO/O2 in a Nanoceria-Supported Copper Oxide Catalyst. *The Journal of Physical Chemistry B* **2004,** *108* (46), 17983-17991; (c) Yi-Yang Tsai, J. O.-C., Kristina Agering, Nicholas Simpson, Mark Atkinson, Clive Wasserfall, Ioannis Constantinidis, and Wolfgang Sigmund, Novel synthesis of cerium oxide nanoparticles for free radical scavenging. *Nanomedicine* **2007,** *2* (3), 325-332.

8. Ornatska, M.; Sharpe, E.; Andreescu, D.; Andreescu, S., Paper Bioassay Based on Ceria Nanoparticles as Colorimetric Probes. *Analytical Chemistry* **2011,** *83* (11), 4273-4280.

9. (a) Baer, D., Amonette, J., Engelhard, M., Gaspar, D., Karakoti, A., Kuchibhatla, S., Nachimuthu, P., Nurmi, J., Qiang, Y., Sarathy, V., Seal, S., Sharma, A., Tratnyek, P., Want, C., Characterization Challenges for Nanomaterials. *Science Interface Analysis* **2008,** *40,* 529-537; (b) Karakoti, A., Kuchibhatla, A., Babu, K., Seal, S., Direct Synthesis of Nanoceria in Aqueous

Polyhydroxyl Solutions. *Journal of Physical Chemistry B* **2007,** *111* (46), 17232-17240; (c) Kuchibhatla, S., Karakoti, A., Seal, S., Hierarchical assembly of inorganic nanostructure building blocks to octahedral superstructures — a true template-free self-assembly. *Nanotechnology* **2007,** *18*, 075303-307.

10. Mehta, A.; Patil, S.; Bang, H.; Cho, H. J.; Seal, S., A novel multivalent nanomaterial based hydrogen peroxide sensor. *Sensors and Actuators A: Physical* **2007,** *134* (1), 146-151.

11. Asati, A.; Santra, S.; Kaittanis, C.; Nath, S.; Perez, J. M., Oxidase-Like Activity of Polymer-Coated Cerium Oxide Nanoparticles. *Angew. Chem. Int. Ed.* **2009,** *48*, 2308 –2312.

12. Holt-Hindle, P.; Nigro, S.; Asmussen, M.; Chen, A., Amperometric glucose sensor based on platinum–iridium nanomaterials. *Electrochemistry Communications* **2008,** *10*, 1438–1441.

13. Gavin, J. R., The Importance of Monitoring Blood Glucose. *US Endocrinology* **2007,** *2*, 42-45.

14. Heller, A.; Feldman, B., Electrochemistry in Diabetes Management. *Accounts of Chemical Research* **2010,** *43* (7), 963-973.

15. Wang, J. T., Dan.; Chen, Aicheng, Nonenzymatic Electrochemical Glucose Sensor Based on Nanoporous PtPb Networks. *Analytical Chemistry* **2008,** *80* (4), 997-1004.

16. Updike, S. J.; Hicks, G. P., The Enzyme Electrode. *Nature* **1967,** *214* (5092), 986-988.

17. Wang, Y.; Xu, H.; Zhang, J.; Li, G., Electrochemical Sensors for Clinic Analysis. *Sensors* **2008,** *8* (4), 2043-2081.

18. (a) D'Auria. S., D. C., N., Gryczynski, Z., Gryczynski, I., Rossi, M., Lakowicz, J., A Thermophilic Apoglucose Dehydrogenase as Nonconsuming Glucose Sensor. *Biochemical and Biophysical Research Communications* **2000,** *274* (3), 727-731; (b) Sierra, J. F. G., J.; Castillo, J.

R., Determination of Glucose in Blood Based on the Intrinsic Fluorescence of Glucose Oxidase. *Analytical Chemistry* **1997,** *69* (8), 1471-1476.

19. Gutman, S.; Fuller, J.; Hausman, E., Consumers Report Glucose Meter Problems to FDA. *Diabetes Technology & Therapeutics* **2004,** *6* (6), 767-769.

20. Chen, Z.; Fang, C.; Wang, H.; He, J., Disposable glucose test strip for whole blood with integrated sensing/diffusion-limiting layer. *Electrochimica Acta* **2009,** *55* (2), 544-550.

21. (a) Beden, B.; Largeaud, F.; Kokoh, K. B.; Lamy, C., Fourier transform infrared reflectance spectroscopic investigation of the electrocatalytic oxidation of -glucose: Identification of reactive intermediates and reaction products. *Electrochimica Acta* **1996,** *41* (5), 701-709; (b) Grace, A.; Pandian, K., Synthesis of gold and platinum nanoparticles using tetraaniline as reducing and phase transfer agent--A brief study and their role in the electrocatalytic oxidation of glucose. *Journal of Physics and Chemistry of Solids* **2007,** *68* (12), 2278-2285; (c) Kang, X. H.; Mai, Z. B.; Zou, X. Y.; Cai, P. X.; Mo, J. Y., A novel sensitive non-enzymatic glucose sensor. *Chinese Chemical Letters* **2007,** *18* (2), 189-191.

22. Tominaga, M.; Shimazoe, T.; Nagashima, M.; Kusuda, H.; Kubo, A.; Kuwahara, Y.; Taniguchi, I., Electrocatalytic oxidation of glucose at gold-silver alloy, silver and gold nanoparticles in an alkaline solution. *Journal of Electroanalytical Chemistry* **2006,** *590* (1), 37-46.

23. (a) Sun, Y.; Buck, H.; Mallouk, T. E., Combinatorial Discovery of Alloy Electrocatalysts for Amperometric Glucose Sensors. *Analytical Chemistry* **2001,** *73* (7), 1599-1604; (b) Qiu, R.; Zhang, X. L.; Qiao, R.; Li, Y.; Kim, Y. I.; Kang, Y. S., CuNi Dendritic Material:â€‰ Synthesis, Mechanism Discussion, and Application as Glucose Sensor. *Chemistry of Materials* **2007,** *19* (17), 4174-4180; (c) Aoun, S. B.; Dursun, Z.; Koga, T.; Bang, G. S.; Sotomura, T.; Taniguchi, I.,

Effect of metal ad-layers on Au(1 1 1) electrodes on electrocatalytic oxidation of glucose in an alkaline solution. *Journal of Electroanalytical Chemistry* **2004,** *567* (2), 175-183; (d) Cui, H., Ye. J., Liu. X, Zhang. W., Sheu, F., Pt-Pb alloy nanoparticle/carbon nanotube nanocomposite: a strong electrocatalyst for glucose oxidation. *Nanotechnology* **2006,** *17*, 2334-2339; (e) Wang, J.; Thomas, D. F.; Chen, A., Nonenzymatic Electrochemical Glucose Sensor Based on Nanoporous PtPb Networks. *Analytical Chemistry* **2008,** *80* (4), 997-1004.

24. (a) Jingquan, L.; Alison, C.; Wibowo, R.; Michael , N. P.-R.; Gooding, J. J., Achieving Direct Electrical Connection to Glucose Oxidase Using Aligned Single Walled Carbon Nanotube Arrays. *Electroanalysis* **2005,** *17* (1), 38-46; (b) Wang, S. G.; Zhang, Q.; Wang, R.; Yoon, S. F.; Ahn, J.; Yang, D. J.; Tian, J. Z.; Li, J. Q.; Zhou, Q., Multi-walled carbon nanotubes for the immobilization of enzyme in glucose biosensors. *Electrochemistry Communications* **2003,** *5* (9), 800-803.

25. Chen, J. Z., Wei-De.; Ye, Jian-Shan, Nonenzymatic Electrochemical Glucose Sensor Based on MnO2/MWNTs nanocomposite. *Electrochemistry Communications* **2008,** *10* (9), 1268.

26. Park, S.; Boo, H.; Chung, T. D., Electrochemical non-enzymatic glucose sensors. *Analytica Chimica Acta* **2006,** *556*, 46–57.

27. (a) Park, S.; Chung, T. D.; Kim, H. C., Nonenzymatic Glucose Detection Using Mesoporous Platinum. *Anal. Chem.* **2003,** *75*, 3046-3049; (b) Boo, H.; Park, S.; Ku, B.; Kim, Y.; Park, J. H.; Kim, H. C.; Chung, T. D., Ionic Strength-Controlled Virtual Area of Mesoporous Platinum Electrode. *Journal of the American Chemical Society* **2004,** *126* (14), 4524-4525.

28. Chou, C.-H.; Chen, J.-C.; Tai, C.-C.; Sun, I. W.; Zen, J.-M., A Nonenzymatic Glucose Sensor Using Nanoporous Platinum Electrodes Prepared by Electrochemical

Alloying/Dealloying in a Water-Insensitive Zinc Chloride-1-Ethyl-3-Methylimidazolium Chloride Ionic Liquid. *Electroanalysis* **2008,** *20* (7), 771-775.

29. Ernst, S.; Heitbaum, J., The Electrooxidation of Glucose in Phosphate Buffer Solutions. Part I. Reactivity And Kinetics Below 350 mV/RHE. *Journal of Electroanalytical Chemistry* **1979,** *100*, 173-183.

30. (a) Shoji, E., Freund, M, Potentiometric Sensors Based on the Inductive Effect on the pKa of Poly(aniline): A Nonenzymatic Glucose Sensor. *Journal of American Chemical Society* **2001,** *123* (14), 3383-3384; (b) Shoji, E., Freund, M, Potentiometric Saccharide Detection Based on the pKa Changes of Poly(aniline bronic acid). *Journal of American Chemical Society* **2002,** *124* (42), 12486-12493.

31. (a) Torto, N., Ruzgas, T., Gorton, L., Electrochemical oxidation of mono- and disaccharides at fresh as well as oxidized electrodes in alkaline media. *Journal of Electroanalytical Chemistry* **1999,** *464* (2); (b) Corbo, D.; Bertotti, M., Use of a copper electrode in alkaline medium as an amperometric sensor for sulphite in a flow-through configuration. *Analytical and Bioanalytical Chemistry* **2002,** *374* (3), 416-420.

32. Pereira, A. C.; Fertonani, F. L.; Neto, G. d. O.; Kubota, L. T.; Yamanaka, H., Reagentless biosensor for isocitrate using one step modified Pt-Ir microelectrode. *Talanta* **2001,** *53* (4), 801-806.

33. Myung, Y.; Jang, D. M.; Cho, Y. J.; Kim, H. S.; Park, J., Nonenzymatic Amperometric Glucose Sensing of Platinum, Copper Sulfide, and Tin Oxide Nanoparticle-Carbon Nanotube Hybrid Nanostructures. *J. Phys. Chem. C* **2009,** (113), 1251–1259.

34. (a) Ma, Y.; Hu, G.; Shao, S.; Guo, Y., An amperometric sensor for uric acid based on ordered mesoporous carbon-modified pyrolytic graphite electrode. *Chemical Papers* **2009,** *63*

(6), 641-645; (b) Ndamanisha, J. C.; Guo, L., Nonenzymatic glucose detection at ordered mesoporous carbon modified electrode. *Bioelectrochemistry* **2009,** *77* (1), 60-63.

35. (a) Luo, D.; Wu, L.; Zhi, J., Fabrication of Boron-Doped Diamond Nanorod Forest Electrodes and Their Application in Nonenzymatic Amperometric Glucose Biosensing. *ACS Nano* **2009,** *3* (8), 2121-2128; (b) Su, L.; Qiu, X.; Guo, L.; Zhang, F.; Tung, C., Amperometric glucose sensor based on enzyme-modified boron-doped diamond electrode by cross-linking method. *Sensors and Actuators B: Chemical* **2004,** *99* (2-3), 499-504.

36. (a) Korsvik, C.; Patil, S.; Seal, S.; Self, W. T., Superoxide dismutase mimetic properties exhibited by vacancy engineered ceria nanoparticles. *Chemical Communications* **2007,** (10), 1056-1058; (b) Karakoti, A. S.; Kuchibhatla, S. V. N. T.; Babu, K. S.; Seal, S., Direct Synthesis of Nanoceria in Aqueous Polyhydroxyl Solutions. *The Journal of Physical Chemistry C* **2007,** *111* (46), 17232-17240.

37. Bard, A. J.; Faulkner, L. R., *Electrochemical Methods: Fundamentals and Applications*. Wiley: New York, 2001.

38. Oldham, K. B.; Myland, J. C.; Bond, A. M., *Electrochemical Science and Technology: Fundamentals and Applications*. John Wiley & Sons, Ltd.: Chichester, UK, 2012.

39. Fisher, A. C., *Electrode Dynamics*. Oxford University Press: New York, 1996.

40. (a) Bagotsky, V. S., *Fundamentals of Electrochemistry*. 2nd ed.; JOHN WILEY & SONS, INC.: Hoboken, New Jersey, 2006; (b) Mabbott, G. A., An introduction to cyclic voltammetry. *Journal of Chemical Education* **1983,** *60* (9), 697; (c) Somorjai, G. A.; Yimin, L., *Introduction to Surface Chemistry and Catalysis.* John Wiley & Sons: 2010.

41. (a) Campos, C. L.; Roldán, C.; Aponte, M.; Ishikawa, Y.; Cabrera, C. R., Preparation and methanol oxidation catalysis of Pt-CeO2 electrode. *Journal of Electroanalytical Chemistry* **2005,**

581 (2), 206-215; (b) Díaz, D. J.; Greeneltch, N.; Solanki, A.; Karakoti, A.; Seal, S., Novel Nanoscale Ceria–Platinum Composite Electrodes for Direct Alcohol Electro-Oxidation. *Catal Lett* **2007,** *119* (3-4), 319-326.

42. Díaz, D.; Greenletch, N.; Solanki, A.; Karakoti, A.; Seal, S., Novel Nanoscale Ceria–Platinum Composite Electrodes for Direct Alcohol Electro-Oxidation. *Catalysis Letters* **2007,** *119* (3), 319-326.

43. Zhang, J.; Sung, Y. E.; Rikvold, P. A.; Wieckowski, A., Underpotential deposition of Cu on Au(111) in sulfate-containing electrolytes: A theoretical and experimental study. *J. Chem. Phys.* **1996,** *104* (14), 5699-5712.

44. (a) Beden, B.; Largeaud, F.; Kokoh, K. B.; Lamy, C., Fourier transform infrared reflectance spectroscopic investigation of the electrocatalytic oxidation of d-glucose: Identification of reactive intermediates and reaction products. *Electrochimica Acta* **1996,** *41* (5), 701-709; (b) Vassilyev, Y. B.; Khazova, O. A.; Nikolaeva, N. N., Kinetics and mechanism of glucose electrooxidation on different electrode-catalysts: Part I. Adsorption and oxidation on platinum. *Journal of Electroanalytical Chemistry and Interfacial Electrochemistry* **1985,** *196* (1), 105-125; (c) Bae, I. T.; Yeager, E.; Xing, X.; Liu, C. C., In situ infrared studies of glucose oxidation on platinum in an alkaline medium. *Journal of Electroanalytical Chemistry and Interfacial Electrochemistry* **1991,** *309* (1–2), 131-145.

45. Ernst, S.; Heitbaum, J.; Hamann, C. H., The electrooxidation of glucose in phosphate buffer solutions: Part I. Reactivity and kinetics below 350 mV/RHE. *Journal of Electroanalytical Chemistry and Interfacial Electrochemistry* **1979,** *100* (1–2), 173-183.

46. (a) Attard, G. S.; Bartlett, P. N.; Coleman, N. R. B.; Elliott, J. M.; Owen, J. R., Lyotropic Liquid Crystalline Properties of Nonionic Surfactant/H2O/Hexachloroplatinic Acid Ternary

Mixtures Used for the Production of Nanostructured Platinum. *Langmuir* **1998,** *14* (26), 7340-7342; (b) Attard, G. S.; Corker, J. M.; Göltner, C. G.; Henke, S.; Templer, R. H., Liquid-Crystal Templates for Nanostructured Metals. *Angewandte Chemie International Edition in English* **1997,** *36* (12), 1315-1317; (c) Elliott, J. M.; Attard, G. S.; Bartlett, P. N.; Coleman, N. R. B.; Merckel, D. A. S.; Owen, J. R., Nanostructured Platinum (HI-ePt) Films: Effects of Electrodeposition Conditions on Film Properties. *Chemistry of Materials* **1999,** *11* (12), 3602-3609; (d) Elliott, J. M.; Birkin, P. R.; Bartlett, P. N.; Attard, G. S., Platinum Microelectrodes with Unique High Surface Areas. *Langmuir* **1999,** *15* (22), 7411-7415; (e) Evans, S. A. G.; Elliott, J. M.; Andrews, L. M.; Bartlett, P. N.; Doyle, P. J.; Denuault, G., Detection of Hydrogen Peroxide at Mesoporous Platinum Microelectrodes. *Analytical Chemistry* **2002,** *74* (6), 1322-1326.

47. Park, S. B., Hankil.; Chung Taek, Electrochemical Non-Enzymatic Glucose Sensors. *Analytica Chimica Acta* **2006,** *556* (1), 46-57.

48. Turrens, J. F., Mitochondrial formation of reactive oxygen species. *The Journal of Physiology* **2003,** *552* (2), 335-344.

49. Chabot, F.; Mitchell, J.; Gutteridge, J.; Evans, T., Reactive oxygen species in acute lung injury. *European Respiratory Journal* **1998,** *11* (3), 745-757.

50. Imlay, J. A., Cellular Defenses against Superoxide and Hydrogen Peroxide. *Annual Review of Biochemistry* **2008,** *77* (1), 755-776.

51. Apel, K.; Hirt, H., REACTIVE OXYGEN SPECIES: Metabolism, Oxidative Stress, and Signal Transduction. *Annual Review of Plant Biology* **2004,** *55* (1), 373-399.

52. (a) Bolwell, G. P.; Wojtaszek, P., Mechanisms for the generation of reactive oxygen species in plant defence – a broad perspective. *Physiological and Molecular Plant Pathology*

1997, *51* (6), 347-366; (b) Fahn, S.; Cohen, G., The oxidant stress hypothesis in Parkinson's disease: Evidence supporting it. *Annals of Neurology* **1992,** *32* (6), 804-812; (c) Hensley, K.; Robinson, K. A.; Gabbita, S. P.; Salsman, S.; Floyd, R. A., Reactive oxygen species, cell signaling, and cell injury. *Free Radical Biology and Medicine* **2000,** *28* (10), 1456-1462; (d) Vallyathan, V.; Shi, X.; Castranova, V., Reactive Oxygen Species: Their Relation to Pneumoconiosis and Carcinogenesis. *Environmental Health Perspectives* **1998,** *106* (Supplement 5), 1151-1155.

53. Ispas, C.; Njagi, J.; Cates, M.; Andreescu, S., Electrochemical Studies of Ceria as Electrode Material for Sensing and Biosensing Applications. *Journal of The Electrochemical Society* **2008,** *155* (8), F169-F176.

54. (a) Farr, S. B.; R., D. A.; Touati, D., Oxygen-dependent mutagenesis in escherichia coli lacking superoxide dismutase. *Proc. natl. Acad. Sci. USA* **1986,** *83*, 8268-72; (b) Levin, D. E.; Hollstein, M.; Christman, M. F.; Schwiers, E. A.; Ames, B. N., A new Salmonella tester strain (TA102) with A X T base pairs at the sire of mutation detects oxidative mutagens. *Proc. Natl. Acad. Sci. USA* **1982,** *79*, 7445-49.

55. Sabine, B., Electrochemical quantification of reactive oxygen and nitrogen: challenges and opportunites. *Analytical and Bioanalytical Chemistry* **2009,** *394*, 95-105.

56. (a) Cai, L.-T.; Chen, H.-Y., Electrocatalytic reduction of hydrogen peroxide at platinum microparticles dispersed in a poly(o-phenylenediamine) film. *Sensors and Actuators B: Chemical* **1999,** *55* (1), 14-18; (b) Garcıa Armada, M.; Losada, J.; Cuadrado, I.; Alonso, B.; González, B.; Ramı; rez-Oliva, E.; Casado, C. M., Electrodes modified with a siloxane copolymer containing interacting ferrocenes for determination of hydrogen peroxide and glucose. *Sensors and Actuators B: Chemical* **2003,** *88* (2), 190-197; (c) Yu, H.; Sheng, Q. L.;

Zheng, J. B., Preparation, electrochemical behavior and performance of gallium hexacyanoferrate as electrocatalyst of H_2O_2. *Electrochimica Acta* **2007,** *52* (13), 4403-4410; (d) Martel, D.; Kuhn, A., Electrocatalytic reduction of H_2O_2 at $P_2Mo_{18}O_{62}^{6-}$ modified glassy carbon. *Electrochimica Acta* **2000,** *45* (11), 1829-1836; (e) Wang, G.; Zhou, J.; Li, J., Layer-by-layer self-assembly aluminum Keggin ions/Prussian blur nanoparticles ultrathin films towards multifunctional sensing applications. *Biosensors and Bioelectronics* **2007,** *22*, 2921-2925.

57. Berchmans, S.; Gomathi, H.; Prabhakara Rao, G., Enzymeless approach for the determination of some biologically important species. *Sensors and Actuators B: Chemical* **1998,** *50* (2), 156-163.

58. (a) Hall, S. B.; Khudaish, E. A.; Hart, A. L., Electrochemical oxidation of hydrogen peroxide at platinum electrodes. Part IV: phosphate buffer dependence. *Electrochimica Acta* **1999,** *44* (25), 4573-4582; (b) Terashima, C.; Rao, T. N.; Sarada, B. V.; Spataru, N.; Fujishima, A., Electrodeposition of hydrous iridium oxide on conductive diamond electrodes for catalytic sensor applications. *Journal of Electroanalytical Chemistry* **2003,** *544* (0), 65-74; (c) Chikae, M.; Idegami, K.; Kerman, K.; Nagatani, N.; Ishikawa, M.; Takamura, Y.; Tamiya, E., Direct fabrication of catalytic metal nanoparticles onto the surface of a screen-printed carbon electrode. *Electrochemistry Communications* **2006,** *8* (8), 1375-1380.

59. (a) Hrbac, J.; Halouzka, V.; Zboril, R.; Papadopoulos, K.; Triantis, T., Carbon Electrodes Modified by Nanoscopic Iron(III) Oxides to Assemble Chemical Sensors for the Hydrogen Peroxide Amperometric Detection. *Electroanalysis* **2007,** *19* (17), 1850-1854; (b) Salimi, A.; Hallaj, R.; Soltanian, S.; Mamkhezri, H., Nanomolar detection of hydrogen peroxide on glassy carbon electrode modified with electrodeposited cobalt oxide nanoparticles. *Analytica Chimica Acta* **2007,** *594* (1), 24-31; (c) Schachl, K.; Alemu, H.; Kalcher, K.; Jezkova, J.; Svancara, I.;

Vytras, K., Amperometric Determination of Hydrogen Peroxide With a Manganese Dioxide-modified Carbon Paste Electrode Using Flow Injection Analysis. *Analyst* **1997,** *122* (9); (d) Yao, S.; Xu, J.; Wang, Y.; Chen, X.; Xu, Y.; Hu, S., A highly sensitive hydrogen peroxide amperometric sensor based on MnO2 nanoparticles and dihexadecyl hydrogen phosphate composite film. *Analytica Chimica Acta* **2006,** *557* (1–2), 78-84; (e) Hermanek, M.; Zboril, R.; Medrik, I.; Pechousek, J.; Gregor, C., Catalytic Efficiency of Iron(III) Oxides in Decomposition of Hydrogen Peroxide: Competition between the Surface Area and Crystallinity of Nanoparticles. *Journal of the American Chemical Society* **2007,** *129* (35), 10929-10936.

60. Babu, S.; Velez, A.; Wozniak, K.; Szydlowska, J.; Seal, S., Electron paramagnetic study on radical scavenging properties of ceria nanoparticles. *Chemical Physics Letters* **2007,** *442* (4–6), 405-408.

61. Heinemann, C.; Cornehl, H. H.; Schroeder, D., The CeO2+ cation: Gas-phase reactivity and electronic structure. *Journal Name: Inorganic Chemistry; Journal Volume: 35; Journal Issue: 9; Other Information: PBD: 24 Apr 1996* **1996**, Medium: X; Size: pp. 2463-2475.

62. Hall, S. B.; Khudaish, E. A.; Hart, A. L., Electrochemical oxidation of hydrogen peroxide at platinum electrodes. Part 1. An adsorption-controlled mechanism. *Electrochimica Acta* **1997,** *43* (5–6), 579-588.

63. Treimer, S.; Tang, A.; Johnson, D. C., A Consideration of the Application of Koutecký-Levich Plots in the Diagnoses of Charge-Transfer Mechanisms at Rotated Disk Electrodes. *Electroanalysis* **2002,** *14* (3), 165-171.

64. Prabhu, V. G.; Zarapkar, L. R.; Dhaneshwar, R. G., Electrochemical studies of hydrogen peroxide at a platinum disc electrode. *Electrochimica Acta* **1981,** *26* (6), 725-729.

65. (a) Mopper, K.; Zhou, X., Hydroxyl Radical Photoproduction in the Sea and Its Potential Impact on Marine Processes. *Science* **1990,** *250* (4981), 661-664; (b) Zhou, X.; Mopper, K., Determination of photochemically produced hydroxyl radicals in seawater and freshwater. *Marine Chemistry* **1990,** *30* (0), 71-88.

66. Page, S. E. W., Kyle T.; Pierre, Valerie C., Sensitive and Selective Time-Gated Luminescence Detection of Hydroxyl Radical in Water. *ChemComm* **2010,** *46*, 2423-2425.

67. Stasinakis, A. S., Use of selected advanced oxidation processes (AOPs) for wastewater treatment- a mini review. *Global NEST Journal* **2008,** *10* (3), 376-385.

68. (a) He, Y. Z. M., W. G.; Tsang, W. , Kinetics of Hydrogen and Hydroxyl Radical Attack on Phenol at High Temperatures. *J. Phys. Chem.* **1988,** *92* (8), 2196-2201; (b) Otsuka, K. K., Mitsuhiro; Yamagata, Hideaki, Direct Synthesis of Phenol from Benzene During O2-H2 Fuel Cell Reactions. *J. Electrochem. Soc.* **1992,** *139* (9), 2381-2386.

69. Bahidsky, M. H., Milan, Direct Hydroxylation of Benzene to Phenol. *Petroleum and Coal* **2004,** *46* (3), 49-55.

70. Takeda, K. T., Hiroshi; Yamaji, Shuhei; Ohta, Keiichi; Sakugawa, Hiroshi., Determination of Hydroxyl Radical Photoproduction Rates in Natural Waters. *Analytical Chemistry* **2004,** *20*, 153-158.

71. Li, B. G., Peter L.; Blough, Neil V., Trace Determination of Hydroxyl Radical in Biological Systems. *Analytical Chemistry* **1997,** *69*, 4295-4302.

72. Joseph, J. M. L., Teene L.; Aravind, Usha K.; Aravindakumar, Charuvila T., Photochemical Production of Hydroxyl Radical from Aqueous Iron(III)-Hydroxyl Complex: Determination of its Reaction Rate Constants with Some Substituted Benzene Using Deoxyribose-Thiobarbituric Acid Assay. *Water Environment Research* **2010,** *73* (2), 243-247.

73. Jen, J.-F. L., Meei-Fan; Yang, Thomas C., Determination of Hydroxyl Radicals in an Advanced Oxidation Process with Salicylic Acid Trapping and Liquid Chromatography. *Journal of Chromatography A.* **1997,** *796*, 283-288.

74. (a) Chen, X. M., Kenneth., Determination of Tropospheric Hydroxyl Radical by Liquid Phase Scrubbing and HPLC: Preliminary Results. *Journal of Atmospheric Chemistry* **2000,** *36*, 81-105; (b) Nakatani, N. H., Norichika; Shindo, Hirotaka; Yamamoto, Masatoshi; Kikkawa, Megumi; Sakugawa, Hirishi., Determination of Photophormation Rates and Scavenging Rate Constants of Hydroxyl Radicals in Natural Waters Using and Automatic Light Radiation and Injection System. *Analytica Chimica Acta* **2007,** *581*, 260-267; (c) Stokes, N. J. T., Brian J.; Hewitt, C. Nicholas, The Determination of Hydroxyl Radical Concentrations in Environmental Chambers Using electron Spin Resonance. *Chemosphere* **1994,** *28* (5), 999-1008; (d) Wang, L. Z., Changbo; Wu, Feng; Deng, Nansheng; Glebov, Evgeni M.; Bazhin, Nikolai M. , Determination of Hydroxyl Radicals from Photolysis of Fe(III)-Pyruvate Complexes in Homogeneous aqueous Solution. *React. Kinet. Catal. Lett* **2006,** *89* (1), 183-192; (e) Wang, L. Z., Changbo; Wu, Feng; Deng, Nansheng., Photoproduction and Determination of Hydroxyl Radicals in Aqueous Solutions of Fe(III)-tetrate Complexes: A Quantitative Assessment. *Journal of Coordination Chemistry* **2006,** *59* (7), 803-813; (f) White, E. M. C., Yu-Ping, Determination of Photochemical Production of Hydroxyl Radicals by Natural Dissolved Organic Matter. *Preprints of Extended Abstracts* **2000,** *40* (2), 10-13; (g) Kilinc, E., Determination of the hydroxyl radical by its adduct formation with phenol and liquid chromatography/electrochemical detection. *Talanta* **2005,** *65* (4), 876-881.

75. Balakrishnan, I.; Reddy, M. P., Mechanism of reaction of hydroxyl radicals with benzene in the .gamma. radiolysis of the aerated aqueous benzene system. *The Journal of Physical Chemistry* **1970,** *74* (4), 850-855.

76. Agarwal, A.; Ng, W. J.; Liu, Y., Principle and applications of microbubble and nanobubble technology for water treatment. *Chemosphere* **2011,** *84* (9), 1175-1180.

77. (a) Takahashi, M.; Chiba, K.; Li, P., Formation of Hydroxyl Radicals by Collapsing Ozone Microbubbles under Strongly Acidic Conditions. *The Journal of Physical Chemistry B* **2007,** *111* (39), 11443-11446; (b) Takahashi, M.; Chiba, K.; Li, P., Free-Radical Generation from Collapsing Microbubbles in the Absence of a Dynamic Stimulus. *The Journal of Physical Chemistry B* **2007,** *111* (6), 1343-1347.

78. Glotfelty, D. E.; Majewski, M. S.; Seiber, J. N., Distribution of several organophosphorus insecticides and their oxygen analogs in a foggy atmosphere. *Environmental Science & Technology* **1990,** *24* (3), 353-357.

79. Valsaraj, K. T.; Thoma, G. J.; Reible, D. D.; Thibodeaux, L. J., On the enrichment of hydrophobic organic compounds in fog droplets. *Atmospheric Environment. Part A. General Topics* **1993,** *27* (2), 203-210.

80. Raja, S.; Valsaraj, K. T., Adsorption and Transport of Gas-Phase Naphthalene on Micron-Size Fog Droplets in Air. *Environmental Science & Technology* **2003,** *38* (3), 763-768.

81. Li, P.; Takahashi, M.; Chiba, K., Enhanced free-radical generation by shrinking microbubbles using a copper catalyst. *Chemosphere* **2009,** *77* (8), 1157-1160.

82. Kimura, T., Ando, T.,, Physical Control of chemical reaction by ultrasonic waves. *Ultranson. Technol.* **2002,** *14*, 7-8.

83. Sumikura, M. H., M.; Murakami, H.; Nobutomo, Y.; Murakami, T., Ozone micro-bubble disinfection method for watewater reuse system. *Water Science & Technology* **2007,** *56* (5), 53-61.

84. Arnold, D. S. P., C.A.; Erickson, E.E.; Pike, F.P., Solubility Of Benzene in Water. *Chemical and Engineering Data Series* **1958,** *3* (2), 253-256.

85. Erb, E. W.; Resch, D. R. Odor control atomizer utilizing ozone and water. US6076748 A, 2000.

86. Zhang, Q. Z., F.; Kai, X.M., Simultaneous Determination of Phenol and Resorcinol by dual-wavelength Spectrophotometric Linear Regreassion Method. *PubMed* **2006,** *26* (11), 2110-2121.

87. Beltran, F. J., *Ozone Reaction Kinetics for Water and Wastewater Systems*. Lewis Publishers: 2004.

88. (a) Tully, F. P. R., A. R.; Thompson, R. L.; Nicolich, R. C.; Shah, R. C.; Kreutter, N. M.; Wine, P. H., Kinetics of the Reactions of Hydroxyl Radical with Benzene and Toluene. *American Chemical Society* **1981,** *85* (15), 2262-2269; (b) Mehta, Y. M.; George, C. E.; Kuo, C. H., Mass transfer and selectivity of ozone reactions. *The Canadian Journal of Chemical Engineering* **1989,** *67* (1), 118-126.

89. Riva, G. Sewage and Wasterwater Odor Control. (accessed April 28, 2013).

90. Gregor, I.; Martin, R., The Reaction between Ozonized Oxygen and Hydrogen Sulphide in the Gaseous Phase. *Australian Journal of Chemistry* **1961,** *14* (3), 462-468.